

Copper catalysts for the conversion of polyunsaturated hydrocarbons

Giorgio Totarella

Author: Giorgio Totarella

Title: Copper catalysts for the conversion of polyunsaturated hydrocarbons

This research has received funding from the Dutch Research Council (De Nederlandse organisatie voor Wetenschappelijk Onderzoek, NWO), NWO Vici 16.130.344

Cover design: Giorgio Totarella

Printing: Ridderprint, the Netherlands

Copper catalysts for the conversion of polyunsaturated hydrocarbons

Koperkatalysatoren voor de omzetting van meervoudig onverzadigde koolwaterstoffen

(met een samenvatting in het Nederlands)

Catalizzatori a base di rame per la conversione di idrocarburi polinsaturi

(con riassunto in italiano)

Proefschrift

ter verkrijging van de graad van doctor aan de
Universiteit Utrecht
op gezag van de
rector magnificus, prof. dr. H.R.B.M. Kummeling,
ingevolge het besluit van het college voor promoties
in het openbaar te verdedigen op

woensdag 19 juni 2024 des ochtends te 10.15 uur

door

Giorgio Totarella

geboren op 30 mei 1992
te Campobasso, Italië

Promotor:

Prof. dr. P.E. de Jongh

Copromotor:

Dr. L. Delannoy

Beoordelingscommissie:

Dr. J.E.S. van der Hoeven

Prof. dr. A. Meijerink

Dr. M. Moret

Dr. F.T. Rabouw

Prof. M. Rønning

Table of contents

Chapter 1	General introduction	1
Chapter 2	Hydrogenation of 1,3-butadiene on Cu nanoparticles immobilized on inert supports: catalyst stability and selectivity	21
Chapter 3	Particle size effects	43
Chapter 4	Metal/metal oxide additives	63
Chapter 5	Selective hydrogenation of 2-methyl-3-butyn-2-ol over supported Cu nanocatalysts	79
	Summary and Outlook	93
	Nederlandse samenvatting	97
	Riepilogo in italiano	101
	References	107
	List of publications and presentations	125
	Curriculum vitae	127

1 General introduction

Summary

Copper, one of the first metal used by humans, has a significant impact on society. It has interesting physicochemical properties that spur technological applications. In catalysis, the metal is often used in the hydrogenation of organic molecules, both for bulk and fine chemical synthesis. An important example is the production of methanol from synthesis gas (a mixture of CO, CO₂ and H₂). Methanol is one the most important building blocks in industrial chemistry and used for the synthesis of sustainable fuels as well as specialty chemicals. Cu nanoparticles are particularly promising for selective hydrogenation reactions such as the hydrogenation of triple C≡C bonds to double C=C bonds, and the hydrogenation of a specific double C=C bond while leaving other unsaturated moieties in the molecule untouched. The selective hydrogenation of 1,3-butadiene is introduced which, together with acetylene, represents a major disruptor in the efficient synthesis of olefin-based high-quality polymers and fine chemicals and it's the main reaction discussed in this thesis. Also, an introduction to particle size effects, the dependence of activity, selectivity, and stability on particle size, is provided. Finally, an overview of the content of this thesis is presented.

1.1 – Copper

Copper is regarded as the first metal used by humans for the fabrication of tools and weapons.¹ The main reason for its early success is that copper can be easily found in nature in its metallic form (example of “native copper” in Figure 1.1 on the right). Estimates place the earliest use of native copper for the manufacturing of utensils and ornaments at around 9000 B.C.¹ The ability to extract copper from ores, however, was developed only 5000 years later. Some of the most important copper-containing minerals that can be found in nature are azurite ($\text{Cu}_2(\text{CO}_3)_2(\text{OH})_2$), malachite ($\text{Cu}_2(\text{CO}_3)(\text{OH})_2$) and chalcopyrite (CuFeS_2). Present-day Israel, Egypt, Iran, and Jordan were some of the earliest locations of copper smelting sites. Early societies here traded and used copper to produce pots, trays, saucers, and drinking vessels.



Figure 1.1 Native copper about 1½ inches (4 cm) in size. Author photograph: “Jonathan Zander”. <https://commons.wikimedia.org/wiki/File:NatCopper.jpg>. Reproduced under license: CC BY-SA 3.0.



Figure 1.2 A copper alloy Roman sestertius, possibly of Septimius Severus (AD 193-211). The coin is quite worn making identification difficult, although the figure on the reverse may be female and may be holding a phoenix. Rights holder: PAS, Oxfordshire County Council. Record number BERK-BC7832. Reproduced under license CC BY-SA 4.0 DEED.

Tools made of bronze or other copper alloys, including chisels, razors, harpoons, arrows, spearheads and even plumbing parts, have been discovered dating from to the third millennium BCE.^{2,3} Around the same period, Cu was also used as coinage metal, together with Ag and Au (Figure 1.2: copper alloy Roman sestertius, possibly of Septimius Severus, AD 193-211). This is still the case for many currencies around the world (even though Cu is usually alloyed with other metals to avoid surface

oxidation). A few thousands of years have passed since, yet our society still heavily relies on the shiny reddish metal. The laptop on which I am writing these lines of text, power cables, electric cars, fridges, air-conditioners would not exist, or would be very expensive, without copper.

But why is this metal so popular? This is due to its distinctive properties. Copper is a relatively malleable metal, it’s corrosion-resistant (due to surface passivation) and has

antimicrobial properties. However, it is mostly known for its superior electrical conductivity (59.6 MS m^{-1}), second only to silver, and its high thermal conductivity ($400 \text{ W m}^{-1} \text{ K}^{-1}$). Copper not only possesses fascinating macroscopic properties. If shaped in the form of nanoparticles (NPs) - ensembles of typically ~ 10 to 10^3 atoms - it has tunable physical properties, which makes it suitable for applications that range from regenerative medicine to catalysis.⁴

Catalysis, in particular, is an important branch of (industrial) chemistry and is responsible for around 35% of the world's GDP⁵ and production of 90% of the chemicals (by volume).⁶ Copper-based catalysts (promoted via zinc oxide⁷⁻⁹) are for instance used for the production of methanol, an important building block for a vast amount of compounds such as resins, pharmaceuticals and perfumes. Hydrogen production via the water gas shift reaction (the conversion of CO and H₂O into CO₂ and H₂), is a crucial step for the production of ammonia and thus fertilizers, and is carried out on ZnO-modified Cu-Al₂O₃ catalysts.^{10,11} Cu-based catalysts are also used in pollutants control, e.g. Cu-functionalized zeolites used for the removal of toxic NO_x fumes from exhaust gas of large ships and urban incinerators via ammonia SCR (Selective Catalytic Reduction).^{12,13} Other important use of Cu-based nanoparticles can be found in electrocatalysis,^{14,15} hydrogen evolution,¹⁶⁻¹⁸ photocatalytic water splitting,^{19,20} and numerous organic couplings,²¹⁻²³ reduction²⁴⁻²⁸ and oxidation²⁹⁻³¹ reactions.

The following sections will introduce the basics of metal nanoparticle catalysis, with specific focus on particle size effects and hydrogenation reactions.

1.2 – Copper nanoparticles in catalysis

A catalyst is a “substance that increases the rate of a given reaction without undergoing changes and without modifying the stability of either reactants or products”.³² In practice, catalysts make a reaction occur faster by allowing it to run via a lower energy pathway (schematic representation in Figure 1.3), enabling the production of several products such as plastics, fuels, and pharmaceuticals. In addition, environmental catalysis contributes to a more sustainable human activity and healthier environment by lowering the impact of chemical processes, achieve carbon circularity, produce renewable fuels, and improve the sustainability of the transportation industry.³³⁻³⁶

Most catalytic processes involve metals as active sites, often a transition metals.³² These metals have partially filled d-orbitals with well-defined energy levels and that extend far and in specific directions, and hence are able to interact with the electronic orbitals of atoms and molecules. Metals used in catalysis are often noble metals, such as Pt, Pd, Rh, Ru, Ir, known for their high catalytic activity in industrially relevant reactions. However, base metals, such as Ni and Cu, are also frequently used in chemical industry, not only for their cost effectiveness, but also for their high selectivity to desired products.

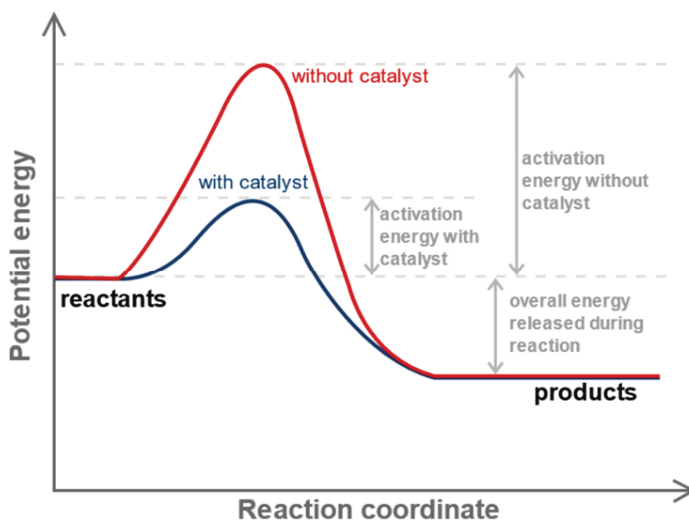


Figure 1.3 Potential energy diagram for a reaction without (red) and with (blue) catalyst. Here, the overall energy released during the reaction represents the relative stability of the products compared to the reactants, that remains unaltered upon addition of a catalyst.

Apart from the type of metal used in a given process, how the metal is placed in the final catalyst is also of great importance. Catalysts can be used in form of a single metal cation (or few, such as in multi-metallic homogeneous complexes) stabilized by ligands, with this complex dissolved in a reaction solution. This class of materials is referred to as homogeneous catalysts. Alternatively, the metal can also be present as an ensemble of atoms in a solid material (monoliths, foams, gauges, supported nanoparticles) leading to what is known as a “heterogeneous” catalyst. In this case the reaction occurs between reactants being gas, vapor, or liquid, on the surface of a solid catalytic phase. The third class of catalysts are biocatalysts, which are key to life on earth, but their industrial application is limited (e.g., enzymes). Heterogeneous catalysts are often preferred for large scale industrial applications, due to their good stability and recoverability, and relatively low cost.

Copper finds wide application in different fields of catalysis. Homogeneous Cu-based catalysts are omnipresent in organic synthesis because of their flexible oxidation state (typically ranging between Cu^0 , Cu^{I} , and Cu^{II}) and lower price than noble metals (e.g. Pt and Rh).^{37,38} Its flexible oxidation state and ability to bind heteroatoms allows Cu to assist in bond formation (and breaking), both via radical pathways and via two-electron transfer mechanisms.³⁷ This has made Cu-based complexes the catalyst of choice for reactions such as Ullmann coupling,^{37,39} Ullmann-Goldberg coupling,^{37,39} Ullmann-Hurtley condensation,^{37,39} as well as other C-C, C-heteroatom bond formation and organic oxidations.^{37,39–43}

Heterogeneous Cu-based catalysts (typically in the form of supported nanoparticles) find application in hydrogenation. Hydrogenation involves the activation of H_2 and subsequent

transfer of H to unsaturated bonds. Typical reactants are alkenes/alkynes, alkadienes, aldehydes and ketones, and even smaller molecules such as CO and CO₂.^{8,44–52} There is extensive knowledge on noble metals such as Pt and Pd and their interaction with H₂, but much less is known about solid Cu-based hydrogenation catalysts.

So called Platinum Group Metals (“PGM”) such as Ru, Rh, Pd, Os, Ir, are able to bind the H₂ molecule strongly and activate it, and hence they are excellent hydrogenation metals, at least in terms of activity. However, other transition metals outside this group also show interesting hydrogenation properties. These metals are often much less active, but more selective. To understand why and how activity depends on the nature of the metal, we must consider the interaction between the electronic states of the metal and the adsorbate, as well as the final electronic states of the adsorbed atoms (if dissociative binding occurs). Considering only the highest occupied electronic levels of the metal, adsorption, and activation of reactants (e.g., H₂) mostly involves interaction of molecular/atomic orbitals with the metal broad *s*-band (broad= extends in a broad range of energies), and the narrow *d*-band. Schematics of a typical DOS (Density Of States) for a transition metal is schematically represented in Figure 1.4A.

Interaction between the orbitals of the adsorbate atoms and the *s*-band of the metal leads to attraction and is characterized by the broadening of the adsorbate states and lowering them.⁵³ This interaction is similar for all the transition metals, especially the ones at the right part of the transition series. For this reason, it is not the interaction that typically drives differences in metal activity.^{53–56} The interaction between the *d*-band of the metal with the orbitals of the adsorbate is, on the contrary, strongly element specific. In fact, it is the one that generates bonding and antibonding states for the metal-molecule and metal-molecular fragment (e.g., atom) systems (Figure 1.4B, orbital at the top-center has antibonding character, the one at the bottom-center has bonding character). The relative filling of bonding and antibonding states, ultimately, drives the metal ability to bind the molecule and eventually activate dissociation.⁵³

According to the “*d*-band model”,⁵³ the type of interaction between molecule and the metal surface depends on two main factors. First, the characteristic of the *d*-band, which are 1) band width, 2) band filling and 3) band center (of mass) respective to the metal Fermi level (the highest energy state occupied by electrons in a material at absolute zero temperature). As *d*-band center, filling and width are all correlated, the “*d*-band model” can be rationalized and simplified by focusing on only one of the three band characteristics. Often, the one that is used is the *d*-band center, as easier to quantify and visualize.^{53,57} The second factor playing a significant role in metal surface-molecule interaction is the geometric extent of the *d*-band of the metal.

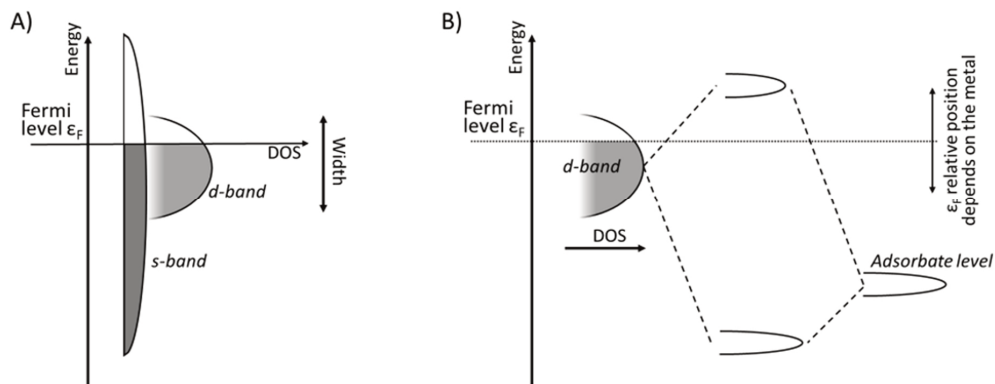


Figure 1.4 A) Illustration of the density of states (DOS) of a typical transition metal, showing the broad *s*-band and the narrow *d*-band around the Fermi level. Shaded area represents the band filling (at 0 K, there would be zero possibility to find electrons above the Fermi level). Note the partially filled *d*-band (typical of transition metals); B) Adsorbate level (orbitals) splitting due to interaction with the metal *d*-band. The position of the *d*-band relative to the Fermi level depends on the nature of the metal. For transition metals, the *d*-band is only partially filled (strictly speaking, Au, Ag, Cu are not transition metals, as the *d*-band is completely filled).

The *d*-band model suggests that when the *d*-band is broad its center is hence relatively low e.g. ~ 3 eV or more below the Fermi level energy (which by definition is within the *d*-band and at its top for d^{10} metals), not only the bonding states but also the antibonding ones can end up below Fermi level. This means that antibonding states can be populated, thus leading only to a net weak metal-adsorbate interaction. As soon as the *d*-band moves closer to the Fermi level (high-lying *d*-band), antibonding states are “pushed” upward in energy. Some of these states might hence end up above the Fermi level, and thus they will remain empty. The result is that the net metal-adsorbate interaction is stronger, and chemisorption is usually observed.^{53,57}

Figure 1.5 reports an example of such metal-adsorbate interaction between the (111) surfaces of Ni, Pt, Cu, Au, and the H atom. The shaded area represents the (occupied) density of one-electron states for atomic hydrogen chemisorbed on the four clean surfaces, while the dotted curves are the metal *d*-projected states. Peaks between -5 and -10 eV are the dominant H *1s* – metal *d*-bonding resonances, while the peaks of the corresponding antibonding states are highlighted with arrows (Figure 1.5). In all cases, the energies are relative to the Fermi energy of the metal (which is set to zero). Both Ni(111) and Pt(111) have high-lying *d*-bands (equivalently, high *d*-bands centers, specifically -1.29 and -2.25 eV respectively; band centers ϵ_d for transition metals can be found in ref.⁵³). For these two surfaces, the antibonding states (arrows) are unpopulated, hence both surfaces can strongly bind H. Cu(111) and Au(111), on the contrary, have deeper-lying *d*-bands (*d*-band centers equal to -2.67 and -3.56 eV, respectively),⁵³ which leads to more populated antibonding states, hence both surfaces are less efficient in binding H.^{53–55} In this case, however, the interaction is not completely repulsive thanks to the coupling of the H *1s* orbital with the metal *s*-band.⁵³

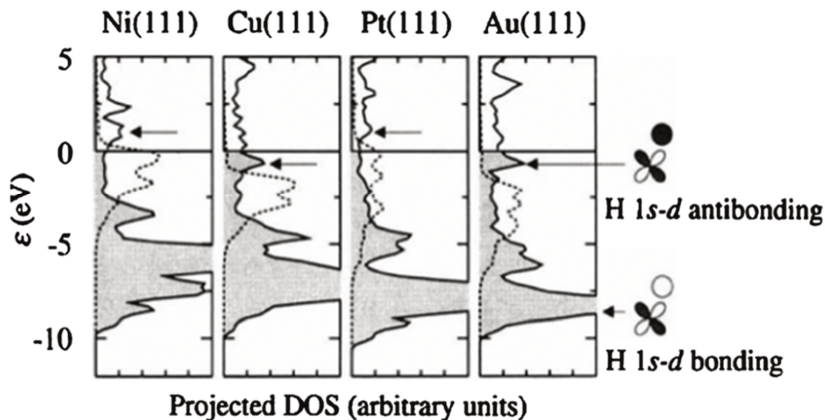


Figure 1.5: Solid lines: density of one-electron states (DOS) for H chemisorbed on Ni(111), Cu(111), Pt(111) and Au(111) surfaces. The DOS is projected onto the atomic H 1s state. Dotted lines: surface d -bands DOS of the four clean metal surfaces, for reference. Reproduced with permission from Springer Nature, ref.⁵⁴

The second factor playing a role is the spatial extension of the d -band. Cu(111) has a relatively small size of its d orbitals, with antibonding states occupied, but little Pauli repulsion. There is an optimal H-Cu(111) distance for which the net interaction is bonding.⁵³ Moving down the groups of the transition metal series, the size of the d orbitals increases ($3d < 4d < 5d$). This leads to increased Pauli repulsion, which decreasing the stability of the metal-bound molecule/atom complex.⁵³ This effect is large enough to make the Au(111)-H interaction repulsive. A very similar argument is valid for the interaction of the H_2 molecule with the metal surface. The combined effect is that H_2 is easily dissociated on Pt(111) and Ni(111), an activation energy needs to be overcome to bind H to Cu(111), and atomic H adsorption is not facilitated by Au(111).⁵⁴ This is confirmed by experimental results, as for instance Pt and Ni (111) surfaces have a low barrier and readily dissociate H_2 , while Cu has a significant barrier for H_2 dissociation, and no dissociation is observed on Au(111).^{53,54}

Following the theory and generalizing for small molecules (H_2 , N_2 , $CO\dots$), it is clear that moving to the left of the transition series (towards higher d -band centers⁵³) gives lower activation barriers and stronger bonds. Bonds are stronger for elements higher in the period table. The search for the perfect transition metal for a specific reaction involves a compromise between its ability to bind/dissociate the adsorbate, and a sufficiently weak adsorption between metal-reaction intermediate to avoid bonding irreversibly. Another important parameter to take in consideration is metal oxidizability. For instance, metals such as Mn and Fe could be poorly active in typical hydrogenation reactions also because it might actually be difficult to pass from their oxidic to the metal form under typical hydrogenation conditions in virtue of their strongly negative reduction potential. Noble metals, on the other hand, are typically in their zero-valent (metallic) state under typical reaction conditions, while Cu can

be reduced fairly easily (1bar H₂, T>100-150°C, see also **Chapter 2**). Activity of hydrogenation metals also depends on the molecule to be hydrogenated, as well as the exposed metal surface.

Focusing only on the ability to bind and activate H₂, it is clear that Cu occupies a rather unique position in the periodic table. The H₂ binding process is activated, and the adsorption strength is below that of Pd and Pt. This means that the activity of Cu can be more easily controlled e.g., by altering environmental conditions such as temperature. Additionally, the description above is based on well-defined extended metal surfaces. For nanoparticles, the picture is more complex. In general, the smaller the nanoparticle the more the energy of the electronic bands resembles the one of the single atom or hypothetical “metal molecule” (M-M). This gives narrower energy bands, and at higher energies than the one of the bulk.⁵⁸ The milder activity of Cu hence allows electronic tuning and catalyst design, for instance by nanosizing.⁵⁸

Experimental results for Cu-based catalysts for hydrogenation reactions show that the adsorption of H₂ on Cu surfaces highly depends on the facet concerned. Low index facets such as (111), (100), (110) only show physisorption of the H₂ molecule.⁵⁹ On the contrary, high index faces such as (211) and (311) can show activated hydrogen chemisorption, with a heat of adsorption of 40 kJ/mol, or -0.4 eV (Cu-H binding energy of 474 kJ/mol_{H₂}, 4.9eV)⁵⁹ and activation energy of adsorption of 21 kJ/mol (-0.2 eV).⁵⁹ For Cu, the M-H dissociation energy is around 237 kJ/mol_H (~2.5 eV), H-H bond energy is equal to 436 kJ/mol_{H₂} (or ~4.5 eV, at room temperature), similar but lower than the M-H of other well-known hydrogenation metals such as Pd (around 320 kJ/mol, 3.3 eV) and Pt (350 kJ/mol, 3.6 eV). Hence, the hydrogen coverage of Cu is generally low. In conditions in which the availability of hydrogen is the rate limiting step, this enables higher selectivity (to partially hydrogenated intermediates, e.g., as in conversion of poly- to mono-unsaturated compounds, see **Chapter 2**) than for conventional Pd and Pt catalysts.^{28,59}

In conclusion, metallic Cu represents an interesting alternative to noble metal hydrogenation catalysts, specifically when dealing with processes that requires high selectivity. More information, in particular for alkyne and alkadiene conversion to alkenes, can be found in **section 1.5** of this Chapter.

1.3 – Particle size effects

Heterogeneous catalysts require an efficient interaction between a solid and a liquid or gas, due to the bi- or three-phasic nature of the catalytic processes. To optimize the catalytic activity per gram of metal, the specific surface area has to be high, which is achieved by shaping the metal into very small particles containing tens to few thousands of atoms. In practical applications, the particle size varies between small metal clusters to particles of around one hundred nanometers in size (hence the terminology “nanoparticles”).

The fraction of the atoms that resides at the surface (also known as dispersion) scales inversely with the particle diameter, with 1 nm particles/clusters displaying almost 100% dispersion and 10 nm particles around 10% dispersion. Assuming that the intrinsic catalytic activity (i.e., the turnover frequency, TOF, defined as the ratio between $\text{mol}_{\text{converted}}/\text{mol}_{\text{metal_surf_atoms}}$ per unit time) remains constant, the weight-based catalyst activity scales with the dispersion, and hence also inversely with the particle diameter.

However, reality deviates from this model for a variety of reasons. First of all, small clusters of atoms (typically <100) display electronic quantum size effects, strongly dependent on the exact number of valence electrons present. According to the superatom model, metal clusters with a “magic number” of free (valence) electrons (2, 8, 18, 20, 34, 40, 58, 92, 138...) have a high stability due to electron shell closure, while metal clusters with a few electrons more or less are much less stable.^{60,61} Another type of effect is related to discontinuous variations in dispersion for small metal particles: metal clusters or particles that have such a number of atoms that they form closed surfaces or facets are more stable than particles with a few atoms more or less, due to the difference in average coordination number. For instance, for a dodecahedron (an increasing number of shells surrounding a central atom, with 12 coordination in the interior of the particle), this results in particles with a higher stability if they contain 13, 55, 147, 309 etc. atoms.⁶²

For larger particles, the trends as a function of size become more continuous. An effect that is specifically relevant for catalysis is the type of facets and surface sites that is exposed at the surface to the reactants. Particles smaller than 10-20 nm do not just expose facets, but also a significant fraction of kink, step and corner sites. For metals possessing fcc structure, *kink* sites have half the number of neighboring atoms (6) compared to an atom in the bulk of the crystal (12), while *terrace* can have 8 to 9 and *step* sites have 7 neighboring atoms respectively. More strongly undercoordinated sites adsorb molecules and atoms more strongly. This is due to both electronic and geometrical properties (e.g., a bulky molecule might be adsorbed more easily on a kink site rather than a terrace). This leads to a particle size effect that is generally known as “structure sensitivity” in catalysis, leading to trends in catalytic activity and selectivity as a function of particle size.^{63,64} This is illustrated for an fcc cuboctahedral particle in Figure 1.6A.

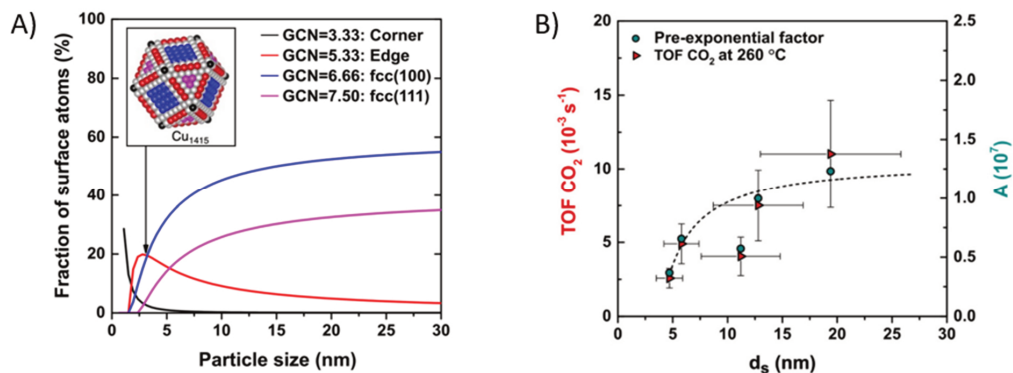


Figure 1.6 A) Fraction of surface atoms with a specific GCN (generalized coordination number)³⁶ as a function of the particle diameter for the cuboctahedral geometry. B) TOF and pre-exponential factor as a function of Cu particle size for the hydrogenation of CO₂ to methanol. Reproduced from ref.³⁶ with permission from the Royal Society of Chemistry. Licensed under: CC BY 3.0 DEED.

Increasing the particle diameter while retaining the particle geometry, changes the fraction of surface atoms. The fraction of corners atoms decreases by increasing the particle size, while terrace sites increase for particles up to 10 nm, flattening out at above 30 nm. As facets and sites have different activities, the average TOF depends on the particle diameter. In the example depicted in Figure 1.6A, reactions that would occur preferentially on edge sites benefit of particles of around 3 nm, while both smaller and bigger diameters would lead to a lower TOF. Highly undercoordinated sites, such as steps, kinks, and corners, usually bind molecules more strongly than flat and dense terrace sites (e.g., fcc(111)). Hence, small molecules such as CO, N₂, O₂ and NO are usually activated on step sites, such as the edges of (111) terraces of metal crystals.⁶⁵

Step-edge sites seems crucial in almost every reaction involving a dissociative adsorption step, with cleavage of a π -bond of a diatomic molecule.^{53,65–67} Removing an atom present in the row of a step site leads to the formation of a kink. Surfaces with a high fraction of these (highly unsaturated) kink sites can show high selectivity towards cleavage/activation of σ type bonds, such as C-C bonds (i.e., kink sites cause hydrogenolysis rather than for isomerization).^{65,68} Also hydrogenation processes for which H₂ dissociation is rate limiting, are expected to benefit of the presence of kink sites. In this case, dissociating/activating the H-H bond requires effective interaction with a σ type of molecular bond. The rate of structure sensitive reactions hence depends on the nanoparticle diameter distribution (and possibly different relative abundance of catalytic sites). Notable examples of structure sensitive reactions are Co and Fe-catalyzed Fisher-Tropsch synthesis,^{69–71} numerous Pt and Pd-catalyzed hydrogenations and oxidations,^{65,72–78} methanation over Ru and Ni,^{79–81} as well as numerous electrocatalytic processes.^{14,65,82–86}

Copper nanoparticles, which recently gained much attention as catalysts for hydrogenation reactions, also show particle size effects.^{7,26,27,36} Recent work on Cu and Cu/Zn on SiO₂ catalysts for methanol synthesis from synthesis gas (CO/H₂, usually with addition of CO₂)⁷

suggests that the surface-dependent activity of sub-10 nm copper is due to geometric rather than electronic effects. The authors observed a three-fold increase in TOF by going from particles of 2 to 8 nm, regardless of the presence of ZnO_x as promoter.⁷ In the hydrogenation of ethyl acetate to ethanol²⁷ for Cu/C catalysts a similar size-dependence of the activity was reported with a 4-fold increase in TOF when going from 3 to 10 nm particles. In both cases the authors ascribed the observed effect to the fraction of different surface sites responsible for H₂ activation as well as ethyl acetate uptake. This is consistent with the observation that particles with a size above 2-3 nm usually have size-insensitive local density of state of surface sites,^{65,87} hence electronic effects are unlikely.

Also, Cu-catalyzed methanol synthesis by CO₂ hydrogenation is structure sensitive: small nanoparticles displayed a lower activity, but higher methanol selectivity (the side product being CO);³⁶ see Figure 1.6B. The turnover frequency for the methanol synthesis increased around 3-fold by moving from 5 to 13 nm Cu nanoparticles, while the apparent activation energy for MeOH formation was size-independent, hence it is the density of active sites rather than their nature that changes. DFT calculations indicated that formate (main intermediate of the reaction) has lowest formation energy on low density Cu(211) and Cu(110) (step/edge sites), which abundance is expected to be higher for particles above 10 nm.³⁶

In this thesis we report on particle size effects for Cu nanoparticles in the case of selective hydrogenation of 1,3-butadiene. An in-depth discussion of the impact of particle size on the activity and selectivity of silica supported Cu catalysts can be found in **Chapter 3**.

1.4 – Copper nanoparticles preparation and control over particle size

Conventional methods to prepare supported Cu nanoparticles (and other metal nanoparticles) include incipient wetness impregnation and drying, precipitation methods (deposition-precipitation and co-precipitation), ion adsorption and colloidal synthesis.^{58,88} Each route has its specific advantages and disadvantages. The different steps in the synthesis can greatly affect the catalyst final structure and hence performance. Control over the particle size can almost always be achieved, but the methodology needs to be adjusted to the type of metal and precursor, and reported methods include a fair dose of trial-and-error.

In **precipitation**, a metal precursor is precipitated from a liquid phase solution in the form of a low-solubility compound (often, but not exclusively, a metal oxide or hydroxide). The most used methods involve a gradual increase in the pH of the solution, the direct reduction of the metal precursor, or removal of ligands from metal complexes. The method requires control over nucleation and growth. When a support material is present, nucleation is favored on the surface of the solid due to lowering of the surface free energy of the precipitate. In this case the method is referred to as **(homogeneous) deposition-precipitation, (H)DP**, and it can be used for the preparation of high metal loading catalysts (>20%).⁸⁸

Another precipitation-based method is **coprecipitation**. The method involves simultaneous precipitation of both the metal and the support. Compared to (H)DP, it has the major advantage of achieving even higher metal loadings (60-80%). For this reason, a large number of commercial catalysts, such as for methanol production, steam reforming, water gas shift reaction, hydrogenation, and hydrocarbon oxidation are produced in this way.⁸⁸⁻⁹⁰

Academic literature on Cu precipitation mainly involves two supports: TiO₂ and SiO₂. DP-prepared Cu-TiO₂ is usually obtained by urea-mediated (CO(NH₂)₂) precipitation of copper nitrate (Cu(NO₃)₂) on suspended titania.^{52,91} The reaction is carried out in double-walled vessels and has duration of several hours (typically 24 h). The reaction mixture is heated to 80 °C, causing decomposition of the urea into NH₃, which increases the pH of the solution causing precipitation of typically copper hydroxide. Reduction of the precipitated copper species at temperatures around 250 °C in H₂- or CO- rich atmosphere yields to Cu metal nanoparticles. Delannoy *et al.* demonstrated that a method to vary the metal particle size is to change the weight loading of Cu. For instance, 1, 2 and 4 wt% loadings yield 0.6, 4.5 and 8.5 nm Cu particles upon reduction.^{52,91}

SiO₂-based supports dissolve at high pH and can react with Cu. High weight loadings (>30%) of uniformly distributed Cu particles are achieved by reduction of Cu phyllosilicate. This compound is obtained by precipitation/recrystallization of Cu nitrate onto suspended silica via hydrolysis of urea at 90 °C.⁹²⁻⁹⁴ The clay-like material is then reduced at 250 °C under N₂/H₂ in order to yield a Cu/SiO₂ catalyst. Particle size control can be achieved by choosing a specific heating ramp as well as reductant type (most often H₂ and CO) and concentration. For example, particles of 12, 17 and 24 nm were obtained with a heating ramp of 2 °C min⁻¹ in 10, 20 and 50 % H₂ gas, respectively.⁹² Smaller particles (8 nm) were obtained with faster heating (5 °C min⁻¹)⁹² or by reducing the weight loading of Cu (5 to 2 nm with weight loadings of 18% and 5%, respectively).⁹⁵

Electrostatic (or ion-) adsorption of metal ions from solution onto support materials is another well-known synthesis route for metal-based catalysts. The technique relies on the interaction between charged surface groups of the support and oppositely charged metal cations or metal complexes. Control over the charged of the surface groups is obtained by tuning the pH of the solution with respect to the point-of-zero-charge of the support. The metal loading is limited by the density of charged surface groups on the support. The technique yields low weight loadings of highly dispersed precious metals, but it's impractical for the preparation of low-activity metals that require high metal loadings. Examples of application of the technique are the preparation of single-atom catalysts⁹⁶ (which however applications are limited mostly to research) ion-exchanged zeolites.^{12,97,98}

Colloidal synthesis offers control over the metal particle size and shape. The colloids are prepared by nucleation and particle growth from a precursor solution, with reduction of the metal cations being achieved via addition of reducing agents,⁸⁸ while stabilizing agents (such as PVA or PVP) are present to regulate nanoparticles growth. Particle sizes can be tuned by controlling the nucleation rate and growth rates.⁸⁸ Complete removal of the ligands, as well

as the low stability of ligand free particles, potential organic waste generated, and low concentration (needed for synthesizing stable colloids) makes their large-scale implementation challenging. At this time, there is only one successful example of industrial manufacturing of colloidal (Pd, Pt) based catalyst.⁹⁹ Regarding Cu, usage of colloids in catalysis is very uncommon due to their low stability in solution. However, successful preparation of Cu colloidal suspensions was recently reported.^{100–104}

Incipient wetness impregnation (IWI) and drying is a synthesis technique involving filling the pores of a support (90 to 100% of the pore volume) with a metal precursor solution, followed by heat- or vacuum-assisted removal of the solvent. Ideally, this yields homogeneously distributed solid metal precursor inside the porous structure. The metal precursor is then decomposed at elevated temperatures, yielding metal or metal oxide nanoparticles. The choice of the metal precursor is of foremost importance since it must decompose under relatively mild conditions and yield only gaseous by-products (preferably non-hazardous and non-flammable gases and vapors) and the target solid metal or metal oxide. Strong interaction between the metal precursor and support limits metal redistribution during the heating step, giving additional control on the particle size distribution. A final treatment such as reduction or sulfidation can be applied, depending on the desired phase for catalysis.

Impregnation is widely applied for preparing Cu-based catalyst with high Cu loadings on supports such as Al₂O₃, SiO₂, CeO₂ and TiO₂.^{88,90} Due to the nature of the method, the support needs to be moderately porous (>0.10 ml g⁻¹) in order to achieve medium weight loadings and homogeneous distribution of the metal in the final solid. The most common precursor is Cu(NO₃)₂, which has a high solubility in water (3 g mL⁻¹) and a low decomposition temperature (<300 °C). In the past decade, several methods to control Cu particle size have been explored in our group. On carbon, a good strategy is to start from smaller Cu particles and thermally sinter them. For instance, for 6.3 wt% Cu/OxGNP (surface-oxidized graphitic nanoplatelets) first copper nitrate was decomposed under N₂, to yield to 3 nm CuO particles, followed by thermal sintering under H₂. Cu particles between 3 and 7 nm were obtained by varying the sintering temperature between 250 and 400 °C.⁹² By combining different thermal sintering methods, carbon modification, and modulation of the weight loading (6 to 12 wt%) the particle size range was extended from basically single Cu species⁴⁵ up to 14 nm²⁷ or even 23 nm⁴⁵. The thermal sintering method can however be applied only when the particles weakly bind to the surface of the support.

For SiO₂, particle size control can be obtained by using supports having different pore sizes. A similar method was used for preparing Cu₂O particles for electrocatalytic H₂ generation.¹⁰⁵ E.g. silica gels with pores of 3, 6, 15 and 23 nm were impregnated with 18.7 Cu wt% *ex* Cu(NO₃)₂ and decomposed under 2% NO/N₂ atmosphere, yielding 4, 6, 7 and 10 nm CuO particles.¹⁰⁵ Also the gas atmosphere during the heat treatments influenced the Cu nanoparticles sizes; Cu particles of 2-4 nm were obtained on both SiO₂ gel and mesocellular SiO₂ foam via decomposition under N₂^{8,92,106} or H₂-N₂^{92,107}. To the best of our knowledge,

there are no systematic studies on the effect of the synthesis conditions on IWI-prepared Cu nanoparticles supported onto other metal oxides, such as Al₂O₃, TiO₂ and CeO₂.

In our work, we focused mainly on incipient wetness impregnation as technique for the preparation of Cu nanoparticles. Control on the Cu particle size (in the range 2-10 nm) was achieved by tuning the Cu weight loading, the temperature of the nitrate decomposition step as well as the gas atmosphere used for the decomposition of the Cu nanoparticles.

1.5 – Selective hydrogenation of 1,3-butadiene

Hydrogenation reactions play a crucial role in fine and bulk chemicals production. Many processes are based on the addition of hydrogen to an unsaturated carbon-carbon bond, often using a supported catalyst. Examples include the hydrogenation of polyunsaturated hydrocarbons to mono-olefins,²⁸ hardening of vegetable oils,¹⁰⁸ and selective hydrogenation of various organic compounds such as vitamin intermediates,^{109,110} pharmaceutical and agrochemical active ingredients.^{109,111}

The H₂ molecule is rather inert due to its high binding energy of 4.52 eV (~450 kJ mol⁻¹). A catalyst (most often a transition metal) is hence required to bind and activate the molecule. This can occur in different ways: the adsorption of H₂ on the surface of the catalyst can lead to homolytic cleavage of the bond (2 H·, typical of metal surfaces), heterolytic cleavage (H⁺ and H⁻, in case of highly polarized single cation catalysts) or the bond can be just weakened, instead of broken, via partial occupation of the antibonding σ orbitals of the H–H adsorbed molecule (see **section 1.2**). Transition metals such as Ni, Pd, Pt, Rh, are extensively used in both homogeneously and heterogeneously catalyzed hydrogenation. Examples are the Wilkinson catalyst ([RhCl(PPh₃)₃]) used for the hydrogenation of unsaturated hydrocarbons,^{112,113} Raney nickel (porous Ni) for the hydrogenation of aromatic and nitro compounds,^{114,115} and palladium on carbon using in organic synthesis.^{116–119}

Heterogeneously catalyzed hydrogenation is also extensively used in industry for the removal of impurities from crude streams.^{120–125} An example is the removal of highly unsaturated molecules from olefin streams. Polyunsaturated compounds, such as dienes and alkynes, are present in the product stream from steam-cracking of naphtha to olefins (e.g., 1,3-butadiene, up to 1-5 wt.% in C₂–C₄ steam cracking mixtures¹²⁶). The products are light alkenes (typically C₂ to C₄) used in subsequent reactions such as polymerization and selective oxidation to form polyethylene, polypropylene, epoxides, methanol, ethanol, as well as detergents and fuels. In almost all cases, the presence of polyunsaturated compounds is highly undesirable, as they interfere with subsequent processing due to their ready oxidation, oligomerization, or their ability to poison various metal-based catalysts.^{28,127,128} Consequently, their concentration should be reduced to below tens of ppms, ideally by reducing them to useful alkenes, which are already present in large excess, without (further) hydrogenating the alkenes to alkanes.^{28,127,129}

This challenge is commonly addressed by palladium-based hydrogenation catalysts.^{130–135} Pure Pd has a high hydrogenation activity, but a poor selectivity at high alkyne/alkadiene conversions. Therefore, the metal is often diluted or partially deactivated with appropriate modifiers, in catalysts such as PdAg/Al₂O₃, PdS/CaCO₃ and PdPb/CaCO₃.^{130,131,133} However, restructuring and metal segregation (e.g., when a large excess of diluting metal is present¹³⁶ or after oxidative regeneration of the catalyst¹³⁷) can decrease the selectivity and stability by allowing side reactions such as isomerization, polymerization as well as over-hydrogenation.^{51,136} Little is known about reaction mechanism and catalyst stability and selectivity for non-noble metal catalysts such as Cu.¹³⁸ Before discussing this catalysts further, it is worth reviewing the properties and reactivity of 1,3-butadiene.

1,3-butadiene is the smallest possible conjugated diene. The molecule is essentially flat, with all 4 carbons being sp²-hybridized and hence sharing a conjugated π system. The molecule is typically adsorbed in a di- π structure, with the plane of the molecule parallel to the metal surface.²⁸ The reaction has been examined in detail over supported metal nanoparticles, in particular using Ni,^{139–141} Pd,^{142–147} and Au.^{52,134,148,149} Important information regarding the reaction mechanism was obtained by experiments in hydrogen/deuterium mixtures under mild conditions (<1 bar, <100 °C).^{28,141,147} D exchange was limited, and little HD was formed, suggesting a low coverage of H species on the surface of the metals. A maximum number of two deuterium atoms in each butene molecule (whether 1-butene, trans-2-butene, or cis-2-butene) showed that isomerization did not occur at a significant rate, as this would involve the cleavage of C-H bonds and formation of new C-H/D ones (possibly increasing the deuterium content of the molecule produced by the isomerization step). The formation of any of the olefins thus follows a 1,2- or 1,4- addition.^{28,141,147} Over hydrogenation can occur both via hydrogenation of the produced alkenes or via 2,3-addition, since the intermediate product (*CH₂CH₂CH₂CH₂*) is unstable and readily reacts with another two H atoms.

The negligible isomerization rate of butenes on different metals (at low diene conversion levels) simplifies the study of the reaction mechanism, in particular regarding structural and electronic effects on the possible modes of coordination of the semi-hydrogenated intermediates (reaction mechanism reported in Figure 1.7). Metals such as Cu, Ni, Pd, Pt, Ag give a high selectivity to 1-butene (50–75%) with trans-2-butene as the second product and with a cis-2-butene concentration either equal or slightly lower than trans-2-butene (Au is an exception, as it can give a larger selectivity towards cis-2-butene than trans-2-butene).^{28,148} Metals and metal sulphides such as Rh, Ir, Ti, V, Zr, Nb, Ni(S), Pd(S), Co(S), Fe(S) seem to increase the yield in trans-2-butene at the expense of 1-butene.^{28,150} This observation led to the conclusion that metals that are stronger electron-acceptors favor the adsorption of the mono-olefins in $\pi\sigma$ mode (π -butenyl, Figure 1.7), which leads to the rearrangement of the double bond between C2 and C3, yielding trans-2-butene. On the contrary, metals and metal particles that are weaker electron acceptors tend to stabilize the σ -coordinated intermediate (σ -butenyl) leading to the formation of a terminal double bond (1-butene).

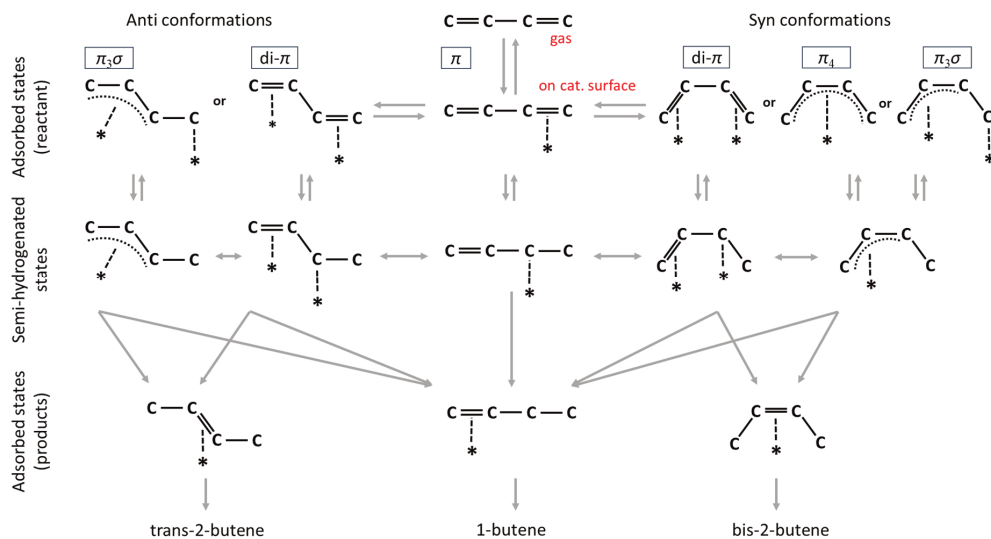


Figure 1.7 Mechanistic scheme for the hydrogenation of 1,3-butadiene.²⁸ Adsorbed state of 1,3-butadiene explicitly indicated in the first row. The way the reaction proceeds (the structure of the half-hydrogenated state, central row) depends on the structure of 1,3-butadiene once adsorbed on the surface of the metal.

Cu has been reported as a reasonably active catalyst for the selective hydrogenation of alkynes and alkydienes since the 1970's. The reactants investigated include propyne,¹⁵¹ 1,3-butadiene,^{46,152} 1-butyne¹⁵³ and 1-butene-3-yne.¹⁵³ The catalysts were prepared by reduction of precipitated Cu species¹⁵³ or Cu²⁺ ions adsorbed onto silica.^{154,155} Cu was 3 to 4 orders of magnitude in terms of 1,3-butadiene turnover frequency less active than Pd-based catalysts,^{111,156} but particularly selective (selectivity to butenes usually above >90% up to 90% conversion).¹⁵¹⁻¹⁵³ Unfortunately, the stability of the investigated catalysts was generally poor, due to oligomer formation, often referred to as “green oil formation”, which limited further interest in this type of catalysts.^{52,151,157}

Renewed interest in Cu as a selective hydrogenation catalyst was spurred by a paper from Studt *et al.*¹⁵⁸, who computationally predicted that not only Pd-alloys, but also base metals and related alloys such as NiZn, FeZn, monometallic Ni and Cu were good catalysts.¹⁵⁸ Recent experimental developments on Cu-based catalysts were reported by the group of Louis *et al.*¹⁵⁷ In particular, the authors showed that the addition of Zn species to TiO₂-supported Cu catalysts helped to stabilize the catalytic performance. The monometallic copper lost more than 90% activity within 4 h on stream, while for the Cu₃Zn₁ sample the decrease in activity was ~30% during 20 h on stream. Partial alloying of Zn with Cu and passivation of TiO₂ surface Lewis acid sites by Zn species might play an important role in stabilizing the samples.¹⁵⁷

Insight regarding the support effect on catalyst stability was recently reported by Masoud *et al.* for Au-based catalysts.¹⁴⁸ SiO₂-supported Au nanoparticles demonstrated much more

stable catalytic performance than TiO₂-supported ones (10% loss of the initial activity for Au/SiO₂ after 5 days on stream at 200 °C, while Au/TiO₂ loses 90% of its initial activity after 15 h on stream, same conditions). The steady loss in activity in the case of Au/TiO₂ was due to green oil formation on the TiO₂ support surface, which gradually also covered the active metal surface. Full recovery of the initial catalyst activity was obtained by heating in air.¹⁴⁸

More details regarding the use of Cu and Cu based catalysts for the selective hydrogenation 1,3-butadiene investigated in the context of this thesis are reported in **Chapter 2, 3 and 4**.

1.6 – Selective hydrogenation of 2-methyl-3-butyn-2-ol

Selective carbon-carbon triple bond hydrogenation of alkynols to alkenols is important for the production of fine chemicals. The reaction is widely used for the manufacture of fragrances, agrochemicals, biologically active compounds, pharmaceuticals and fat-soluble vitamins.^{110,159–161} Alkenols contain both a carbon-carbon double bond and a C–OH unit. They are extensively used as nucleophiles in C–C couplings with carbonyl electrophiles. For example, *cis*-2-butene-1,4-diol is an intermediate in the syntheses of vitamin A and vitamin B6 and is also used as a monomer to generate poly(2-butenediol), an unsaturated telechelic polyether diol.^{162–164} Another important example is the hydrogenation of dehydroisophytol to isophytol, an intermediate step in the production of α -tocopherol, one of the components with the highest vitamin E activity.^{110,165} An example of reaction scheme for the synthesis of α -tocopherol, is reported in Figure 1.8. Two important selective hydrogenation steps are involved in the process: the hydrogenation of 2-methyl-3-butyn-2-ol to 2-methyl-3-buten-2-ol, and the hydrogenation of dehydroisophytol to isophytol.¹¹⁰

The selective hydrogenation of alkynols to alkenols poses challenges, since hydrogenation of acetylenes moieties with a metal catalyst can result in the formation of fully saturated C–C bonds. This unselective process is kinetically favoured if the second hydrogenation step (alkene to alkane) is faster than the first (alkyne to alkene).¹¹⁰ The selectivity of the catalyst is enhanced by adding selective catalyst poisons.¹¹⁰ Catalysts used for this type of reaction are noble metals (Pt, Pd, Rh) or other transition metals (mostly Ni), and the process is usually carried out in a three-phase, slurry type semibatch reactor. One of the most used catalyst for this transformation is Pd in the form of Lindlar-type catalysts.^{162–164,166} These consist of Pd nanoparticles supported on CaCO₃, with 5% Pd weight loading and 2-5% Pb loading, depending on the application.^{110,167,168} These catalysts showed high selectivities (>95%) and activities of substrate conversion in hydrogenation of alkynols.⁹⁹ However, the use of environmentally unfriendly modifiers such as lead acetate and quinoline, which eventually contaminate target products, is not desirable.^{110,167,168}

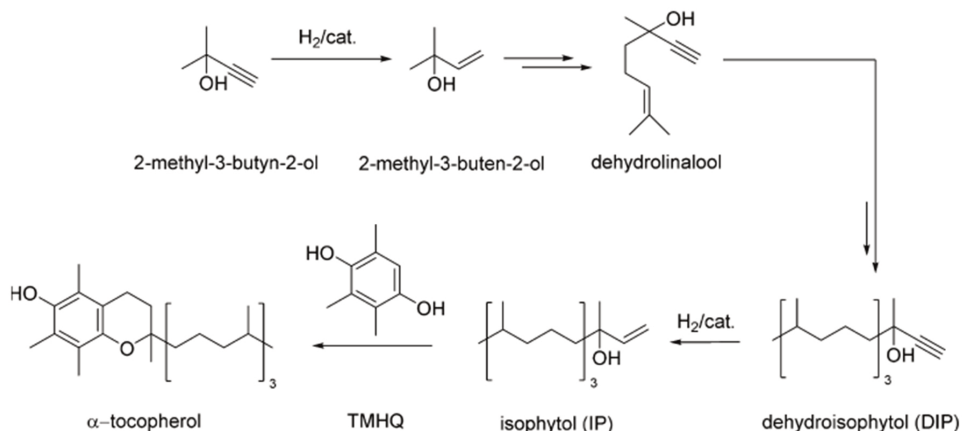


Figure 1.8 Simplified reaction scheme of the synthesis of α -tocopherol, a component with the highest vitamin E activity (Vitamin E is a group of 8 fat-soluble vitamins, all with antioxidant properties). Reprinted (adapted) with permission from ref.¹⁶⁵. Copyright 2017 American Chemical Society.

As discussed in section 1.2, Cu represents a viable alternative to Pd-based catalysts for the gas phase hydrogenation of alkadienes and alkynes. However, few studies addressed supported Cu catalysts for liquid phase hydrogenation. Copper chromite ($\text{Cu}_2\text{Cr}_2\text{O}_5$) was studied for the hydrogenation of vegetable oils.^{169–173} The major drawback of copper chromite catalysts is the high toxicity of certain Cr compounds.^{174,175} Only during the last decade supported Cu nanoparticles gained attention as potential catalyst for the selective hydrogenation of organic compounds in liquid phase. Villaverde *et al.*¹⁷⁴ reported that Cu/ SiO_2 prepared via deposition precipitation has a similar activity as Cu-Cr (TOF: 0.55 vs. 1.33 min^{-1} , respectively) in the selective hydrogenation of furfural to furfuryl alcohol. Modifications of the catalyst, such as preparation of co-precipitated CuMgAl, can lead to even higher activity, around twice that of the reference Cu-Cr catalyst.¹⁷⁴

Cu/ SiO_2 was also studied for the hydrogenation of acetophenone to 1-phenylethanol, an important pharmaceutical intermediate. The authors observed close to 100% product yield, so no hydrogenolysis or cracking leading to side products. The reaction displayed a negative order in acetophenone, first order in hydrogen and typical Langmuir-Hinshelwood reaction kinetics. Another important well-known reaction used to study selective hydrogenation catalysts is the hydrogenation of cinnamaldehyde to cinnamyl alcohol. Gutierrez *et al.* prepared a series of Cu catalyst (supported onto Al_2O_3 , SiO_2 , MCM-48, CeO_3 , Fe_2O_3) and tested for the hydrogenation of cinnamaldehyde in isopropyl alcohol at 100 °C and 10 bar. The highest selectivity was observed for Cu/ SiO_2 (48% at 30% conversion).⁴⁸ Liu *et al.* reported a higher selectivity to cinnamyl alcohol of 80% at around 50% conversion of cinnamaldehyde for 6 nm Cu supported on ordered mesoporous carbon. Clearly, the choice of a suitable preparation method, support and reaction conditions is very important.

In our study, we explored Cu/SiO₂ catalysts for the selective hydrogenation of 2-methyl-3-butyn-2-ol, an important intermediate in the production of fat-soluble vitamins and fragrances.¹¹⁰ Results and discussion can be found in **Chapter 5**.

1.7 – Scope of this thesis

The main aim of the research described in this thesis was to study the activity, stability and selectivity of supported Cu catalysts for industrially relevant gas- and liquid- phase selective hydrogenation reactions. Focus was on the reaction mechanism, selectivity mechanism, as well as on the influence of Cu particle size. Synthesis method development was crucial to tune the Cu nanoparticle size on silica. Transmission electron microscopy, X-ray powder diffraction, thermogravimetric analysis, temperature programmed reduction, were applied in order to elucidate the collective structure-performance relationships in the gas phase hydrogenation of 1,3-butadiene in excess of propene and in the liquid phase hydrogenation of 2-methyl-3-butyn-2-ol.

2 Hydrogenation of 1,3-butadiene on Cu nanoparticles immobilized on inert supports: catalyst stability and selectivity

Abstract

In this chapter, the catalytic performance of copper nanoparticles (3 and 7 nm) supported on either silica gel or graphitic carbon is discussed in the selective hydrogenation of 1,3-butadiene in the presence of a 100-fold excess of propene. We demonstrate that the routinely used temperature ramp-up method is not suitable in this case to reliably measure catalyst activity, and we present an alternative measurement method. The catalysts exhibited selectivity to butenes as high as 99% at nearly complete 1,3-butadiene conversion (95%). Kinetic analysis showed that the high selectivity can be explained by considering H₂ activation as the rate limiting step, and the occurrence of a strong adsorption of 1,3-butadiene with respect to mono-olefins on the Cu surface. The 7 nm Cu nanoparticles on SiO₂ displayed high stability, with almost full retention of their initial activity over 60 h of time-on-stream at 140 °C. This remarkable long-term stability and high selectivity towards alkenes indicate that Cu nanoparticles are a promising alternative to replace precious metal-based catalysts in selective hydrogenation.

Chapter based on: Totarella, G., Beerthuis, R., Masoud, N., Louis, C., Delannoy, L., & De Jongh, P. E. (2020). Supported Cu Nanoparticles as Selective and Stable Catalysts for the Gas Phase Hydrogenation of 1, 3-Butadiene in Alkene-Rich Feeds. *The Journal of Physical Chemistry C*, 125(1), 366-375. First authors Giorgio Totarella and Rolf Beerthuis contributed equally.

2.1 – Introduction

Hydrogenation reactions play an important role in fine and bulk chemicals production. Notable processes that are based on the catalytic addition of molecular hydrogen to an unsaturated carbon-carbon bond are the hydrogenation of polyunsaturated hydrocarbons to olefins,²⁸ hardening of vegetable oils,¹⁰⁸ and selective hydrogenation of various organic compounds such as vitamin intermediates,^{109,110} pharmaceutical and agrochemical active ingredients.^{109,111} The selective removal of polyunsaturated hydrocarbons, for example 1,3-butadiene, from monounsaturated hydrocarbons via hydrogenation is an essential alkenes purification step. In particular, removal of alkadienes and alkynes is necessary to guarantee good process ability of light olefins for the production of polymer- and alkene-derived intermediates.^{28,52,135,142,153,126–128,130–134} At the same time, the reaction is interesting for fundamental hydrogenation studies. The physicochemical property and type of metal catalyst used for the reaction can, in fact, have a significant effect on observed hydrogenation rate, distribution of isomers, polyunsaturated to monounsaturated hydrogenation ratio and over-hydrogenation behavior (hence hydrogenation selectivity).

Cu-based catalysts have already been reported as moderately active in the hydrogenation of different unsaturated hydrocarbons, such as propyne,¹⁵¹ butadiene,^{46,152} 1-butyne¹⁵³ and 1-butene-3-yne.¹⁵³ Although Cu catalysts displayed activities around 4 orders of magnitude lower than the one of Pd-based materials (the catalysts of choice for hydrogenation reactions), they presented much desirable selectivities (>>90%) as over-hydrogenation was very limited.^{111,151–153,156} However, the Cu-based catalysts can generally be rather unstable, and deactivate in few hours of testing due to production of oligomers (often referred to as “green oils”). This limited applications and further interest in this type of catalysts.^{52,151,157}

Only recently, investigation on Cu-based materials regain the deserved attention, also thanks to computational studies confirming Cu as one of the ideal candidates for selective hydrogenations of hydrocarbons (Studt *et al.*¹⁵⁸). Concerning the selective conversion of 1,3-butadiene to butenes, an important experimental milestone was achieved by Louis *et al.*¹⁵⁷ In particular, the authors showed that the addition of Zn species to TiO₂-supported Cu nanoparticles helped to stabilize the catalytic performance of the catalyst, guaranteeing retention of ~70% of the initial activity during 20h on stream (contrary to pure Cu that suffered almost complete activity loss under 4h).¹⁵⁷ The behavior of Cu nanoparticles, however, can't be untangled completely from the support and Zn promoter, as TiO₂ can potentially boost hydrogenation activity and Zn is needed to suppress side reactions on the defective TiO₂ surface.^{148,157}

In this chapter, we discuss the selective hydrogenation of 1,3-butadiene in 100-fold excess of propene using supported Cu nanoparticles. We specifically focused on monometallic Cu supported on silica and graphitic carbon. These supports were chosen based on their relative inertness towards oligomer formation (fouling), as well as towards the main and side reactions. This guarantees that the behavior of the nanosized Cu can be isolated from the one of the supports. In addition, the samples were prepared by incipient wetness

impregnation,^{90,106} which we show being a robust synthesis methodology for the production of well-defined Cu particles distributions.

The Cu samples were fully characterized and tested in continuous flow reaction conditions.^{148,149} We investigated in detail both the catalysts selectivity and stability. Attention was also paid to the catalytic testing methodology, which was shown to be of paramount importance to obtain reliable results for copper-based hydrogenation catalysts.

2.2 – Experimental section

Materials. The following chemicals were used without any further purification: silica gel high purity grade (Davisil Grade 645, $\geq 99\%$ purity, Sigma Aldrich), average pore size 150 Å, BET surface area 300 m² g⁻¹, 60-100 mesh; turbostratic graphitic support (high surface area graphitic carbon, HSAG-500, kindly provided by Timcal Ltd.), average pore size 250 Å, BET surface area 500 m² g⁻¹, <100 mesh; Copper(II) nitrate trihydrate, 99% (for analysis, ACROS Organics™); Nitric acid 65%, AnalaR NORMAPUR® analytical reagent. MilliQ water was used for the preparation of all the impregnating solutions (Direct-Q® 3 UV, water resistivity of 18.2 MΩ.cm at 25°C). The gases used during the catalyst preparation and testing were purchased from Air Liquide Benelux Industry: Propylene 3.5 (99.95% purity), 1,3-butadiene 2.5 (99.5% purity), Hydrogen 5.0 (99.9990% purity), Helium 5.0 (99.9990% purity), Nitrogen 5.0 (99.9990% purity) and 10% NO/Ar (99.90% purity).

Functionalization of the carbon support. The pristine carbon support (HSAG-500, high surface area turbostratic graphitic carbon, average pore size 250 Å, BET surface area 500 m² g⁻¹; kindly provided by Timcal Ltd) was surface functionalized by liquid-phase oxidation using concentrated nitric acid.¹²⁵ Herein, ~10 gram of the pristine carbon material was suspended in HNO₃ (aq) (65%; 40 mL g⁻¹), inside a 1 L round-bottom flask fitted with a reflux condenser. The pristine graphite material was heated to 80 °C in approximately 25 min, and kept at 80 °C for 110 min. Thereafter, the reaction was quenched by diluting the suspensions with ~1.6 L of cold deionized water (25 °C). The surface-oxidized carbon was allowed to sediment for 30 min and the supernatants were decanted. The solids were washed with deionized water until a pH of around 7 was reached. After the final washing step, the carbons were dried overnight at 120 °C and crushed into powders. Finally, the carbon support was dried for 90 min at 170 °C, under dynamic vacuum, to remove traces of adsorbed water, and kept inside an Ar-filled glovebox (Mbraun LABmaster; <1 ppm H₂O; <1 ppm O₂).

Synthesis of Cu/SiO₂. Cu nanoparticles on silica gel were prepared via adaptation of the impregnation and drying method reported elsewhere for SiO₂-based supports.^{105,106} In particular, the impregnation solution concentration and the thermal treatment conditions were adjusted in order to obtain particles of ~3 and ~7 nm (final Cu weight loading equal to 5.7 wt.%). Around 2 g of bare support (Davisil Grade 645, $\geq 99\%$ purity, average pore size 150 Å, BET surface area 300 m² g⁻¹; Sigma Aldrich) were dried at 230 °C for 2 h in a double-neck

round-bottom flask. The material was then impregnated under static vacuum with dropwise addition of a 1 M $\text{Cu}(\text{NO}_3)_2$ solution acidified to pH ~ 1 with HNO_3 to incipient wetness (the volume of the solution used was equal to 90% of the total pore volume of the support). The impregnated solid was then transferred in a 4A zeolite-filled desiccator and kept there for 2 days. Subsequently, it was further dried under dynamic vacuum at room temperature for 5 days and then transferred to a tubular plug flow reactor for the final thermal decomposition treatment.

Nanosized Cu^0 particles of 3 nm (sample 3nm_Cu/SiO₂) were obtained by heating the solid to 250 °C under 20% H_2/N_2 . The sample was left to cool down to room temperature, purged with 20 vol% O_2/N_2 flow (100 mL min^{-1} g^{-1}) and heated up to 250 °C in the same gas mixture (heating ramp of 2 °C min^{-1} , isothermal hold of 2 h, 100 mL min^{-1} gas flow for each gram of dry material). It was found that particles cannot be grown larger on silica gel by simply increasing the reduction or the nitrate decomposition temperature. Larger crystallites were thus prepared by using 2% NO/N_2 as gaseous atmosphere during the copper nitrate decomposition step, as previously described by Munnik *et al.*¹⁰⁶ In particular, particles of around 7 nm (sample 7nm_Cu/SiO₂) were obtained by performing the thermal treatment at 350 °C under 2% NO/N_2 (heating ramp of 2 °C min^{-1} , isothermal hold of 2 h, 300 mL min^{-1} gas flow for each gram of dry material). The samples (supported CuO) were exposed to air and stored in closed vials at room temperature.

Synthesis of Cu/C. Cu/C catalysts were prepared with a similar impregnation and drying method.^{27,125} As for Cu/SiO₂, the synthesis parameters were chosen to obtain particles of ~ 3 and ~ 7 nm and guarantee homogeneous distribution of the Cu NPs over the surface of the support. For the preparation, around 2 g of dry oxidized carbon were impregnated by dropwise addition of a 2M $\text{Cu}(\text{NO}_3)_2$ solution acidified to pH ~ 1 with HNO_3 to incipient wetness (the volume of the solution used was equal to 90% of the total pore volume of the support; resulting Cu weight loading equal to 6.3 wt.%). The dried impregnate was heated to 230 °C (0.5 °C min^{-1}), followed by 1 h isothermal hold at 230 °C, under N_2 flow (100 mL min^{-1} g^{-1}) to decompose the nitrate precursor. The sample was left to cool down to room temperature, purged with 20 vol% O_2/N_2 flow (100 mL min^{-1} g^{-1}) for 3 h at room temperature, then purged with pure N_2 flow (100 mL min^{-1} g^{-1}) for 30 min. Subsequently, the material was reduced by heating to 150 °C (2 °C min^{-1}), with 2 h isothermal hold at 150 °C, under 5 vol% H_2/N_2 flow (100 mL min^{-1} g^{-1}). Next, the temperature was increased to either 250 or 400 °C (2 °C min^{-1}), with 1 h isothermal hold at the final temperature, to obtain the 3nm_Cu/C and 7nm_Cu/C catalysts, respectively. The final catalyst was collected after letting it cool down to room temperature and passivating it by exposure to air (overnight) at room temperature, then stored in closed vials at RT. Prior to X-ray powder diffraction analysis and TEM imaging, the nanoparticles were fully oxidized under 20 vol% O_2/N_2 flow (100 mL min^{-1} g^{-1}) at 250 °C (heating ramp of 2 °C min^{-1} , isothermal hold of 2 h).

X-ray powder diffraction and TEM imaging. Characterization measurements were performed on XRD analysis was carried out on the as-prepared samples with a Bruker D2

Phaser. Radiation source: Co K α (1.78897 Å). The diffractogram were recorded in the 2 θ interval 15–90° with a step size of 0.05°. Rietveld refinement was conducted with DIFFRAC.SUITE TOPAS software. Transmission electron micrographs of the Cu/C and Cu/SiO₂ catalysts were obtained on a Tecnai F20 apparatus, operated at 200 kV. Scanning transmission electron microscopy was performed in high-angle annular dark-field (HAADF) mode on a Talos F200X (FEI), equipped with a high-brightness field emission gun (X-FEG) and operated at 200 kV.

Prior to TEM imaging, the two silica-supported samples were both ultramicrotomed in order to increase the contrast between the amorphous silica gel support and the Cu nanoparticles. The catalyst grains (<75 μm) were embedded in a two-component epoxy resin (Epofix, EMS) and cured at 60 °C for 24 h. The embedded catalysts were sliced into 50 nm nominal thickness sections by means of a Diatome Ultra 35° diamond knife mounted on a Reichert-Jung Ultracut E microtome. The sections were then deposited on a TEM grid and analyzed. Graphitic carbon supported materials were finely grinded via mortar and pestle and dry deposited onto the TEM grids. Average particle sizes were defined as $d_{TEM} = \Sigma_i d_{NP,i}^3 / \Sigma_i d_{NP,i}^2$, while particle size dispersion was described as standard deviation. The number of surface copper atoms was calculated using a copper dispersion of 1.46×10^{19} atoms per square meters of Cu exposed surface area. The latter was calculated by assuming a spherical particle shape and using the equation $S_{Cu} = 6000/d_{TEM} \rho_{Cu}$ where S_{Cu} is the specific copper surface area ($\text{m}_{Cu}^2 \text{g}_{Cu}^{-1}$), d_{TEM} is the mean particle diameter and ρ_{Cu} is the copper density (8.92 g cm^{-3}).¹⁰⁶ The CuO and Cu particle sizes (after reduction of the pre-catalyst prior to catalytic tests) were assumed to be the same.

Temperature programmed reduction tests. Temperature programmed reduction (H₂-TPR) profiles for the as-prepared 3 and 7 nm CuO particles on SiO₂ and C were performed using a Micromeritics Autochem II ASAP 2920 apparatus, with H₂ consumption measured using a thermal conductivity detector. The sample (~150 mg) was first dried at 120 °C for 30 min under an Ar flow (~1 L min⁻¹ g⁻¹) and cooled down to room temperature. Subsequently, the samples were heated at constant rate to 450 °C (5 °C min⁻¹ for Cu on SiO₂, 2 °C min⁻¹ for Cu on C) under 5 vol% H₂/Ar gas flow (~2 mL min⁻¹ g⁻¹). Small (3 nm) and large (7 nm) CuO particles on both SiO₂ and C were fully reduced at temperatures below 250 °C. The reduction onset temperature was between 100 and 125 °C.

Catalytic tests. The catalytic tests were performed with the use of a tailor made gas-phase hydrogenation set-up previously described by Masoud *et al.*¹⁴⁸ The experiments were carried out by loading a homogeneous mixture of each individual sample (sieve fraction 75–150 μm ; total amount of copper loaded in the reactor equal to 1.28 mg) and 150 mg of SiC as thermal diluent (sieve fraction 212–425 μm) in a U-shaped Pyrex packed bed microreactor (internal diameter of 4 mm). Prior to the test, the catalysts were reduced in situ under pure H₂ flow (50 mL min⁻¹) from RT to 250 °C (ramp 2 °C min⁻¹) and kept at 250 °C for 90 min. Hereafter, the catalyst was put into contact with the reaction mixture (0.3% butadiene, 30% propene, 20% hydrogen, and helium for balance with a flow rate of 50 NmL min⁻¹, 1 bar). The reactor

temperature was either linearly increased from RT to 150 °C at 0.5 °C/min or held constant for 2 h long isothermal steps in the range 110–180 °C. More details on the methodology can be found later in the text (see **sections 2.4 and 2.5**).

The concentration of the products and unconverted reactants was monitored every 15 minutes via gas chromatography using a Flame Ionization Detector (GC-FID, hydrocarbons detected: C₁-C₄). The composition of the gas mixture fed to the reactor was monitored at the beginning and at the end of each catalytic run by by-passing the reactor bed. Calculated turnover frequencies (TOF, s⁻¹) were defined as the molecules of 1,3-butadiene consumed per unit time per Cu surface atom, calculated as follows:

$$TOF = \frac{p Q_{1,3-bd} X_{1,3-bd}}{R T} * \frac{1}{S_{Cu} w_{Cu} 1.46 \cdot 10^{19} / N_{AV}}$$

where p is the reactor pressure (1 bar), $Q_{1,3-bd}$ is the butadiene volumetric flow rate to the reactor (0.15 NmL min⁻¹), R is the ideal gas constant, T is the temperature at which the TOF is calculated, $X_{1,3-bd}$ is the conversion of 1,3-butadiene to butenes at a temperature equal to T , S_{Cu} is the exposed Cu surface area (expressed in m² g_{Cu}⁻¹ and calculated as $S_{Cu} = 6000/d_{TEM} \rho_{Cu}$, where d_{TEM} is the mean particle diameter in nm, and ρ_{Cu} is the copper density, 8.92 g cm⁻³), w_{Cu} is the amount of Cu loaded inside the reactor (1.28 mg), $1.46 \cdot 10^{19}$ is the number of Cu atoms per square meters of Cu exposed surface area and N_{AV} is the Avogadro number ($6.022 \cdot 10^{23}$).^{106,176}

The total selectivity to butenes was defined as follows:

$$Total\ selectivity\ to\ butenes = \frac{C_{1-butene} + C_{trans-2-butene} + C_{cis-2-butene}}{C_{1-butene} + C_{trans-2-butene} + C_{cis-2-butene} + C_{butane} + C_{propane}}$$

Where C_i denotes the concentration (expressed as ppmv) of each individual product of the reaction.

Reaction orders were calculated by varying the partial pressure of one reactant (propene, 1,3-butadiene, H₂) at a time. The standard mixture is obtained by mixing 0.15 NmL min⁻¹ of 1,3-butadiene, 15 NmL min⁻¹ of propene, 10 mL min⁻¹ of hydrogen, He as balance. The volumetric flow rate is kept constant by decreasing/increasing the volumetric flow rate of He.

2.3 – Structural characterization

The structural properties of the prepared catalysts (oxidized form) were investigated by X-ray powder diffraction, and results are reported in Figure 2.1. CuO crystallite sizes obtained via Rietveld refinement are shown in Table 2.1. Both silica-supported samples (3nm_Cu/SiO₂ and 7nm_Cu/SiO₂) display two main characteristic CuO reflections peaks at 42° and 45.5° (corresponding to the [002] and [111] diffractions, respectively), while the broad scattering band at 25° is ascribed to the disordered silica gel support. The peak broadening for 3nm_Cu/SiO₂ indicates the presence of only small CuO crystallites in this sample. For 7nm_Cu/SiO₂ the intense and much sharper diffraction peaks demonstrate the presence of large CuO crystallites. The average CuO crystallite sizes were 3.1 and 10.4 nm in 3nm_Cu/SiO₂ and 7nm_Cu/SiO₂, respectively (Table 2.1). The diffractogram of the 3nm_Cu/C did not show any CuO or Cu₂O reflections, implying a high copper dispersion. Lastly, the sample 7nm_Cu/C exhibited intense CuO peaks, and the calculated average crystallite size was 10.1 nm, similar to the 7nm_Cu/SiO₂ sample.

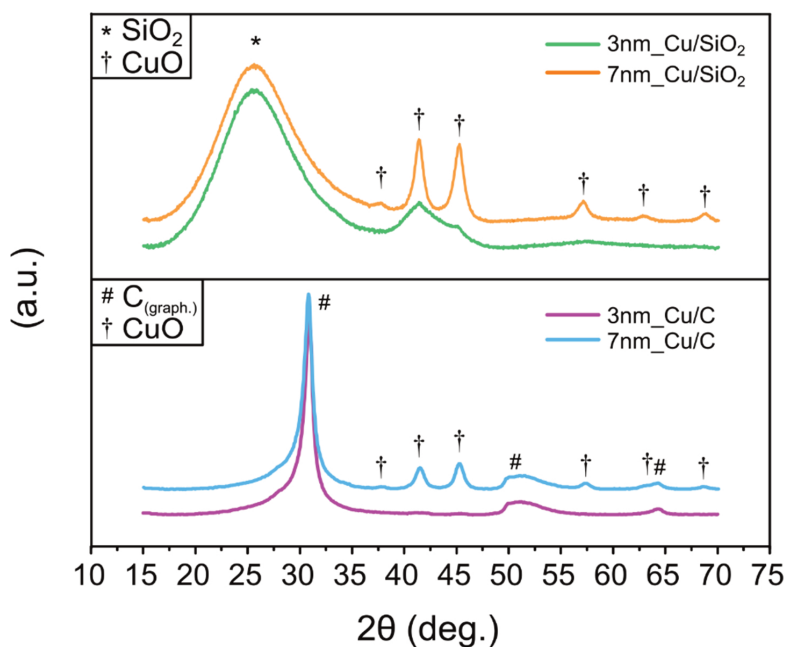


Figure 2.1 X-ray powder diffraction patterns of the oxidized 3nm_Cu/SiO₂, 7nm_Cu/SiO₂, 3nm_Cu/C and 7nm_Cu/C. X-ray source: Co K α .

Table 2.1 Structural properties for the as-prepared samples.

Catalysts	Cu ⁰ weight loading	Particle size		Cu dispersion
	(%)	d _{TEM} (nm)	d _{XRD} (nm)	(%)
3nm_Cu/SiO ₂	5.7	3.5 ± 1.0	3.1	20
7nm_Cu/SiO ₂	5.7	7.3 ± 2.4	10.4	14
3nm_Cu/C	6.3	3.1 ± 0.9	n.a.	34
7nm_Cu/C	6.3	7.3 ± 1.8	10.1	14

The XRD results show that the crystallite sizes on carbon can be tuned by changing the temperature at which the catalyst is treated. A reduction step conducted at 400 °C led to larger and more crystalline CuO nanoparticles (sample: 7nm_Cu/C), while at 250 °C particle growth was limited (sample: 3nm_Cu/C). This was not observed by HAADF-STEM in the case of CuO over SiO₂ (see Figure 2.2, 3nm_Cu/SiO₂ prepared at 250 and 450 °C). The difference between carbon and silica supports suggests that Cu (or CuO) particles are more strongly anchored on the surface of the silica rather than on the modified graphitic carbon. Moreover, preparation via reduction under H₂ at 250 °C results (upon further oxidation) in measurable CuO crystallites on SiO₂ but not on oxidized carbon, which may indicate a different interaction of the copper species with these two supports, such as the presence of amorphous CuO phase over the carbon support.

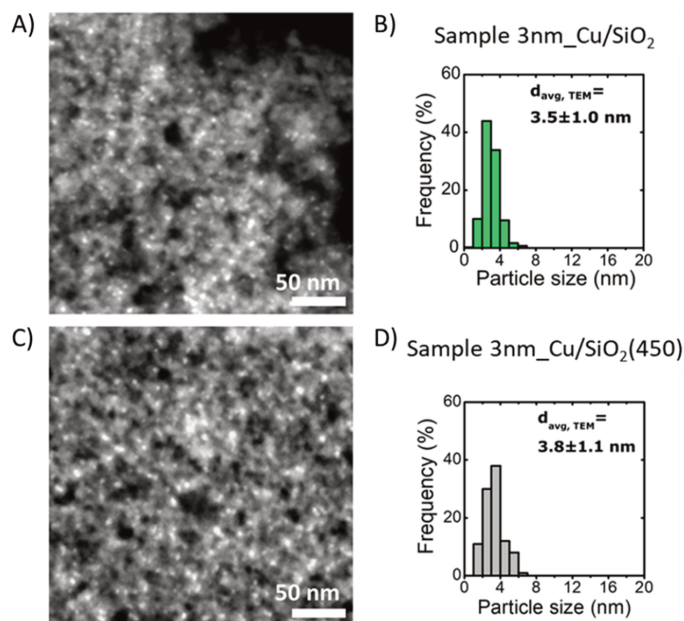


Figure 2.2 HAADF-STEM images for the as synthesized (A) 3nm_Cu/SiO₂ (with corresponding particle size distribution in frame B) and (C) 3nm_Cu/SiO₂(450) catalysts (with corresponding particle size distribution in frame D). Cu particles do not grow larger by increasing the reduction temperature at which the impregnated support is treated (in this case, from 250 °C to 450 °C for 3nm_Cu/SiO₂ and 3nm_Cu/SiO₂(450) respectively).

The CuO nanoparticle sizes and distributions on both silica and surface-oxidized graphitic carbon were investigated with TEM (Figure 2.3). A uniform distribution of the CuO particles over the surface of the support was observed for both the silica and the graphitic carbon. Interestingly, the 3nm_Cu/C sample contained small particles all over the surface of the carbon, which had not been detected via XRD probably due to low crystallinity. Unimodal particle size distributions were found for all the four samples and no particles above 20 nm in diameter were present.

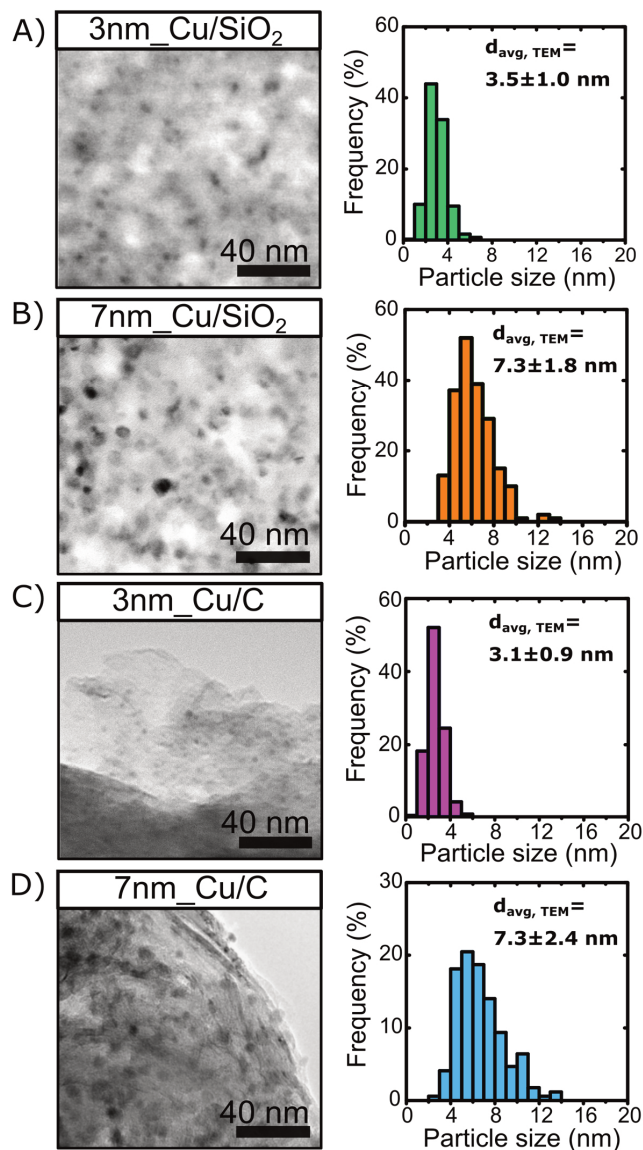


Figure 2.3 Representative transmission electron micrographs for the as synthesized (A) 3nm_Cu/SiO₂, (B) 7nm_Cu/SiO₂, (C) 3nm_Cu/C and (D) 7nm_Cu/C catalysts, with the corresponding particle size distributions. Silica-supported samples were ultramicrotomed to 50 nm slices (nominal thickness) prior to imaging.

The particle diameters as determined by TEM are in good agreement with the crystallite sizes as estimated by XRD (Table 2.1). In the case of 7nm_Cu/C and 7nm_Cu/SiO₂, XRD data analysis gives a slightly larger crystallite diameter (about 10 nm) in both cases. This could be explained by considering the higher degree of crystallinity and hence diffraction intensity of the larger particles present in those samples (most probably caused by slight over-impregnation of a fraction of the support) which leads to a stronger contribution to the overall signal by the larger crystallites. Hence the effective copper dispersion used for the evaluation of the catalytic data was based on the CuO particle sizes determined from TEM data (Table 2.1).

2.4 – Activity measured during a temperature ramp

The results of the temperature ramp catalytic experiments are reported in Figure 2.4 in terms of 1,3-butadiene conversion vs. temperature. Specifically, a comparison of the conversion data for the 3 and 7 nm Cu on SiO₂ and C is shown in Figure 2.4A, while Figure 2.4B reports the data collected for a heating-and-cooling cycle for the sample 3nm_Cu/SiO₂. All test data were collected while linearly heating (or cooling) the in situ pre-reduced samples from 50 to 175 °C with 0.5 °C min⁻¹.

The bare supports did not show any hydrogenation activity when exposed to the reactant mixture at temperatures up to 200 °C. Both silica-supported and carbon-supported catalysts (3 and 7 nm) showed a similar concentration profile for the consumption of 1,3-butadiene versus temperature (Figure 2.4A, for raw and full product distribution refer to Supporting Information of ref.²⁶). In particular, the onset of 1,3-butadiene consumption was around 105 °C, with a sharp decrease in 1,3-butadiene concentration until full conversion (>98%) at 120–130 °C (indicated later in the text as T_{98%}). In all cases, the catalysts were almost fully selective towards butenes, and the main product of the reaction was 1-butene (selectivity 60–70%, significantly higher for carbon-supported catalysts than for the silica-supported catalysts). Smaller amounts (10–15%) of cis-2-butene and trans-2-butene were also detected and their concentration increased with the temperature. Butenes and propene conversions were generally below 1.5% and 1%, respectively, at almost full (>95%) 1,3-butadiene conversion (see SI in ref.²⁶ for more details, as well as **section 2.7**)

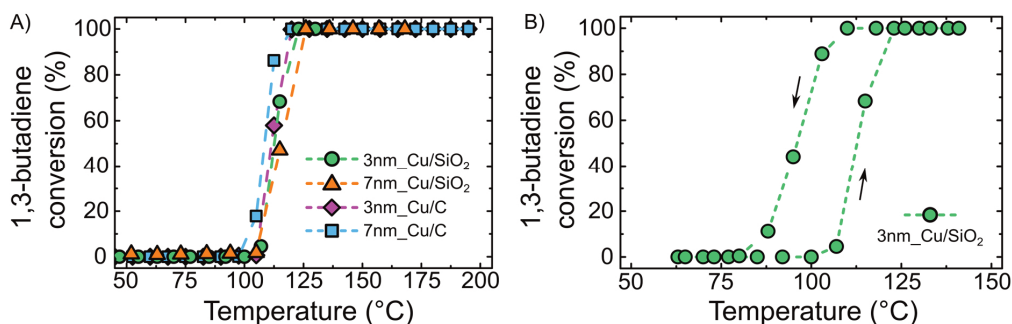


Figure 2.4 A) 1,3-butadiene conversion as a function of temperature for the 3nm_Cu/SiO₂, 7nm_Cu/SiO₂, 3nm_Cu/C and 7nm_Cu/C samples. B) 1,3-butadiene conversion as a function of the temperature for the sample 3nm_Cu/SiO₂; the datapoints were collected while heating the in situ pre-reduced catalyst from 50 °C to 175 °C and then cooling down the used catalyst back to room temperature (temperature ramp: 0.5 °C min⁻¹). Reaction conditions: butadiene/propene/H₂/He= 0.15/15/10/24.85 mL min⁻¹, 1 bar(a), and 1.28 mg of Cu loaded. GHSV: 35 000 h⁻¹.

All catalysts displayed the same activity (per unit Cu mass) within error at temperatures between 105 and 125 °C, as evident from the almost perfect overlap of conversion data (see Figure 2.4A). This is surprising as differences due to the different particles sizes and supports might be expected. Hence, we started a more detailed study of the activity by temperature cycling experiments, with as an example results for 3nm_Cu/SiO₂, reported in Figure 2.4B. In this case, a pronounced hysteresis was observed; the high 1,3-butadiene conversion was retained to temperatures below 105 °C during cooling. A possible explanation might be the formation of local hotspots in the catalyst bed due to the exothermicity of the hydrogenation reaction, although this is not expected under the given conditions (ref.²⁶ and associated SI). Another possibility is that the low activity between 85 and 105 °C during the first heating ramp is due to deactivation of the surface of the copper nanoparticles by oxidation.

Oxidation of copper is favored at low temperatures (e.g., during cooling and preparation steps after in situ activation or at the beginning of the catalytic test heating ramp) and can be caused by trace amounts of oxygen and/or water that are always present in commercial gas mixtures. The onset of activity might correspond to the reduction of Cu oxides by the H₂ present in the reaction mixture. Temperature programmed reduction (TPR) experiments were carried out on both silica and carbon supported samples in order to verify the reduction temperature of the Cu nanoparticles for the catalyst pre-treatment, as well as for investigating reduction onset (Figure 2.5).

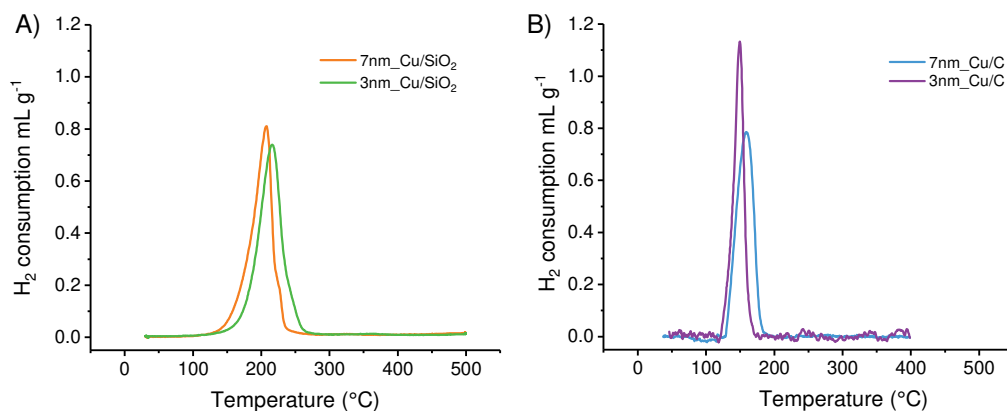


Figure 2.5 H₂ consumption while heating for the as-prepared 3 (A) and 7 nm (B) CuO particles on SiO₂ and C (initially oxidized under 20 vol% O₂/N₂ flow, 100 mL min⁻¹ g⁻¹, at 250 °C 2h hold).

All four samples showed one unique reduction peak at the testing conditions employed for the TPR experiment (5%vol H₂/Ar flow, ~2 mL min⁻¹ g⁻¹, and heating ramp equal to 5 °C min⁻¹). Regarding SiO₂ supported samples, the onset of reduction was 135 and 160 °C and peak temperature equal to 210 and 215 °C for 7 and 3 nm Cu, respectively. In both cases, the Cu was completely reduced at a temperature of 250 °C. For C supported samples, the onset was slightly lower (125-130°C) and peak temperature equal to 150 and 160 °C for 3 and 7 nm particles, respectively. Cu on C was completely reduced at 200 °C. The results suggests that the reduction step carried out before any catalytic test (2 °C min⁻¹, 250 °C, see also **section 2.2 – Experimental Section**) should guarantee full reduction of CuO to metallic Cu nanoparticles. As anticipated, however, temperatures below 100-120 °C might lead to slow formation of Cu oxides on the surface of the nanoparticles if traces of O₂ or H₂O are present. This might explain the similar reaction onset observed for the experiments reported in Figure 2.4A.

To evaluate that the Cu can retain its metallic oxidation state (Cu⁰) at high temperature (>100-120 °C) and under reaction conditions, we additionally simulated the thermodynamic equilibrium of Cu/Cu₂O/CuO, considering the worst-case scenario of 50 ppm of O₂ present in the gas mixture as impurity. We assumed a molar ratio in Cu:H₂:O₂:He of 1:10:10⁻²:10². The relative amount of CuO and Cu₂O at temperature between 100 °C and 250 °C was negligible (Cu:Cu₂O:CuO molar ratio in the orders 1:10⁻³²:10⁻³², hence absence of Cu oxides). These calculations, together with H₂-TPR results, indicate that the Cu nanoparticles will consist of metallic Cu under the highly reducing reaction conditions (T= 150-250 °C).

Interestingly, a sudden increase in conversion between 100–120 °C was previously reported also in the case of hydrogenation of various alkynes using Cu-based catalysts.¹⁵³ Using a single heating ramp is a common way to assess the activity of catalysts. Although this might be a valid method when measuring catalytic performance of more noble metals such as Pd,¹⁷⁷ Pt¹⁷⁸ or Au,^{148,179} clearly for Cu-based catalysts the intrinsic properties might be obscured by oxidation. Therefore, another type of testing protocol was developed, as described in the next section.

2.5 – Activity under steady state conditions

The new measurements protocol involved a first step of catalyst pre-conditioning for 15 hours under reaction mixture at $T = 110\text{--}130\text{ }^{\circ}\text{C}$. Subsequently, the catalyst was heated (or cooled) to the desired temperature and kinetic data were recorded for 2 h in isothermal conditions. The datapoints used for performance evaluation were collected at the end of a 2 h hold, in order to reach a steady state in terms of solid-to-gas interface composition and thermal equilibrium. The process was iterated at each temperature level and multiple points were collected at one chosen temperature to detect possible activation/deactivation. An example of such a measurement is illustrated in Figure 2.6A for 3nm_Cu/SiO₂. Additionally, data at the same temperature were collected multiple times over the entire course of the test in order to verify possible catalyst deactivation. An example is reported in 2.6B, where the multiple datapoints collected at a temperature of 120 °C are highlighted.

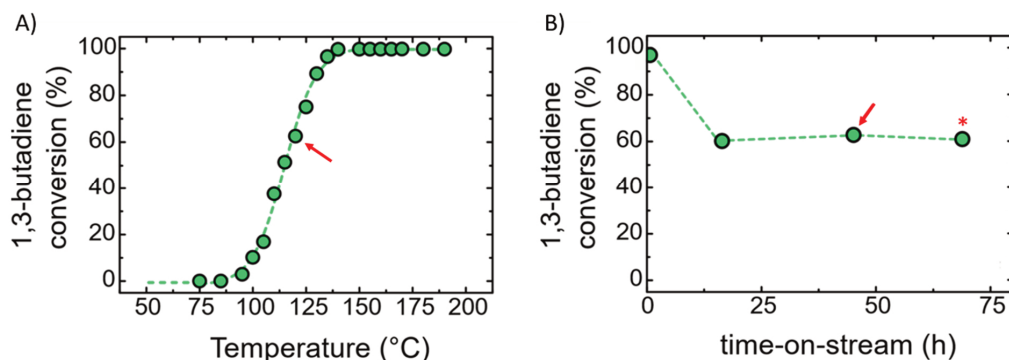


Figure 2.6 (A) 1,3-butadiene conversion as a function of the temperature for the 3nm_Cu/SiO₂ sample. The data were collected at steady state conditions after 15 h pre-conditioning ($T = 110\text{--}130\text{ }^{\circ}\text{C}$). Additionally, data were collected at the same temperature multiple times during the same test in order to check for possible catalyst deactivation (B). The points marked with the red arrow on both plots represents the same datapoint. The datapoint marked with an asterisk was used as control (for stability/reproducibility). Conditions: as in Figure 2.4.

As it can be observed in Figure 2.6A, the new protocol yielded a well-defined onset temperature of activity (and no hysteresis, here not shown), and clear conversion gradient vs. Temperature, different from the sudden conversion jump observed in Figure 2.4A. In addition, the test enabled the sampling of the catalyst conversion at the same temperature multiple times. In Figure 2.6B, it is clear that after the first pre-conditioning step (first 15h), the catalyst reached steady state, as the datapoint collected between 15 and 75h at 120 °C were the same within measurement uncertainty. Hence, no change in catalyst activity is expected during the test (after pre-conditioning).

The 1,3-butadiene conversion profiles as function of the temperature obtained with the described protocol are given in Figure 2.7A and 2.7B for three selected catalysts, 3nm_Cu/SiO₂, 7nm_Cu/SiO₂ and 7nm_Cu/C. With this new measurement protocol, the

activity plot looked very different from the one obtained by linearly heating the catalyst (Figure 2.4A), with clear differences between the various catalysts. Both 7nm_Cu/C and 7nm_Cu/SiO₂ showed very similar conversion profiles (Figure 2.7A). Hydrogenation activity was measurable starting at around 115 °C with almost full 1,3-butadiene conversion reached at around 170 °C. However, the sample 3nm_Cu/SiO₂ (Figure 2.7B) displayed a higher activity than the 7nm_Cu/SiO₂, with full hydrogenation at 135 °C.

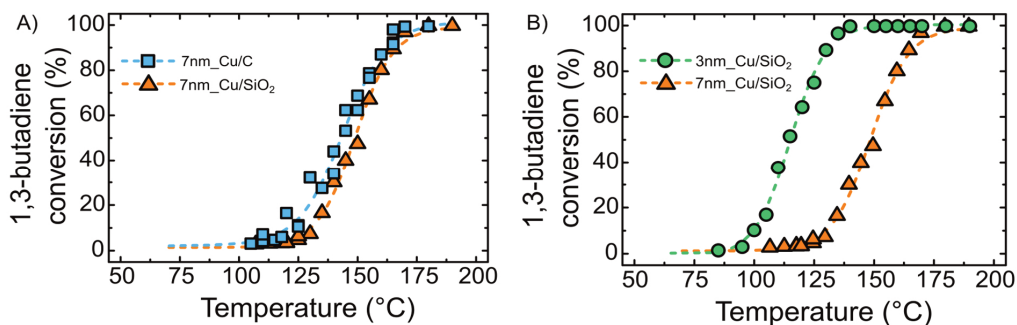


Figure 2.7 1,3-butadiene conversion as function of temperature for A) 7nm_Cu/SiO₂ and 7nm_Cu/C and B) 3nm_Cu/SiO₂ and 7nm_Cu/SiO₂ samples. The catalysts were preconditioned for at least 15 hours at 110–130 °C prior to measurements (see Figure 2.6). The catalytic data were collected after allowing at least 2 h at a given T for reaching stable state conditions. Conditions: 1,3-butadiene/propene/H₂/He = 0.15/15/10/24.85 mL min⁻¹, 1 bar(a) and 1.28 mg of Cu loaded for each test. GHSV: 35000 h⁻¹.

The turnover frequencies (normalized to the number of exposed copper atoms) measured at 125 °C with the method and conditions described in Figures 2.6 and 2.7 were $6 (\pm 2) \times 10^{-3}$, $5 (\pm 2) \times 10^{-3}$ and $22 (\pm 6) \times 10^{-3} \text{ s}^{-1}$ respectively for 7nm_Cu/C, 7nm_Cu/SiO₂ and 3nm_Cu/SiO₂. The TOFs measured for Cu nanoparticles in this work can be compared for those previously reported in literature. Wang *et al.* measured a turnover frequency of $32 \times 10^{-3} \text{ s}^{-1}$ at 105 °C for 5 nm Cu on TiO₂ (same reaction conditions),⁹¹ higher than for the catalysts hereby reported. The authors stated that the catalyst was able to partially hydrogenate 1,3-butadiene at temperatures as low as 60 °C.⁹¹ The lower Cu-based activity for the catalysts supported on SiO₂ and carbon, compared to TiO₂, may be caused by support effects for small nanoparticles on reducible metal oxide supports. For example, Masoud *et al.* reported a 4-fold higher activity (but much lower stability) for <5 nm Au nanoparticles supported on TiO₂ compared to Au/SiO₂.¹⁴⁸ The activity may also be strongly influenced by the specific catalyst pre-treatment and reaction conditions.

The Cu-based activities for 1,3-butadiene hydrogenation investigated in our work were higher than for Au/SiO₂ catalysts ($4 \times 10^{-3} \text{ s}^{-1}$ at 120 °C)¹⁴⁸ as well as for Ag/SiO₂ systems ($0.2 \times 10^{-3} \text{ s}^{-1}$ at 120 °C)¹⁴⁹ yet much lower than for Pd/Al₂O₃ (10.5 s^{-1} at 40 °C) as measured under similar reaction conditions.¹⁵⁶ Hence our results confirm that supported Cu nanoparticles are reasonably active catalysts for 1,3-butadiene hydrogenation. However, at least as important as the activity, is the catalyst stability, which is discussed in the next section.

2.6 – Stability

Measurements carried out at steady state conditions revealed that the catalysts, after proper pre-conditioning, displayed stable and reproducible activity (see Figure 2.7). However, TEM analysis of the used catalysts revealed that the 7nm Cu supported on carbon, sample 7nm_Cu/C, suffered from extensive particle growth (from ~7 to ~23 nm) during the catalytic testing described in section 2.5 (Figure 2.7), while all silica-supported samples retained their initial particle size (see also ref.²⁶ and associated Supporting Information). Hence, we focused in more detail on the Cu/SiO₂ system and more specifically on the activated (reduced) 3nm_Cu/SiO₂ and 7nm_Cu/SiO₂ catalysts (more details on the Cu/C samples can be found in ref.²⁶). Silica supported samples were hence tested for stability during a 60h run at a given temperature. The results are reported in Figure 2.8A, while total selectivity to butenes and C₄ composition can be found in Figures 2.8B and 2.8C.

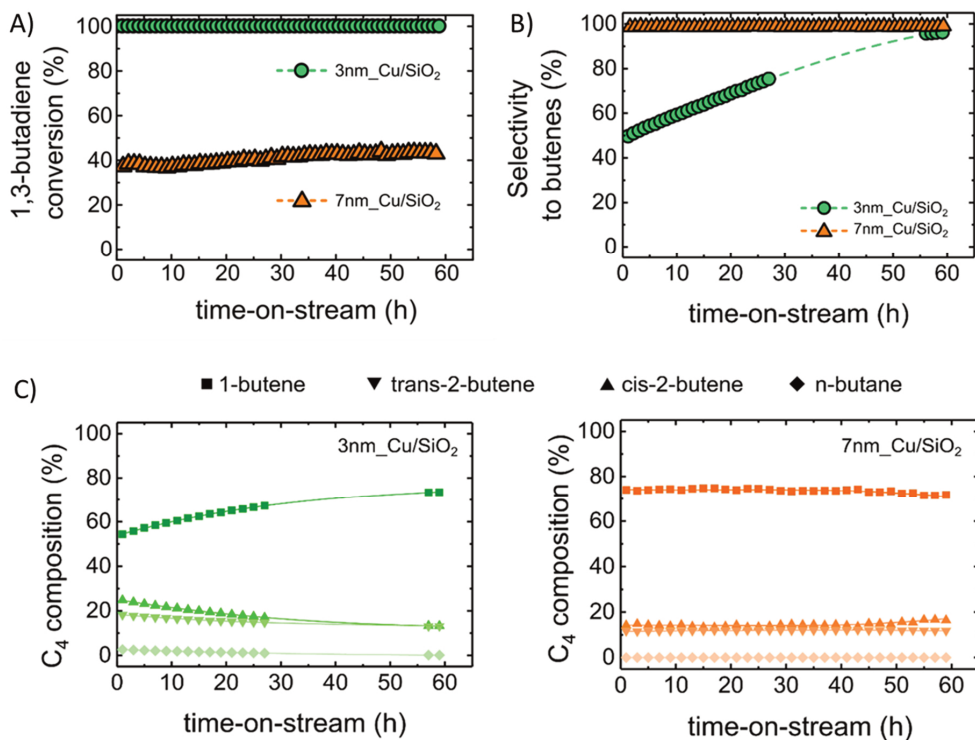


Figure 2.8 A) 1,3-butadiene conversion as a function of the time-on-stream for the 3nm_Cu/SiO₂ (test carried out at 130 °C) and 7nm_Cu/SiO₂ (140 °C) samples. Conditions: 1,3-butadiene/propene/H₂/He = 0.15/15/10/24.85 mL min⁻¹, 1 bar(a) and 1.28 mg of Cu loaded for each test. GHSV: 35 000 h⁻¹. B) Selectivity to butenes and C) C₄ products composition (bottom) as a function of the time-on-stream. Lines: guide for the eye.

The 3 nm catalyst tested at 130 °C exhibited full conversion for the entire 60 hours of catalytic test (Figure 2.8A). Full conversion does not allow to assess stability changes. Long term tests on 7nm_Cu/SiO₂ (140 °C, same conditions) revealed a high stability, with the 1,3-butadiene conversion equal to ~40% from the beginning to the end of the run. It is interesting to note a good agreement between these data and the ones collected under steady state conditions (Figure 2.7) for both the samples, which underlines the remarkable stability of these catalysts as well as the robustness of our new measurement protocol.

Regarding the selectivity to butenes (Figure 2.8B), a steady selectivity of around 98.8% was observed for the sample 7nm_Cu/SiO₂ (in good agreement with the results shown in Figure 2.10). For this catalyst, the major component of the C₄ products composition was 1-butene (70%). The product concentration was stable for 60 hours. The sample 3nm_Cu/SiO₂, however, displayed a gradual increase in selectivity (from 50% to 96%, Figure 2.8C). Concomitantly, the selectivity towards 1-butene formation also increased over time until reaching a steady value of 73%. This might suggest restructuring of the catalytic surface over time (yet, the small particle size distribution was retained, see ref.²⁶ and associated SI), or possible deactivation of a small fraction of unselective sites. Ex-situ FT-IR investigations of the fresh and used samples post-test reported in Figure 2.8, are reported in Figure 2.9.

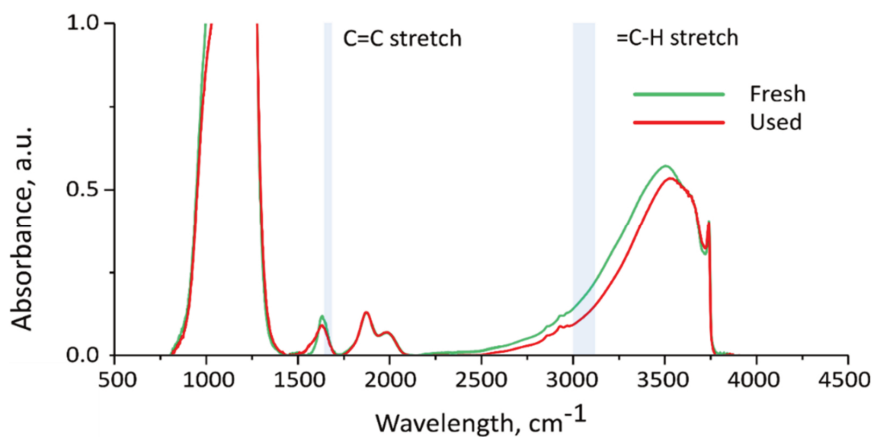


Figure 2.9 Ex situ FT-IR data collected for 3nm_Cu/SiO₂ fresh and used sample (tested at 130 °C for 60 h (same reaction conditions as described in Figure 2.8)).

Regarding formation of possible oligomers starting from 1,3-butadiene, the two main interesting signals are the C=C stretching (1640 – 1680 cm⁻¹) and the =C-H stretch, expected between 3000 and 3100 cm⁻¹. Both the fresh and the used 3nm_Cu/SiO₂ catalysts do not display features in the two areas of interest, suggesting that the formation of carbonaceous oligomers is absent or very limited.

The catalysts described in this work were significantly more stable than Cu catalysts immobilized on oxidic supports reported in literature. For instance, 5 nm Cu/TiO₂ described

by Wang *et al.* measured using the same reaction mixture, but at $T = 90\text{ }^{\circ}\text{C}$, lost more than 90% of its activity in less than 10 hours on stream.¹⁵⁷ Deactivation was mainly ascribed to “green oil” or coke poisoning (formation of C_4+ oligomers or carbonaceous deposit).^{52,151,157} No results for Cu catalysts on SiO_2 have been reported before. However, differences in stability between SiO_2 - and TiO_2 - supported catalysts were reported by our group for Au catalysts used in selective hydrogenation of the same reaction mixture.¹⁴⁸ Higher stability was observed for Au nanoparticles immobilized on the silica support than on titania P25 (almost full retention of the activity for Au/ SiO_2 catalyst after 16 h at $200\text{ }^{\circ}\text{C}$, versus 88% loss in activity for Au/ TiO_2 tested in the same conditions). Analysis revealed coke formation on the TiO_2 support under reaction conditions, even in the absence of Au.¹⁴⁸

An important role of the support was reported for the hydrogenation of alkynes as well. Sárkány,¹⁸⁰ for instance, observed that the amount of carbon deposited over Pd catalyst supported on TiO_2 was twice the one on $\alpha\text{-Al}_2\text{O}_3$ during pulse-flow hydrogenation experiment of ethyne/ethene mixtures (3.9 carbon atoms per Pd surface atom for Pd/ TiO_2 versus 1.66 for Pd/ Al_2O_3). Combination of adjacent vinyl species and/or insertion of ethyne into Pd-C bond of adsorbed vinyl intermediates to form a diene were considered the reason for the formation of green oil in ethyne hydrogenation. The authors postulated that the TiO_2 support, due to the presence of Ti^{3+} sites decorating the Pd particle, enhanced the concentration of retained hydrocarbons over the surface of the catalyst, leading to a greater formation of C_6+ oligomers.¹⁸⁰ It is clear that using more inert supports, as we show here for Cu-based catalysts, is a successful strategy to produce stable catalysts for the hydrogenation of alkadienes.

2.7 – Selectivity

In this section, the selectivities of 3nm_Cu/SiO₂ and 7nm_Cu/SiO₂ (collected during the tests reported in Figure 2.7) are discussed in more detail. Propene conversion and selectivity to butenes are displayed in Figure 2.10A and B, respectively. The total selectivity to butenes (Figure 2.10B, see **section 2.2**) is defined as the ratio between the C₄ alkenes productivity over the total hydrogen consumption (see **section 2.2**).²⁶ For both catalysts, hydrogenation of alkenes to alkanes was limited, with a propene conversion below 0.1% in the entire 1,3-butadiene conversion range (Figure 2.10A). Sample 3nm_Cu/SiO₂ exhibited a maximum propene conversion of 0.06%, while for 7nm_Cu/SiO₂ it is limited to 0.013% at almost full (97%) 1,3-butadiene conversion (corresponding to roughly 40 ppm of propane present in the reactor outlet stream).

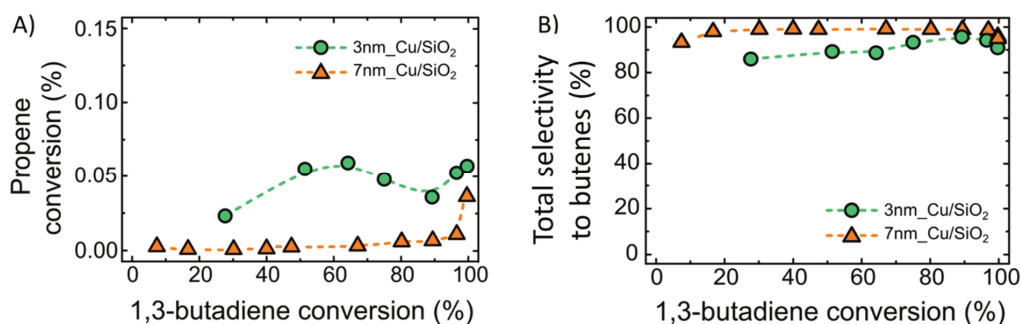


Figure 2.10 A) Propene conversion and B) Total selectivity to butenes data (defined as the ratio between the butenes productivity over the total hydrogen consumption) as function of the 1,3-butadiene conversion for the reduced 3nm_Cu/SiO₂ and 7nm_Cu/SiO₂. Pre-treatment, reaction conditions and testing methodology as in Figure 2.7.

Although the propene conversion is commonly used in the literature to assess the performance of this class of hydrogenation catalysts, it is valuable to additionally look at the total selectivity to butenes (Figure 2.10B). In this way both undesired reactions, hydrogenation of propene (to propane) and over-hydrogenation of 1,3-butadiene (to butane), are taken into consideration. Both silica-supported catalysts presented high selectivities. For instance, at 97% 1,3-butadiene conversion, the total selectivities to butenes were 94% for the 3 nm Cu and an astonishing 99% to butenes for 7nm_Cu/SiO₂. The difference in selectivity between the two catalysts is substantial. The higher overall activity of 3nm_Cu/SiO₂ in terms of 1,3-butadiene hydrogenation to butenes (Figure 2.7) and alkenes hydrogenation with respect to 7nm_Cu/SiO₂ (Figure 2.10), suggests a particle size dependency. More details on particle size effect can be found in **Chapter 3** of this thesis.

In order to better understand the catalyst selectivity, sample 3nm_Cu/SiO₂ was also tested at temperatures well above 140 °C, the T required to achieve full hydrogenation of 1,3-butadiene (T_{98%}). Under these conditions (with top-down flow) at the bottom of the catalytic bed, the 1,3-butadiene concentration is negligible, and the reaction atmosphere consists mainly of propene, butenes and H₂. The fraction of the catalytic bed that experiences these conditions increases with the reaction temperature. The 1,3-butadiene conversion, propene conversion and C₄ composition are reported in Figure 2.11. The propene conversion is low and constant from 110 °C up to 150 °C (temperatures at which the 1,3-butadiene consumption is below 98%). At temperatures higher than 140 °C, i.e., at full conversion with the 1,3-butadiene concentration depleted at the bottom of the catalytic bed, the propene conversion increases. This conversion, however, remains lower than 1% at 50 °C higher than the temperature required for full 1,3-butadiene hydrogenation. Simultaneously, conversion of butenes to butane remains almost absent. These observations highlight the remarkably high selectivity of Cu/SiO₂ catalysts.

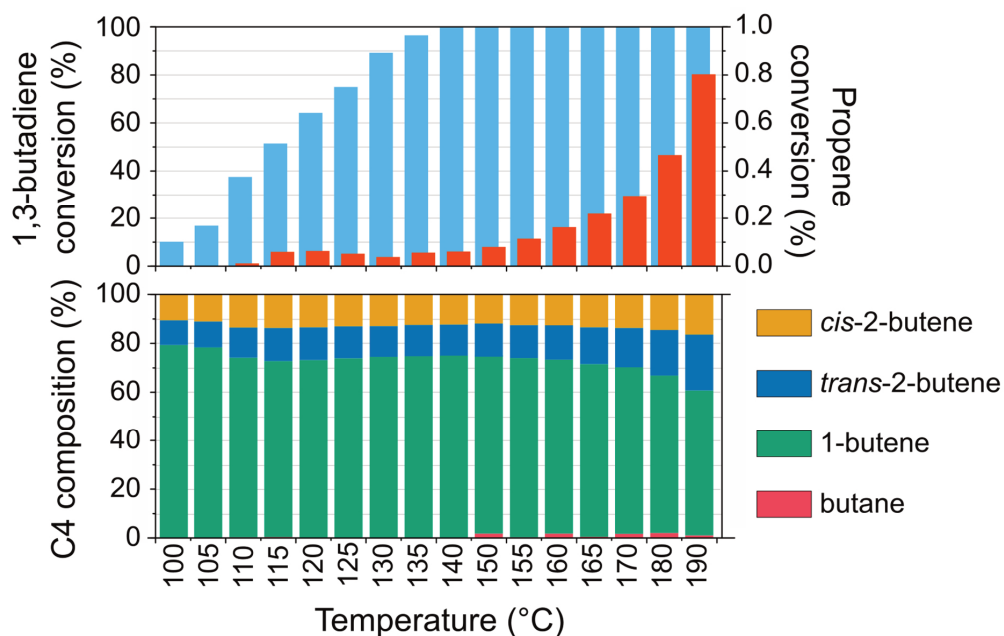


Figure 2.11 1,3-butadiene conversion (blue bars), propene conversion (orange bars) and C₄ (butenes) distribution as a function of temperature for 3nm_Cu/SiO₂. Pre-treatment, reaction conditions and testing methodology as in Figure 2.7.

A similar trend was observed for the C₄ products, with the trans-2-butene concentration increasing with temperature only above 150 °C, at the expense of the less stable 1-butene, a sign that isomerization becomes significant only when 100% conversion is reached and when part of the catalytic bed is depleted in 1,3-butadiene. In fact, from both thermodynamic and

experimental data, the *trans*-2-butene is the most stable molecule, and hence is expected to be present in higher amount, followed then by *cis*-2-butene and finally 1-butene (see Figure 2.12 for butenes thermodynamic data). Concomitantly, *n*-butane appears as a product of the hydrogenation of C₄ species from 150 °C onwards. This clearly suggests that competitive adsorption, hence the strong adsorption of 1,3-butadiene on Cu, is a key factor in the high selectivity for alkadiene conversion, as side reactions such as isomerization or further hydrogenation of alkenes only take place once the 1,3-butadiene concentration is severely depleted in the reactor, and hence also low in concentration at the surface of the Cu particles.

The phenomena described above can be compared to what was observed for the Pd-based catalysts for which the preferential adsorption of alkynes and dienes makes it possible to maintain high alkenes selectivity up to relatively high conversion, although the hydrogenation rate of adsorbed ethene is for instance about one hundred times higher than that of adsorbed ethyne.^{181,182}

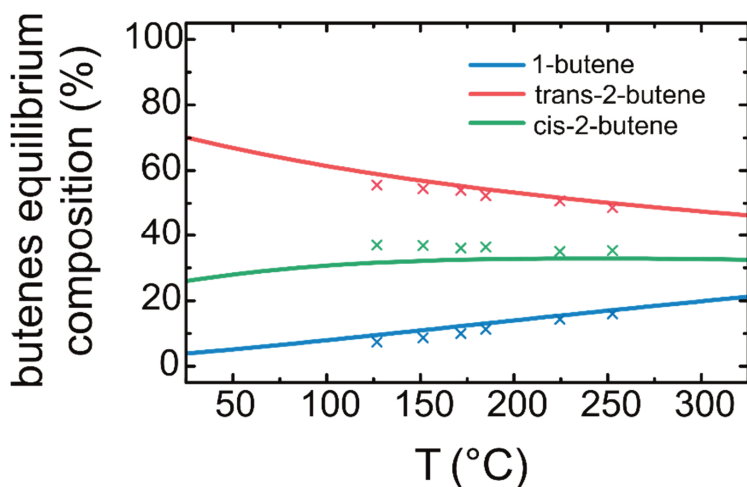
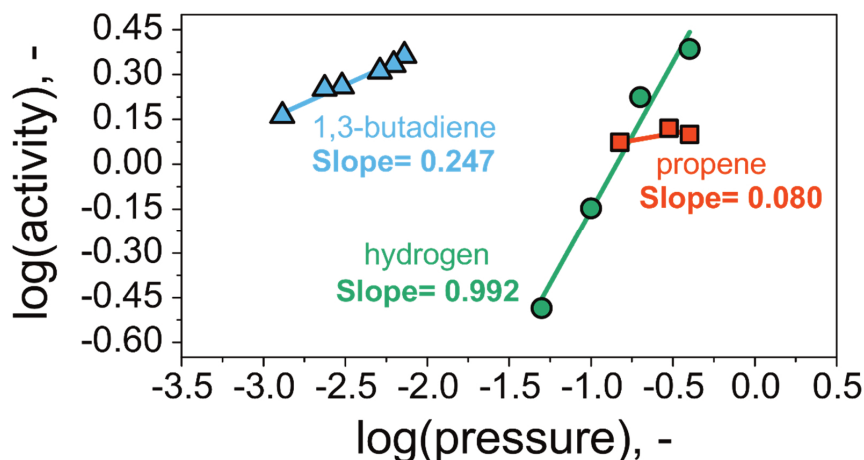


Figure 2.12 C₄ alkenes equilibrium composition as a function of the temperature at atmospheric pressure ($p = 1$ bar). Solid lines: as calculated via HSC Chemistry 7 from an equimolar mixture (1:1:1) of the three butenes (1-butene, *cis*-2-butene, *trans*-2-butene). Crosses: experimentally measured by Maccoll et. al.¹⁸³

Further evidence is provided by analyzing the reaction kinetics data. From the 1,3-butadiene hydrogenation rate as function of the partial pressure of the reactive species (Figure 2.13), we observed a first-order dependency in H₂ pressure, a fractional positive order in 1,3-butadiene (0.25) and a nearly-zeroth order in propene (0.08). The first-order dependency in hydrogen pressure suggests a low hydrogen surface coverage (linear adsorption regime),^{28,46} in line with the general observation that H₂ adsorbs relatively weakly on Cu.^{28,152} The slightly positive order in 1,3-butadiene can be ascribed to its particularly strong affinity to bind the copper nanoparticles, since almost complete surface saturation is reached.

The low reaction order in 1,3-butadiene is in line with literature reports for experiments involving Ni, Au, Pd and Co.^{28,46,142,184} In addition, this kinetic behavior partially resembles what was observed in case of Pd model catalysts (Pd/Al₂O₃/NiAl(110), Pd > 4 nm),¹⁴² for which the 1,3-butadiene adsorption can be so strong that the hydrocarbon can even limit hydrogen penetrating the adsorption layer and adsorbing onto Pd active sites.¹⁴² Lastly, the near-zeroth reaction order in propene partial pressure shows that the competition of adsorption between the butadiene and propene is strongly in favor of the former.



$$r_{1,3\text{-butadiene hydrogenation}} \propto p_{\text{hydrogen}}^1 p_{1,3\text{-butadiene}}^{1/4}$$

Figure 2.13 Reaction rate order for the selective hydrogenation of 1,3-butadiene over 3nm_Cu/SiO₂ as a function of the 1,3-butadiene, H₂ and propene partial pressure. Log of the activity is defined as the log₁₀ of ($\mu\text{mol}_{1,3\text{-butadiene}}^{\text{converted}} \text{ s}^{-1} \text{ g}_{\text{metal}}^{-1}$) versus the log₁₀ of the reactants pressure.

We hence explain the almost full selectivity to butenes of our Cu/SiO₂ system (Figure 2.11) to the strong preferential bonding of polyunsaturated molecules over mono-unsaturated ones. As long as there is an appreciable 1,3-butadiene concentration, the diene almost fully covers the surface of the Cu catalyst, hindering the hydrogenation and/or isomerization of alkenes (Figure 2.12). Assuming similar intrinsic hydrogenation rates for all the adsorbed hydrocarbons, the selectivity measured for 7nm_Cu/SiO₂ at 130 °C would correspond to a 1,3-butadiene to propene surface coverage ratio of 50:1. Conversion of butenes (mainly 1-butene) was limited, which indicates that butenes once formed, then rapidly desorb from the copper surface.

An adsorption/desorption-driven selectivity was already predicted computationally in the case of hydrogenation of alkynes/alkenes mixtures, such as ethyne/ethene,¹⁵⁸

propyne/propene over Cu and Ni¹⁸⁵ as well as the hydrogenation of enynes over Cu.¹⁸⁶ In a recent study on the selective hydrogenation of 1-phenyl-1-propyne in batch reactor, the authors found that Cu/SiO₂ has no intrinsic selectivity towards alkenes formation at full conversion since the apparent rate of hydrogenation of the alkene to the alkane is faster than that of hydrogenation of the alkyne to the alkene.¹⁸⁷ They rather assigned the high selectivity to alkenes to a competitive substrate adsorption on the Cu nanoparticles with the adsorption constant of the alkyne on Cu/SiO₂ being orders of magnitude higher than that of the alkene.

Lastly, a comparison with the literature reveals that the propene conversion values here obtained (Figure 2.11A) are much more favorably low than that for other Cu-based catalysts in literature (0.1-1%), as measured under similar reaction conditions (Cu/TiO₂,⁹¹ Cu-Zn/TiO₂,¹⁵⁷ Cu-Au/TiO₂ and Au/TiO₂⁵²). Our Cu/SiO₂ systems also outperform Pd-based NPs (generally propene conversion >1%, same conditions),¹⁸⁸ single-atom Pd and Pt/Cu (~0.1 and ~1% propene conversion; corresponding gas feed: 1.9/2% butadiene, 70/20% propene, 4.7/16% hydrogen and balance He, respectively),^{146,189} Au/SiO₂ catalysts (for which the conversion of propene was already particularly low, <0.1%, same conditions)^{148,149} or PdAu bimetallic nanorods (selectivity to butenes below 90%, same conditions).¹⁸⁸ To the best of our knowledge our high butenes selectivity (>98%) under these conditions is only rivalled by that reported for Cu-based catalysts obtained via carbonization of MOFs (HKUST-1, 50 wt.% Cu).¹⁹⁰

2.8 – Conclusions

Copper nanoparticles (~3 and ~7 nm) supported either on silica gel or on surface-oxidized graphitic carbon were synthesized and used as catalysts for the selective hydrogenation of 1,3-butadiene in the presence of a 100-fold excess of propene. A new protocol for the measurement of catalytic data for Cu-based hydrogenation catalysts was developed, which is a more reliable alternative to the ramp-up methodology. The catalysts exhibited full conversion of the alkadiene at mild temperatures (130–170 °C). The conversion of propene at almost full 1,3-butadiene consumption was generally less than 0.2 % (0.01% for the 7 nm Cu/SiO₂ system) and the total selectivity to butenes was above 94% for all the catalysts (up to 99% for the same catalyst 7 nm Cu/SiO₂). For both Cu catalysts, conversion of propene and butenes to alkanes remains limited even at temperatures well above the ones required for full 1,3-butadiene conversion (propene conversion <1% at 190 °C). Reaction order and detailed product analysis proved that the exceptionally high selectivity can be ascribed to the strong preferential adsorption on the Cu surface of alkadienes rather than alkenes. Furthermore, the 7 nm Cu/SiO₂ retained its initial activity for the full 60 h time-on-stream test at 140 °C.

3 Particle size effects

Abstract

In the previous chapter we discussed the promising stability and selectivity of nanosized Cu supported on SiO₂. Differences in behavior between 3 and 7 nanometer Cu suggests possible size-dependent catalytic performance. In this chapter we discuss in more details Cu particle size effect in the selective conversion of 1,3-butadiene. To this end, we synthesized and investigated activity and selectivity of 2, 3, 4, 7 and 10 nanometers Cu supported on SiO₂. The catalysts exhibited particle size-dependent activity, with particles above 4 nm being 3 to 4 times more active than the 2 nm ones, and at the same time more selective (up to 99% at almost full butadiene conversion for 7-10 nm particles). The higher activity of larger particles was ascribed to a higher fraction of kinks and step sites, essential to activate hydrogen. The high selectivity of nanoparticulate Cu catalysts was explained by a very strong preferential adsorption of 1,3-butadiene compared to mono-olefin (propene) adsorption on the Cu surface (in particular on larger particles), as proven via adsorption measurements. These findings may guide both testing and catalyst design for reactions where hydrogen surface availability and selectivity play a key role.

This chapter is based on: Totarella, G., de Rijk, J. W., Delannoy, L., de Jongh, P. E. (2022). Particle Size Effects in the Selective Hydrogenation of Alkadienes over Supported Cu Nanoparticles. *ChemCatChem*, 14(19), e202200348.

3.1 – Introduction

As introduced in **Chapter 1** of this thesis, catalytic reaction can be classified as either dependent of or independent of particle size (often referred to as structure insensitive or sensitive, as the exposed facets and active surface sites of the metal nanoparticle changes with particle diameter).^{63,64,191,192} Structure insensitive reactions, or better, reactions for which the weight-based activity scales linearly with the metal specific surface area, benefit from the presence of smaller particles due to increased surface (catalytic) area. In the case of particle-size (or structure) dependent^{63,64,191,192} reactions, certain particle sizes give optimal catalytic performance and non-monotonic dependencies might appear.^{63,64,191,192} In principle, all catalysts based on nanoparticles are actually expected to show activity dependent on size, if the particles are made sufficiently small.

Hydrogenation of (poly)unsaturated hydrocarbons, a well-studied model reaction for selective hydrogenation catalysts and very relevant in industrial applications,^{52,121,140,158,193,194} is considered to be a structure insensitive reaction for most substrates and most transition metal surfaces.^{63,195–197} This is well documented in particular for ethylene hydrogenation and other alkene hydrogenations that do not involve C-C cleavage.¹⁹⁸ Hydrogenation of alkynes and dienes presents more challenges, as multiple hydrogenated products are possible. In this case not only the activity of the catalyst must be taken into consideration, but also its selectivity. Results discussed in **Chapter 2** suggest that the 1,3-butadiene hydrogenation in presence of propene over Cu nanoparticles might indeed display particle size dependent activity and selectivity.

In order to systematically study particle size effects, we prepared a series of supported Cu catalysts with different Cu particle sizes and tested them for the hydrogenation of trace amount (3000 ppm) of 1,3-butadiene in an excess of propene. For the synthesis of differently sized, well-defined Cu particles, we built on previous literature on incipient wetness impregnation for supported Cu.^{26,27,105,106} Methods were adapted in order to synthesize nanoparticles in the size range 2-10 nm supported on SiO₂. The samples were evaluated at different gas flows and reactor loadings in order to compare the catalyst selectivity at similar temperature and 1,3-butadiene conversion. Finally, 1,3-butadiene and propene adsorption/desorption experiments helped to explain the trends in catalyst selectivity.

3.2 – Experimental section

Details on the chemicals used for the synthesis and gas feeds are reported in **Chapter 2** in **section 2.2**. Cu nanoparticles on silica were synthesized via incipient wetness impregnation and drying following a method reported elsewhere for silica (SiO₂) gel supports.^{26,105,106} The impregnation solution concentration and the thermal treatment conditions were tweaked to obtain particles of 2, 3, 4, 7 and 10 nm (final Cu weight loading equal to 5.7 wt.%, except for 4 nm Cu, for which the weight loading was equal to 10.5 wt.%). After synthesis, all samples

were left to cool to room temperature, purged with 20 vol% O₂/N₂ flow (100 mL min⁻¹ g⁻¹) and heated up to 250 °C in the same gas mixture (heating ramp of 2 °C min⁻¹, isothermal hold of 2 h, 100 mL min⁻¹ gas flow for each gram of dry material). The samples (supported CuO nanoparticles) were exposed to air and stored in closed vials at room temperature. Details regarding the methodologies used for the structural characterization of the synthesized catalysts can be found in **Chapter 2 section 2.2**.

Catalytic tests. Catalytic tests were performed using a tailor-made gas-phase hydrogenation set-up described in Chapter 2 section 2.2 (see also ref.¹⁴⁹). The experiments were carried out by loading a mixture of each individual sample (sieve fraction 75–150 μm; total amount of copper loaded in the reactor 1.28 mg unless otherwise specified), and 150 mg SiC as thermal diluent (sieve fraction 212–425 μm) in a U-shaped Pyrex packed bed microreactor (internal diameter 4 mm). Prior to the test, the catalysts were reduced in situ under pure H₂ flow (50 mL min⁻¹) from RT to 250 °C (ramp 2 °C min⁻¹) and kept at 250 °C for 90 min. Hereafter, the catalysts were put into contact with the reaction mixture (0.3% butadiene, 30% propene, 20% hydrogen, and helium for balance with a flow rate of 50 NmL min⁻¹, 1 bar, unless otherwise specified). Tests were conducted at temperatures between 100 and 200 °C. The concentrations of the products and unconverted reactants was monitored every 15 minutes via gas chromatography using a Flame Ionization Detector (GC-FID, hydrocarbons detected: C₁-C₄). The composition of the gas mixture fed into the reactor was monitored at the beginning and at the end of each catalytic run by by-passing the reactor bed.

Calculated turnover frequencies expressed as mmol of H₂ consumed per h per mmol of Cu surface atoms (TOF, h⁻¹) were here defined as follows:

$$TOF = \frac{pQ_{tot}}{RT 10^6} \left[\left(\sum_i C_{butene_i} \right) + C_{n-butane} + C_{propane} \right] * \frac{1}{S_{Cu} w_{Cu} 1.46 \cdot 10^{19} / N_{AV}}$$

Where p is the reactor pressure (1 bar), Q_{tot} is the total volumetric flow rate to the reactor (3 L h⁻¹ @ STP, with the assumption that inlet and outlet flow rate remained constant, since the highly diluted system), R is the ideal gas constant, T is the temperature at which the TOF is calculated, C terms are the concentration, expressed in ppmv, of all products of the reaction (1-butene, trans-2-butene, cis-2-butene, n-butane and propane), S_{Cu} is the exposed Cu surface area (calculated as $S_{Cu} = 6000/d_{TEM}\rho_{Cu}$, where d_{TEM} is the mean particle diameter and ρ_{Cu} is the copper density, 8.92 g cm⁻³), w_{Cu} is the amount of Cu loaded inside the reactor, $1.46 \cdot 10^{19}$ is the number of Cu atoms per square meters of Cu exposed surface area¹⁰⁶ and N_{AV} is the Avogadro number ($6.022 \cdot 10^{23}$).

The total selectivity to butenes was defined as follows:

$$\text{Total selectivity to butenes} = \frac{C_{1\text{-butene}} + C_{\text{trans-2-butene}} + C_{\text{cis-2-butene}}}{C_{1\text{-butene}} + C_{\text{trans-2-butene}} + C_{\text{cis-2-butene}} + C_{\text{butane}} + C_{\text{propane}}}$$

while the 1,3-butadiene to butenes selectivity was calculated as:

$$\text{1,3-butadiene to butenes selectivity} = \frac{C_{1\text{-butene}} + C_{\text{trans-2-butene}} + C_{\text{cis-2-butene}}}{C_{1,3\text{-butadiene}}_{\text{in}} - C_{1,3\text{-butadiene}}_{\text{out}}}$$

In every case, C_i denotes the concentration (expressed as ppmv) of each individual product of the reaction.

Hydrocarbons adsorption/desorption tests. Propene and 1,3-butadiene adsorption tests were carried out by adapting the set-up used for the catalytic tests. In particular, the GC sampling line was connected to a fast mass spectrometer apparatus (Hiden Analytical QGA) and the reactor (4 mm ID) was replaced with a larger one (12 mm ID) to accommodate a larger amount of catalyst. Prior to the measurement, 900 mg of pristine catalyst was loaded into an 8mm ID reactor and pre-reduced in situ under pure H_2 flow (50 mL min^{-1}) from RT to $250 \text{ }^\circ\text{C}$ (ramp $2 \text{ }^\circ\text{C min}^{-1}$) and kept at $250 \text{ }^\circ\text{C}$ for 90 min. The gas atmosphere was then switched to pure N_2 (50 mL min^{-1}) for 5 minutes at $250 \text{ }^\circ\text{C}$ and then the reactor was rapidly cooled down in the same N_2 atmosphere to $30 \text{ }^\circ\text{C}$. After 15 minutes of temperature stabilization and gas mixture background measurement, the gas atmosphere was switched to either 0.3% 1,3-butadiene in He (25 mL min^{-1} total) or 0.6% propene + 0.3% 1,3-butadiene in He (25 mL min^{-1} total; gas mixture concentrations were chosen in order to have a reliable control on the gas flow and optimal temporal resolution).

Data were collected every 15 seconds until steady state concentrations of the gas at the inlet of the reactor were reached. For one selected sample (7 nm Cu particles on SiO_2), a DSC measurement was carried out after saturation in 0.3% 1,3-butadiene in He (25 mL min^{-1} total). The transfer of the sample in DSC sample holder was done in glovebox and the measurement was done in dry and air-free environment, under constant Ar flow (heating/cooling ramp of $10 \text{ }^\circ\text{C min}^{-1}$).

3.3 – Synthesis results and structural characterization

A summary of the parameters used to produce the differently sized Cu nanoparticles is reported in Table 3.1. Transmission electron micrographs as well as particle size distribution for the synthesized catalysts are shown in Figure 3.1, while the relative average Cu particle size and width of the distribution can be found in Table 3.1. In particular, impregnation of the silica gel with 1 M solution of $\text{Cu}(\text{NO}_3)_2$ followed by either heat treatment in i) N_2 (350 mL min^{-1} , $2 \text{ }^\circ\text{C min}^{-1}$, 2 h at $350 \text{ }^\circ\text{C}$), ii) 20% H_2/N_2 (250 mL min^{-1} , $2 \text{ }^\circ\text{C min}^{-1}$, 2 h at $300 \text{ }^\circ\text{C}$) or iii) 2% NO/N_2 (350 mL min^{-1} , $2 \text{ }^\circ\text{C min}^{-1}$, 2 h at $350 \text{ }^\circ\text{C}$) yielded 2, 3 and 7 nm particles respectively (Table 3.1 and Figure 3.1).

For 2 and 3 nm Cu, nanoparticle diameter spread was 0.6 and 1.0 respectively (as 1σ , standard deviation, of the particle diameter distribution), while for the 7 nm the spread was around 2.4 nm. Particles of around 10 nm were also obtained via thermal decomposition under 2% NO/N_2 , with the difference that the flow was applied in bottom-top configuration (fluidized bed, 350 mL min^{-1}). In this case, the spread was larger and around 4.2 nm. The Cu weight loading of 2, 3, 7 and 10 nm was 5.7 wt%. Particles of around 4 nm were obtained by impregnating the silica gel support with a 2 M solution of $\text{Cu}(\text{NO}_3)_2$ (roughly doubling the Cu weight loading, which was equal 10.5 wt.%) followed by direct reduction under 20% H_2/N_2 (250 mL min^{-1} , $2 \text{ }^\circ\text{C min}^{-1}$, 2 h at $300 \text{ }^\circ\text{C}$). For 4 nm, the width of the particle size distribution was 1.2 nm.

These methods were hence effective in tuning the final particle size distribution of Cu, mostly by varying the decomposition process (temperature and gas atmosphere). As expected, larger particles lead to larger spread in diameters distribution. In order to verify the crystallinity and crystallite size of the obtained Cu nanoparticles, XRD measurements were run on pre-oxidized samples ($300 \text{ }^\circ\text{C}$ under simulated air, 1 h). The pre-oxidation step is necessary in order to obtain a stable Cu phase (in this case CuO, see also **Chapter 2**). CuO nanoparticles XRD profiles can be found in Figure 3.2.

Table 3.1 Synthesis parameters and physicochemical properties of the silica-supported Cu catalysts.

Catalyst	Cu loading [wt%]	Gas atmosphere used during thermal treatment	$T_{\text{treatment}}$ [$^\circ\text{C}(\text{ }^\circ\text{C}/\text{min})$]	$D_{\text{TEM}} \pm \sigma_{\text{TEM}}$ [nm]	d_{XRD} [nm]	S_{Cu} [$\text{mCu}_2 \text{ gCu}^{-1}$]
2nm_Cu/SiO₂	5.7	^A N_2 - 350 mL min^{-1}	350(2)	2.0 ± 0.6	n.a	336
3nm_Cu/SiO₂	5.7	^A 20% H_2/N_2 - 250 mL min^{-1}	300(2)	3.5 ± 1.0	3	192
4nm_Cu/SiO₂	10.5	^A 20% H_2/N_2 - 250 mL min^{-1}	300(2)	4.4 ± 1.2	6	152
7nm_Cu/SiO₂	5.7	^A 2% NO/N_2 - 350 mL min^{-1}	350(2)	7.3 ± 2.4	10	92
10nm_Cu/SiO₂	5.7	^B 2% NO/N_2 - 100 mL min^{-1}	350(2)	9.9 ± 4.2	12	68

^A packed-bed configuration

^B bottom-top flow (fluidized bed)

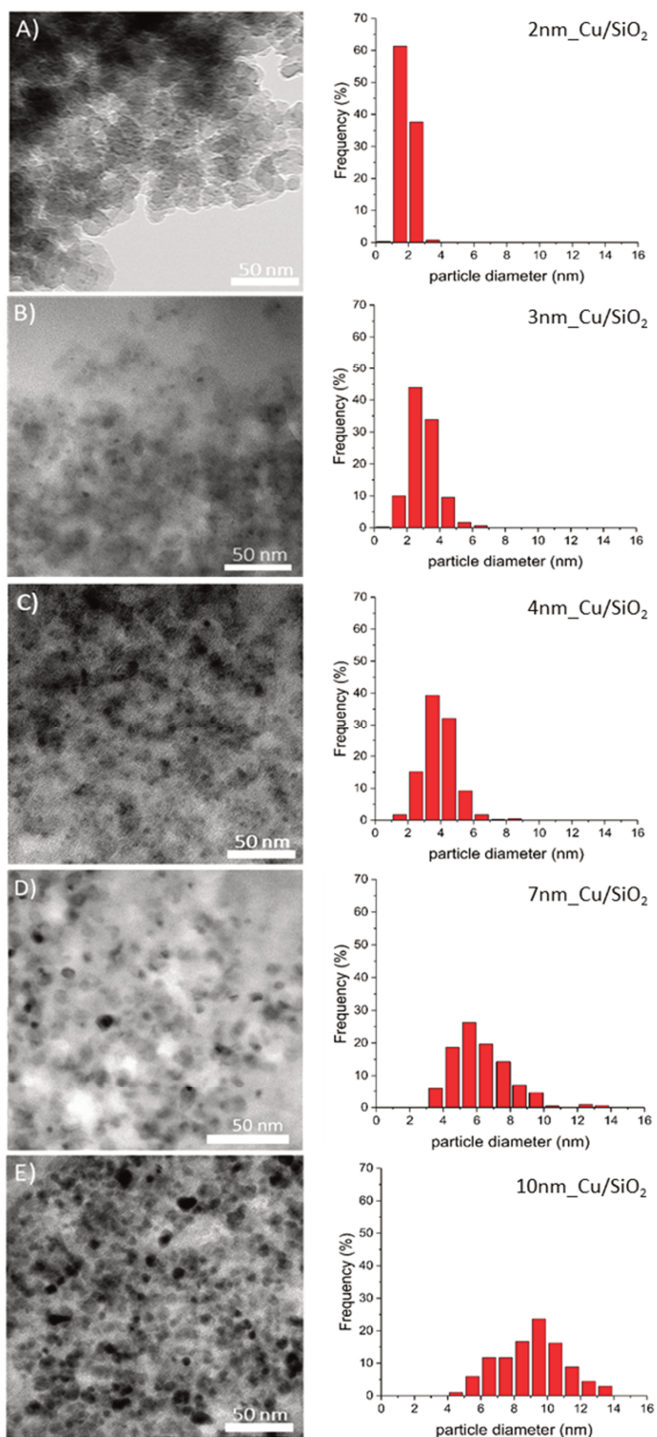


Figure 3.1 Transmission electron micrographs (left) and particle size distributions (frequency counts, right) for the as synthesized A) 2nm_Cu/SiO₂, B) 3nm_Cu/SiO₂, C) 4nm_Cu/SiO₂, D) 7nm_Cu/SiO₂ and E) 10nm_Cu/SiO₂.

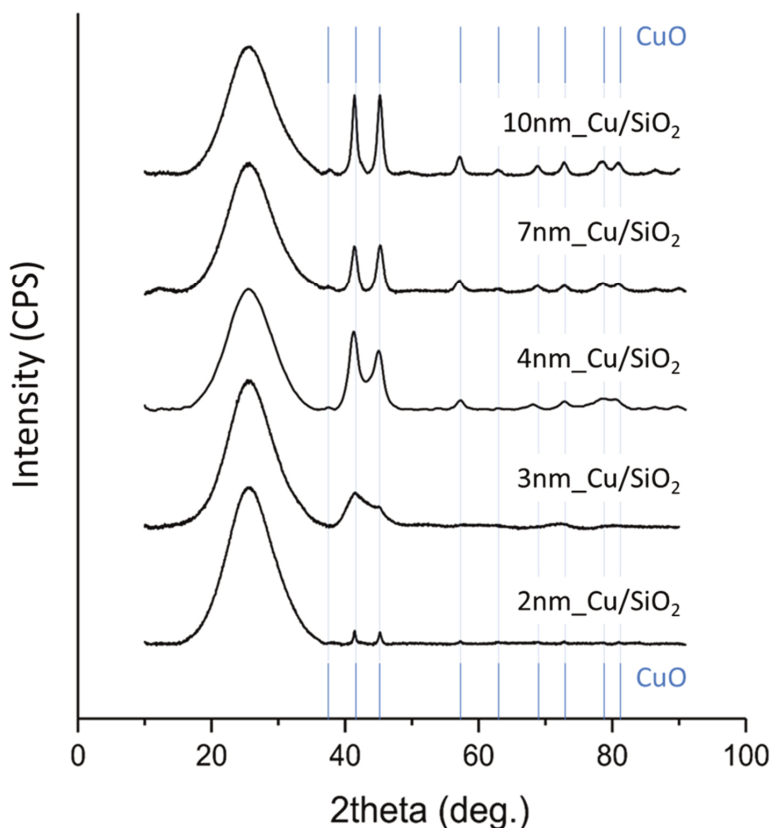


Figure 3.2 X-Ray Diffractograms for the oxidized catalyst samples (CuO) 2nm_Cu/SiO₂, 3nm_Cu/SiO₂, 4nm_Cu/SiO₂, 7nm_Cu/SiO₂ and 10nm_Cu/SiO₂. The materials were prior to the measurements oxidized under dynamic O₂/N₂ atmosphere at 300 °C for 1h. The sample 4nm_Cu/SiO₂ has double the weight loading of the remaining samples (10.5 wt% vs 5.7 wt%). Large peak at 25 2theta degree: SiO₂. CuO peaks marked in the image.

The CuO crystallite sizes obtained from the XRD characterization were in good agreement with the particle sizes measured by TEM in almost all cases. The only exception was 2 nm Cu, which displayed very low-intensity sharp peaks, suggesting a (limited) presence of larger crystallites. However, the low intensity suggests that the vast majority of CuO is present either as amorphous or as very small particles, for which crystalline order is limited due to the restricted diameter. To conclude, we hereby show that controlling the synthesis conditions, such as temperature and reactive atmosphere, can be an excellent method to achieve good control over the CuO/Cu particle size in the range of 2 to 10 nm.

3.4 – Particle size effect on catalyst activity

Figure 3.3 shows the evolution of the concentration of all C₄ species as function of reaction temperature for different catalysts. Data for 3 and 7 nm were shown already in **Chapter 2**, but are repeated here for convenience. All catalysts were pre-conditioned by exposing them to the reaction mixture for 15 h at 130 °C as described in detail in **Chapter 2**. We focus here on discussing the results for 2nm_Cu/SiO₂ and 4nm_Cu/SiO₂, as a detailed comparison of activity and selectivity of all 5 catalysts is reported later in this section as well as in section 3.5.

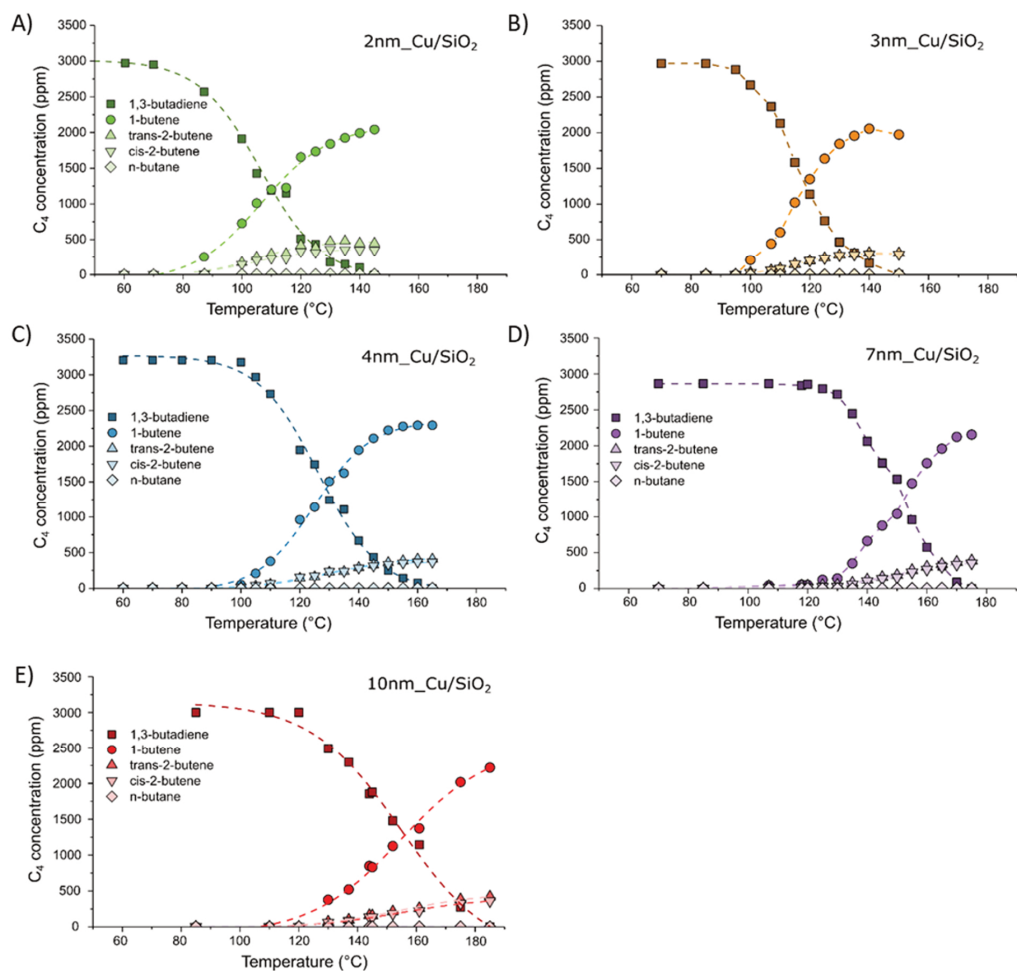


Figure 3.3 Concentration profiles for the reactant 1,3-butadiene and its hydrogenation products, as function of the reactor temperature for the catalysts A) 2nm_Cu/SiO₂, B) 3nm_Cu/SiO₂, C) 4nm_Cu/SiO₂, D) 7nm_Cu/SiO₂ and E) 10nm_Cu/SiO₂. The data were collected under steady-state conditions. Heating ramp= 0.5 °C min⁻¹. Reaction conditions: butadiene/propene/H₂/He= 0.15/15/10/24.85 mL min⁻¹, 1 bar(a) and 1.28 mg of Cu loaded (2.56 mg for 10nm_Cu/SiO₂). GHSV: 35 000 h⁻¹.

For 2 and 4 nm Cu, conversion of 1,3-butadiene was detected at temperatures as low as 100 °C. The main products of hydrogenation were 1-butene (>70%), followed by trans- and cis-2-butene (produced in similar amounts, around 10-15% at $T > 120$ °C). Only traces of butane were formed. Full 1,3-butadiene conversion (1,3-butadiene concentration below 50 ppm) was reached at 140 °C for the 2nm_Cu/SiO₂ catalyst and 160 °C for the 4nm_Cu/SiO₂ sample, respectively. The 1,3-butadiene concentration profiles obtained for 2 and 4 nm Cu on SiO₂ show a similar shape and slope, suggesting that both catalysts have comparable activation energies for the hydrogenation of the alkadiene. The 2 nm catalyst appears to be more active per Cu unit mass than the 4 nm catalyst. In fact, the temperature for which 50% conversion of 1,3-butadiene is reached is 106 °C and 126 °C respectively for 2 and 4 nm particles.

To better compare the differences in activity, the experiments were repeated at similar conversions and in the same temperature range (100 – 170 °C) by adjusting the amount of catalyst loaded in the reactor. An example of 1,3-butadiene conversion vs. temperature profiles is reported for the catalysts 2 and 4 nm Cu in Figure 3.4A (the 1,3-butadiene molar flow rate to the reactor was kept the same, specifically 0.552 mmol h⁻¹ 1,3-butadiene).

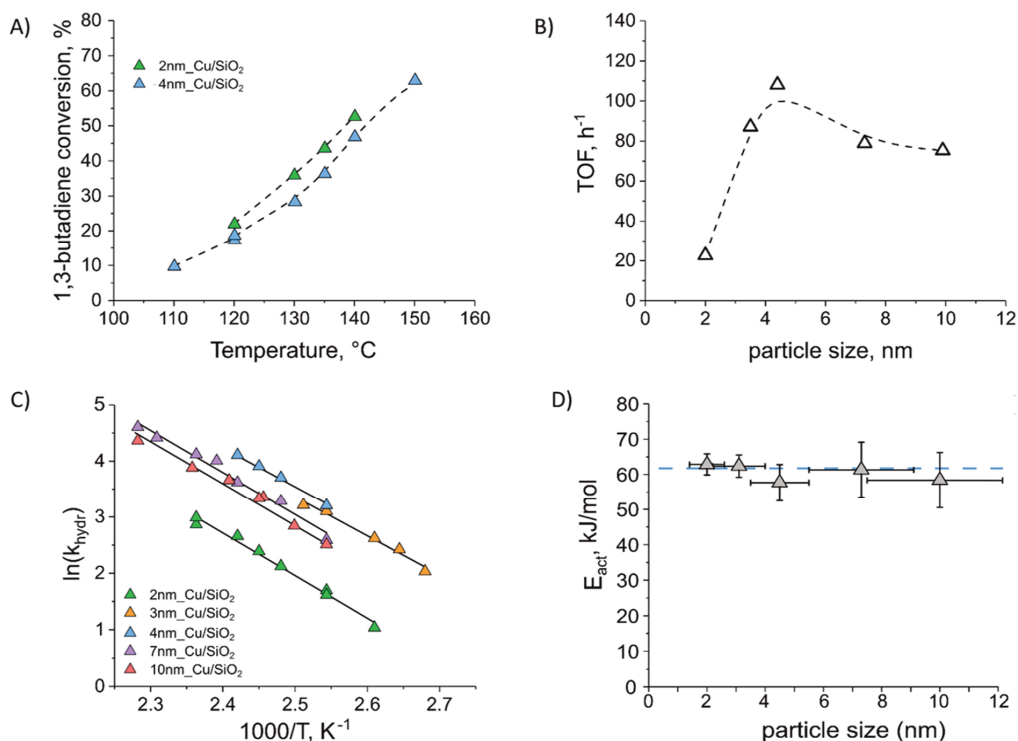


Figure 3.4 A) 1,3-butadiene conversion experiments carried out at similar conversion level for 2 and 4 nm particles. B) turnover frequencies (TOF) calculated at 130 °C from total hydrogen consumptions for all different particle sizes investigated; C) Arrhenius plot and D) activation energy vs. Cu particle size for the 2, 3, 4, 7 and 10 nm Cu on SiO₂ catalysts as calculated from 1,3-butadiene consumption rates.

As it can be observed from the data reported in Figure 3.4A, similar 1,3-butadiene conversions were achieved when tested with copper loadings of $0.417 \text{ m}_{\text{Cu}}^2$ for 2nm_Cu/SiO₂ (45% conversion) and $0.099 \text{ m}_{\text{Cu}}^2$ for 4nm_Cu/SiO₂ (50% conversion). This corresponds to that the 4 nm particles are around 4 times more active than 2 nm ones per unit Cu surface area. This difference is also reflected in the turnover frequencies (mmol of H₂ consumed per hour per mmol of Cu present at the nanoparticle surface, see **section 3.2** for calculation) as calculated at 130 °C for all catalysts. The data for 2, 3, 4, 7 and 10 nm Cu on SiO₂ is reported in Figure 3.4B. As expected from the results discussed in Figure 3.4A, the TOF of Cu nanoparticles increased 4-fold by going from 2 to 4 nm Cu (24 h^{-1} vs. 107 h^{-1} , Figure 3.4B).

To summarize, varying the particle size above 4 nm resulted in a limited change in activity. For instance, 7 and 10 nm Cu only 20% less active than 4 nm Cu on SiO₂, and around >3 times more active than 2 nm particles. Importantly, the 7 and 10 nm particles were already shown to retain their particle size after activity testing during previous experiments (see **Chapter 2** and ref.²⁶). We hereby also tested smaller particles (2 nm) for changes in particle size distribution, as smaller particles might be more prone to growth. Also in this case, we did not observe substantial changes in Cu particles diameter distribution (see Figure 3.5).

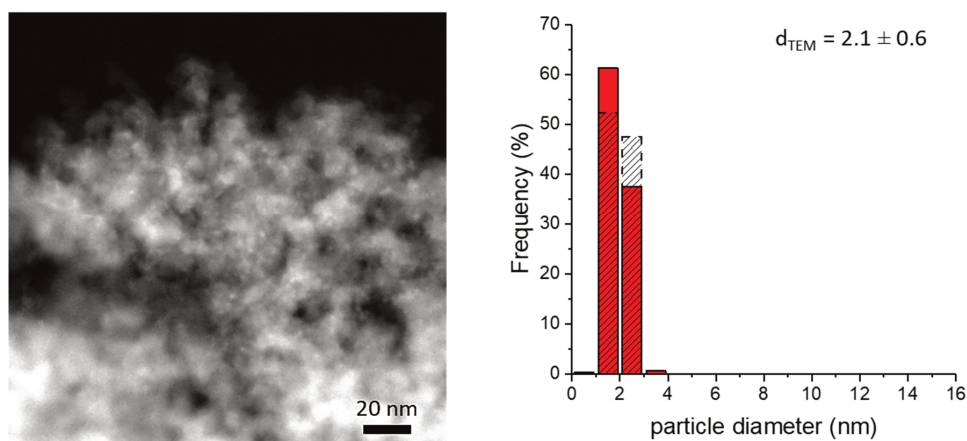


Figure 3.5 DF-TEM A) and particle size distribution B) for the used 2nm_Cu/SiO₂ catalyst. In the histogram, the red area represents the particle size distribution of the fresh catalyst (same as Figure 3.1A), the shaded area represents the particle size distribution of the used catalyst.

Lastly, to assess the origin of the difference in activity between particles, the conversion data were modelled in terms of Arrhenius plots (Figure 3.4C). The kinetic model applied for the study of the 1,3-butadiene conversion data is based on the work described in **Chapter 2**, while the packed bed reactor design equation (integral form) used for extrapolating the kinetic constant is reported in ref.¹⁹⁹ The reaction rates were normalized to the Cu surface area instead of catalyst weight (Cu surface areas are reported in Table 3.1 as S_{Cu} , calculations can be found in **Chapter 2**). The activation energy for the hydrogenation of 1,3-butadiene was

independent of the Cu particle size (Figure 3.4D). In particular, a value of E_{act} equal to 62 ± 3 kJ mol⁻¹ was found, well in line with previously reported data for the hydrogenation of 1,3-butadiene from alkene-free streams on model systems.²⁸ The difference in catalyst activity is hence due to the different pre-exponential A values (reported in Table 3.2 as A_{bd}). The 4 nm Cu on SiO₂, the most active catalyst as normalized per Cu area, showed ~4 times higher pre-exponential factor, hence activity, than the smallest Cu nanoparticles investigated.

Table 3.2 Pre-exponential factor for the 1,3-butadiene hydrogenation to butenes (A_{bd}), propene hydrogenation in absence of 1,3-butadiene (A_{p}), propene hydrogenation in presence of 1,3-butadiene (A_{pwbd}) and the ratio between A_{p} and A_{pwbd} .

Sample name	A_{bd} (mol s ⁻¹ m ⁻² bar ^{-1.25})	A_{p} (mol s ⁻¹ m ⁻²)	A_{pwbd} (mol s ⁻¹ m ⁻²)	Ratio $A_{\text{p}}/A_{\text{pwbd}}$
2nm_Cu/SiO ₂	271	0.093	0.011	8
3nm_Cu/SiO ₂	1168	0.055	0.007	9
4nm_Cu/SiO ₂	1320	0.010	0.001	12
7nm_Cu/SiO ₂	809	0.033	n.a.*	n.a.*
10nm_Cu/SiO ₂	704	0.180	0.0003	700

*propane concentration too low for performing Arrhenius plot fitting.

The same activation energy for the different Cu particle sizes suggests that the nature of the active site involved in the determining step for the hydrogenation of 1,3-butadiene to butenes is the same in all catalysts. This indicates that size-dependency of the activity, especially in the range 2-4 nm, is probably linked to structural/geometric effects than electronic ones.

By assuming the same reaction pathway for the hydrogenation of 1,3-butadiene on all the differently sized Cu nanoparticles, the numerical value of the pre-exponential factor (Table 3.2) can hence be used as an indirect measure of the relative abundancy of active sites, or “active site – reactant” adducts. Furthermore, the 1,3-butadiene reaction rate order is first-order in hydrogen pressure, zeroth order in propene pressure and fractional (0.25) order in 1,3-butadiene partial pressure (see **Chapter 2**). The reaction rate is hence limited by the availability of activated hydrogen on the surface of the Cu nanoparticles.⁷ This is in agreement with literature evidence of low deuterium-hydrogen exchange for Cu catalysts under typical hydrogenation conditions, pointing out to low concentration of activated hydrogen on the Cu surface.^{46,147}

An analogous effect of the nanoparticle size on Cu activity, with a maximum at diameters above 4-6 nm, was observed for other gas phase hydrogenation reactions. In the case of methanol synthesis, van der Berg *et al.*^{7,27}, for instance, observed an increase in TOF by a factor of 3 going from 2 to 8 nm copper particles for both Cu and promoted Cu (CuZn) supported nanoparticles. Structural effects on the hydrogenation activity of Cu nanoparticles were observed also in case of the hydrogenation of ethyl acetate to ethanol for carbon-

supported Cu.²⁷ In this case, a maximum activity was observed at 6 nm, which stayed rather constant up to 13 nm Cu. In both cases the authors ascribed the observed effect to the reaction taking place at surface sites with a unique configuration of several copper atoms such as step-edge and kink sites, identified as responsible for H₂ activation.

The observation that not all Cu atoms on the surface of NPs have the same reactivity (in the size range below 10 nm) has also been reported in recent literature.²⁰⁰ The activity trends described in this work, as well as in ref.^{7,27}, correlate with the theoretical fraction of Cu step (B5A, B5B on fcc metals) and kink (B6) surface sites, usually found at the interface of Cu(111) and Cu(100) (the geometrical equivalent of high Miller index Cu(311), Cu(221), Cu(321) planes). The maximum relative abundance of these sites is interestingly expected at around 4-6 nm.^{7,27,201-203}

In conclusion, the 1,3-butadiene hydrogenation activity described in this work strongly correlates to the abundance of step and kink sites over the Cu surface. These in turn control the surface availability/concentration of hydrogen and henceforth the reaction rate. This activity pattern seems to be in common with other Cu-catalyzed gas phase hydrogenations.

3.5 – Particle size effects on catalyst selectivity

The selectivity of the catalysts was evaluated in terms of butenes produced (1-butene + trans-2-butene + cis-2-butene) against i) the consumption of 1,3-butadiene (Figure 3.6A, see equation in section 3.2) and ii) the total amount of hydrogen consumed by the catalyst (Figure 3.6B, see equation in section 3.2). The first captures the ability of the catalyst to hydrogenate 1,3-butadiene to butenes without further over hydrogenation to butane. The second reflects the ability of the catalyst to hydrogenate 1,3-butadiene preferentially over other alkenes in the stream (i.e., propene), which helps understanding alkadiene-alkene hydrogenation competition as well as being a critical parameter in practical application.^{52,121,140,158,193,194} As the concentration of propene in the gaseous reaction mixture is very high (30%, versus 0.3% 1,3-butadiene), conversion of a small fraction of the propene can drastically lower the total selectivity of the catalyst (e.g. 100% 1,3-butadiene conversion and 1% of propene conversion corresponds to a catalyst selectivity of 50%).

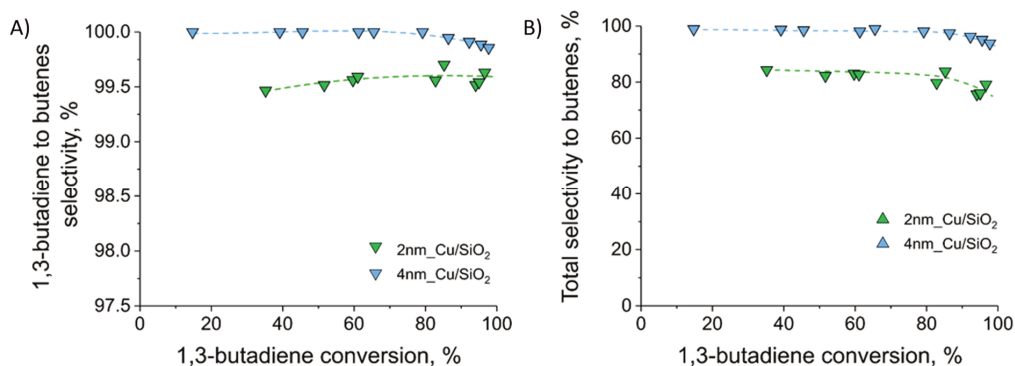


Figure 3.6. A) 1,3-butadiene to butenes selectivity (ratio between production rate of butenes to consumption rate of 1,3-butadiene) as function of 1,3-butadiene conversion; B) total selectivity to butenes as a function of 1,3-butadiene conversion. Samples: pre-reduced 2 and 4 nm Cu. Dashed lines are guide for the eye. Note: axis in figure A and B have different scaling.

The catalyst that displayed the lowest 1,3-butadiene to butenes selectivity in the entire series was 2nm_Cu/SiO₂. The selectivity for this catalyst, however, was still rather high due to very limited formation of n-butane (1,3-butadiene to butenes selectivity above 99%, Figure 3.6A). Catalysts with larger particle size displayed formation of similar amounts of n-butane, usually well below 50 ppm (see Figure 3.3), and hence a 1,3-butadiene to butene selectivity >99.5% in the entire 1,3-butadiene conversion range investigated (e.g., see Figure 3.6A for 4nm_Cu/SiO₂). In terms of n-butane formed, the catalysts displayed similar behavior within measurement error.

The total selectivity to butenes was above 70% for all the catalysts investigated, with the 4nm_Cu/SiO₂ exhibiting the highest selectivity (Figure 3.6B). A minor selectivity decrease

was found at high diene conversions for 4 nm Cu (from 98.8 % to 93.8 % selectivity by going from 65 to 98 % 1,3-butadiene conversion). For the 2nm_Cu/SiO₂, the selectivity also slightly decreases with increasing the 1,3-butadiene conversion, from 85 % at 35 % conversion to 78 % at 98 % 1,3-butadiene conversion.

What really differentiated the different samples was the amount of propene consumed, which varied drastically between the different particle sizes, thus affecting the total selectivity of the catalyst. To better highlight the difference in behavior of the different catalysts regarding the unselective conversion of propane, Figure 3.7 displays the concentration of propane produced against the conversion of 1,3-butadiene. For instance, at 80% 1,3-butadiene conversion the concentration of propane produced by 4 and 2 nm was 10 and 550 ppm, respectively. In addition, the amount of propane formed for 4, 7 and 10 nm particles was below 50 ppm and comparable. As major differences in selectivity were driven by conversion of propane to propene (instead of over-hydrogenation of 1,3-butadiene to butane), the rest of the discussion will focus on the total catalyst selectivity (see **section 3.2**).

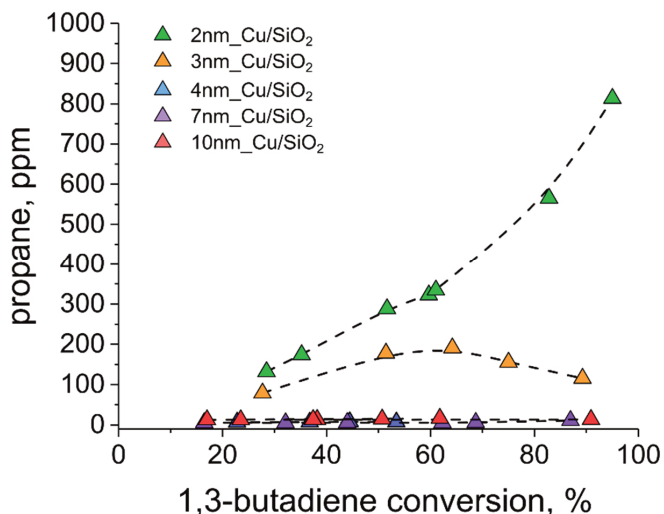


Figure 3.7 Propene concentration vs. 1,3-butadiene conversion for 2nm_Cu/SiO₂, 3nm_Cu/SiO₂, 4nm_Cu/SiO₂, 7nm_Cu/SiO₂ and 10nm_Cu/SiO₂ in the selective hydrogenation of 1,3-butadiene. The conversion of 1,3-butadiene was varied by varying the temperature.

Direct comparison of selectivities is not trivial since the selectivity depends both on the temperature and on the concentration of all the species in the reactor bed during catalysis (see also **Chapter 2**).¹⁸⁴ Hence, tests at the same temperature of 130 °C with varying 1,3-butadiene conversion (5–20 %, see Figure 3.8A) as well as data at a constant 1,3-butadiene conversion of ~80% (Figure 3.8B) are here reported. The data reveal a clear trend in selectivity, with the 2 nm particles being the least selective ones (~75 %) of the entire set (Figure 3.8, frame A and B). Interestingly, the selectivity to butenes increased by going from 2 to 4 nm (74, 87 and 98%, respectively for 2, 3 and 4 nm) and levelled off to more than 95% for 4, 7 and 10 nm

particles (Figure 3.8B). The same trends are observed at higher conversion values. This shows that the larger Cu nanoparticles (equal or above 4 nm) are the most selective ones.

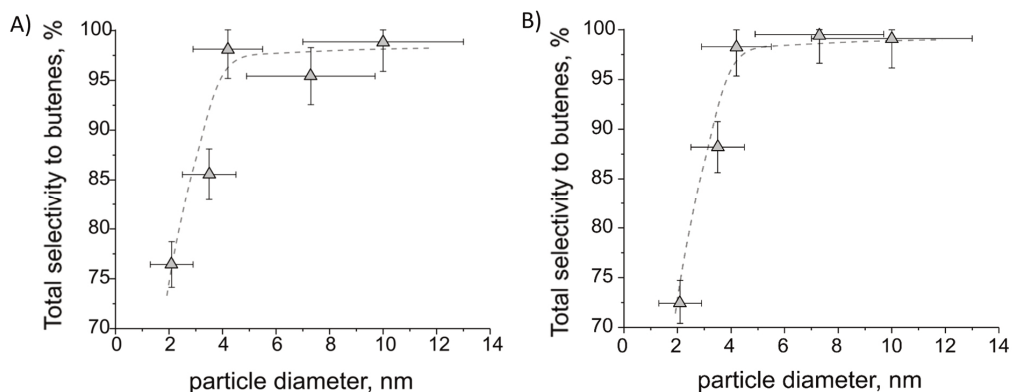


Figure 3.8 Total selectivity to butenes vs. particle diameter for the samples 2nm_Cu/SiO₂, 3nm_Cu/SiO₂, 4nm_Cu/SiO₂, 7nm_Cu/SiO₂ and 10nm_Cu/SiO₂. A) Data measured at constant temperature (130 °C, around 5–20% of 1,3-butadiene conversion); B) Data measured at ~80% 1,3-butadiene conversion. Dashed lines were added to guide the eye.

Separate propene hydrogenation experiments were carried out to clarify the origin of the high catalyst selectivity. The first test was carried out with additional 1,3-butadiene in the reactor feed, the second experiment in its absence. An example of these data can be found in Figure 3.9A for the sample 2nm_Cu/SiO₂. Data are also reported as natural logarithm of the reaction rate of the propene hydrogenation reaction against the reciprocal temperature (frame 3.9B), assuming zero order reaction kinetic in propene and hydrogen (hence the reaction rate is equal to the kinetic constant of the reaction, $k_{\text{prop,hydr}}$). This assumption is justified considering differential conversion conditions, due to rather constant concentrations for propene and hydrogen along the reactor bed. The addition of 1,3-butadiene to the reaction mixture causes a sharp decrease in propane production (almost 10-fold decrease at 150 °C). The drastic decrease of the propene hydrogenation rate by the presence of 1,3-butadiene was observed for all catalysts in the series.

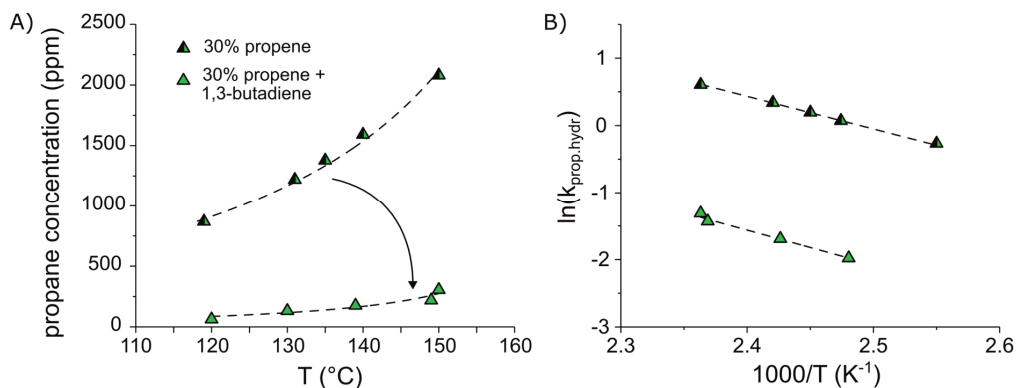


Figure 3.9 A) Concentration of propane produced as function of the temperature during the hydrogenation of 30% propene in He in presence (green half triangles) and absence (green full triangles) of 0.3% of 1,3-butadiene for the sample 2nm_Cu/SiO₂; B) corresponding Arrhenius plot (natural logarithm of the propene hydrogenation kinetic constant vs. 1000/T). Conditions: 1,3-butadiene/propene/H₂/He= 0.15(or 0):15:10:24.85(or 25.00), 1 bar, 5.6 mg Cu. GHSV: 52 500 h⁻¹.

Strikingly, the slope of the Arrhenius curves obtained for the propene-only case (corresponding to $E_{\text{act}} = \text{kJ mol}^{-1}$.) is independent of the presence of 1,3-butadiene (Figure 3.9B; see Figure 3.10A and B for a comparison for all the catalysts). Furthermore, the apparent activation energy for hydrogenation of propene is lower than for 1,3-butadiene (38 vs. 62 kJ mol⁻¹, respectively), but nevertheless propene hydrogenation activity of the sample(s) is strongly hindered by the presence of 1,3-butadiene. The change in reaction rate is hence explained by a change in pre-exponential factor. The ratio between the pre-exponential factors obtained in the case of hydrogenation of propene carried out without and with 3000 ppm of 1,3-butadiene in the reaction mixture was calculated for all the catalysts (see Figure 3.10A and B, as well as Table 3.2, *Ratio A_p/A_{pwb}*). This ratio increases along with the particle size (8, 9, 12 and 700 for 2, 3, 4 and 10 nm Cu on SiO₂ respectively).

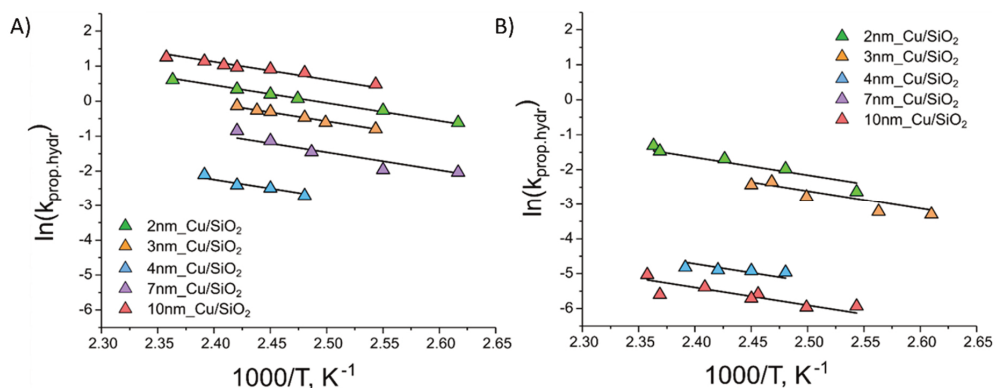


Figure 3.10 Arrhenius plots displaying the natural logarithm of the propene hydrogenation kinetic constant as function of 1000/T for all samples of the series in case of A) absence and B) presence of 3000 ppm of 1,3-butadiene.

Lastly, hydrocarbon adsorption experiments were carried out on two selected catalysts (3nm_Cu/SiO₂, 7nm_Cu/SiO₂) to verify whether the impact of the presence of 1,3-butadiene on the propene hydrogenation can be explained by the stronger adsorption energy for 1,3-butadiene compared to propene (Figure 3.11). During these experiments, pre-reduced catalysts were exposed to either 1,3-butadiene or a mixture of 1,3-butadiene and propene in He (0,6% concentration for each hydrocarbon, 25 mL min⁻¹ total; the conditions were adjusted to have proper time-resolution and hence quantifiable hydrocarbon uptake). The diluent, in this case, acts as both a carrier and a tracer. The delay between the He signal and any of the two hydrocarbons is proportional to the amount of alkadiene or alkene adsorbed. The results, also known as breakthrough curves, are shown in Figure 3.11 in terms of relative amount of 1,3-butadiene and/or propene at the inlet of the reactor (a value of 100% means that the concentration of the specific molecule in the inlet and the outlet of the reactor is the same).

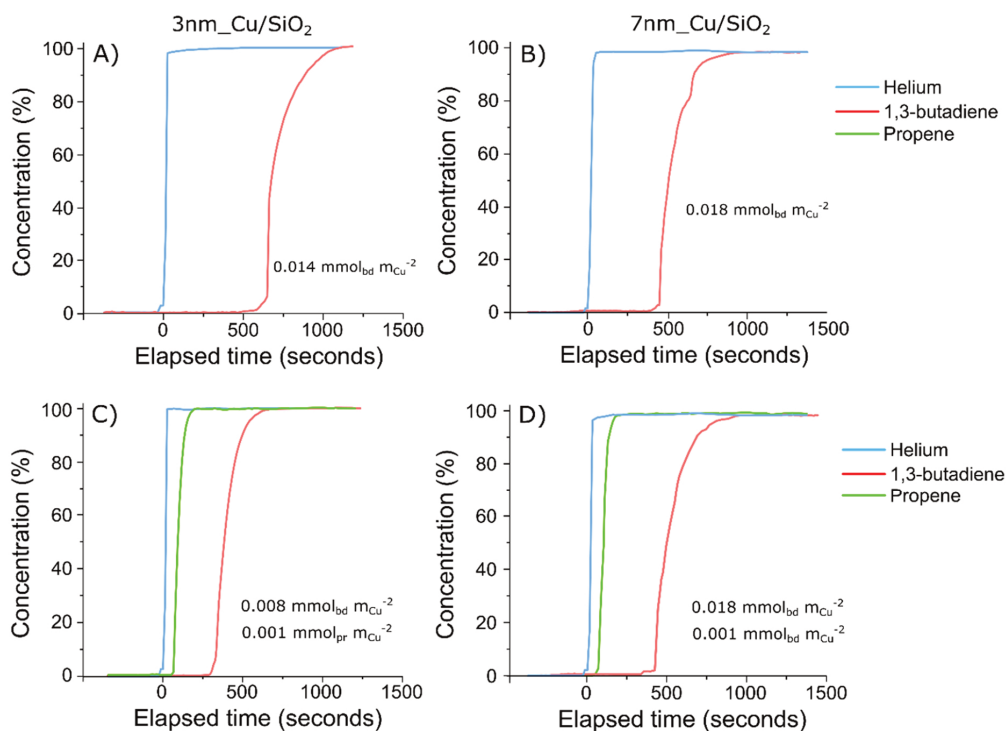


Figure 3.11 Hydrocarbon adsorption experiments for 3nm_Cu/SiO₂ and 7nm_Cu/SiO₂ catalyst. The pre-reduced catalysts were exposed to either i) 0.6% 1,3-butadiene in He (Figure 3.11A: 3nm_Cu/SiO₂, Figure 3.11B: 7nm_Cu/SiO₂) or ii) 0.6% 1,3-butadiene + 0.6% propene in He (the 0.6% propene concentration was adjusted in order to increase the time resolution of the experiment; Figure 3.11C: 3nm_Cu/SiO₂, Figure 3.11D: 7nm_Cu/SiO₂). Helium is used both as diluent and inert tracer. Amount of catalyst loaded = 0.9 g. Gas flow: 25 mL min⁻¹. Temperature = 30 °C.

Reference experiments conducted on pre-dried silica gel only shown simultaneous emission of He and hydrocarbons from the exposed packed bed, hence no hydrocarbon uptake by the support itself. For both the 3 and 7 nm supported Cu nanoparticles, a clear delay in the signal of the hydrocarbons was observed (see Figure 3.11), confirming the uptake of hydrocarbons by Cu nanoparticles. Release of 1,3-butadiene upon heating was verified via DSC experiment for the 7 nm Cu/SiO₂, Figure 3.12. In that case, no endothermic peak was observed for the propene-treated material, while one endothermic peak (with onset at around 120 °C) was observed for 1,3-butadiene treated material (the thermal event was ascribed to the release of 1,3-butadiene from the surface of the catalyst).

In the 1,3-butadiene/He experiments, the amount of 1,3-butadiene adsorbed was equal to 0.014 and 0.018 mmol m_{Cu}⁻² respectively for 3 nm and 7 nm Cu. Upon addition of propene to the mixture, a modest, yet significant amount of propene was adsorbed by both materials (around 0.001 mmol m_{Cu}⁻² for 3 and 7 nm Cu). Interestingly, both materials were able to retain 1,3-butadiene even in presence of propene, with modest to no change in the uptake amount of the diene (unaltered for the 7 nm Cu/SiO₂; while a decrease, from 0.014 mmol m_{Cu}⁻² to 0.008 mmol m_{Cu}⁻² was observed for 3 nm Cu/SiO₂). The observation suggests that the adsorption of 1,3-butadiene was stronger than for propene, in particular for the larger particles. This difference in relative adsorption strength can potentially explain the difference in selectivity between smaller particles (2 and 3 nm) and the more selective larger ones (4 nm and above).

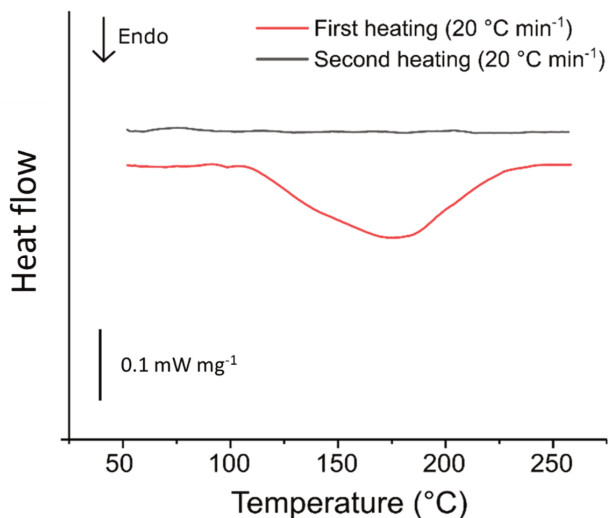


Figure 3.12 Hydrocarbon desorption experiments by means of DSC. The experiment was carried out after saturation pure 1,3-butadiene over 7nm_Cu on SiO₂ particles. The bar on the bottom left represents a heat flow of 0.1 mW per mg of sample loaded. The measurement was done in air-free environment and under Ar flow (heating/cooling ramp of 10 °C min⁻¹). Two consecutive heating ramps were recorded per experiment.

The hydrogenation of 1,3-butadiene and propene displayed different activation energies (62 vs. 38 kJ mol⁻¹, respectively), suggesting that the energy barrier of the hydrogenation reaction is more likely to be the insertion of activated hydrogen on the hydrocarbon substrate rather than hydrogen dissociation. This reinforces the hypothesis that the reaction selectivity depends on the relative concentration of the two hydrocarbons present on the surface, with the reaction kinetic following a Langmuir-Hinshelwood type of mechanism.^{26,145,204} For particles above 2 nm, electronic effects are unlikely. Moreover, electronic effects would be expected to also change the selectivity, as an increase in electron-acceptor character would promote $\pi\sigma$ coordination of the semi-hydrogenated butenyl intermediate (π -butenyl), leading to formation of trans-2-butene at the expenses of 1-butene.^{26,28,150}

A rather similar selectivity to 1-butene was observed for all samples (Figure 3.3), as well as size insensitive activation energies for the hydrogenation of 1,3-butadiene and propene. This strongly suggests that electronic effects cannot explain the dependence of selectivity on particle size. In this work, the lowest selectivity was observed for 2 and 3 nm particles. The surface of these small particles (~2 nm) is known to be rich in corner and edge sites, which concentration drops quickly for larger sizes (5 nm and more, which on the contrary have higher concentration of steps and kinks).^{27,36,201} Their high abundancy can hence lead to a higher coverage and activation of smaller molecules (or smaller semi-hydrogenated intermediates), as in this case propene, lowering the selectivity of the catalyst towards hydrogenation of 1,3-butadiene. In conclusion, while the hydrogen surface concentration dictates the catalyst activity, the difference between the adsorption of the hydrocarbons (butadiene and propene) on the exposed Cu-nanoparticles is responsible for the catalyst selectivity. The ideal Cu catalyst has a surface consisting of a large fraction of steps and kinks sites (high activity) and is poor in corner and edge sites (linked to low selectivity). Optimal activity and almost full selectivity to butenes are thus achieved on Cu particles above 4 nm.

3.4 – Conclusions

Differently sized copper nanoparticles (from 2 to 10 nm) catalysts were synthesized and used for the selective hydrogenation of 1,3-butadiene to butenes in presence of a large excess of propene. The 1,3-butadiene hydrogenation activity of nanoparticulate Cu increased with increasing Cu particle size up to 4 nm (4-fold increase in pre-exponential factor from 2 to 4 nm particles). In addition, the 1,3-butadiene reaction rate appeared to be limited by availability of H on the surface of Cu, with an associated activation energy equal for all five catalysts. The increase in activity with increasing particle size was ascribed to the increase in relative abundance of hydrogenation active sites, in particular steps and kinks, by moving from 2 to 4 – 10 nm. Kinetic analysis of the hydrogenation of 1,3-butadiene and propene, together with hydrocarbon adsorption experiments, proved that the selectivity of Cu nanoparticles is governed by the preferential adsorption on the Cu surface of alkadienes rather than alkenes. This preferential hydrocarbon uptake is also favored by a high surface concentration of step and kink sites. Lastly, near full selectivity to butenes (total, ~99%) was observed for 7-10 Cu nm particles.

4 Metal/metal oxide additives

Abstract

Controlling the Cu particle size is an effective strategy to tune the behavior of Cu based catalysts (see **Chapter 3**). In relevant applications, nanoparticulate Cu is often promoted by metal/metal oxides, typically of period 4 of the transition series. This chapter presents a preliminary investigation on the effect of three different additives, specifically Mn, Fe and Zn oxides, on the catalytic properties of 2 nm Cu supported on SiO₂. The additives had strikingly different effects on the activity and selectivity of Cu. Specifically, 5% (atomic percentage based on metal content) Fe oxides led to a mild decrease in selectivity of the catalyst and showed a marked effect on the activation energy of the hydrogenation process, suppressing H₂ consumption. Zn oxides (5%), which are often used for promoting methanol synthesis catalysts, had a detrimental effect on the selectivity of Cu, which was below 50% in the whole conversion range investigated. The only modifier that showed a positive promotional effect was MnO_x, which led to a roughly 3-fold increase in 1,3-butadiene hydrogenation conversion while preserving the selectivity. Mn hence is a promising promoter for Cu-based catalysts used in the selective (partial) hydrogenation of polyunsaturated hydrocarbons.

4.1 – Introduction

Nowadays, Cu nanoparticles-based catalysts find interesting uses in gas phase hydrogenation processes, and more are currently investigated (see **Chapter 1**). However, Cu is rarely used in its pristine and isolated metal form. In industrial applications, Cu nanoparticles are often combined with metal oxides, for instance ZnO, MnO_x and Cr₂O₃.^{205–207} The addition of these oxides is beneficial in terms of activity, selectivity and/or stability of the catalyst.^{205–207} Examples of application of Cu/M_yO_x based catalysts (M= metal) can be found in major commercial processes such as the conversion of CO/CO₂ into methanol,^{7,8,207,208} ethanol dehydrogenation^{209,210} and the water-gas shift reaction.^{211–213} These additives can affect the performance of the Cu-based catalyst in a number of ways: by the formation of new catalytic active sites,^{44,214,215} synergistic electronic effects,^{216,217} stabilization of more active metallic/metal oxide/alloy phases,^{209,216} structural modifications,^{6,216} as well as passivation of unselective centres.^{6,217}

The most well-known Cu-based catalytic system is Cu/Al₂O₃/ZnO, which is utilized for methanol synthesis via CO/CO₂ conversion.^{7,8,207,208} The promoting effect of ZnO was for long under debate. The initial hypothesis was that ZnO is able to remove sites on the alumina phase, which would otherwise convert methanol to dimethyl ether, causing a yield loss. More importantly, ZnO would supposedly enhance the catalyst activity via hydrogen spillover, a preferred property ideal for any gas phase hydrogenation that display a conversion rate limited by hydrogen availability.²¹⁸

More recent findings on Cu/Zn on more inert support such as graphitic carbon, however, asserts that Zn can actually exist in zerovalent oxidation state during methanol synthesis.²¹⁹ The authors, for instance, observed for Zn an average oxidation state of 0.5, and average coordination number of 8 during in-situ X-ray absorption spectroscopy studies. Hence, Zn can appear not only as partially oxidized surface species (as mostly observed on oxidic support), but also in metallic form and bonded together with other metal atom, as for instance Cu. This is often masked on oxidic supports as strong promoter-support interaction can lead to Zn-oxidic support bonding.²¹⁹ This reduced Zn can form a low-Zn CuZn alloy, which might be responsible of the higher observed catalyst activity, as activity boost by Zn addition is observed also in the case of inert support such as graphitic nanoplatelets.²¹⁹

Other interesting promoters for Cu-based hydrogenation catalysts were studied in ester hydrogenolysis. Brands *et al.*²²⁰, for instance, reported that the activity of Cu could be boosted by adding 3d-transition metal oxides, with the activity increasing in the order Mo > Co ~ Zn ~ Mn > Fe > Ni. In this specific case, the electronegativity of the promoter strongly correlated with the increase in catalyst activity, and the effect was ascribed to the higher electron density of the metal center leading to stronger absorption of the organic substrate.²²⁰

Another promoter worth of special attention is Mn. Recently, MnO_x was found able to boost copper hydrogenation activity. In a recent study,²²¹ the addition of 11% Mn/(Cu+Mn) resulted in a 7-fold increase in hydrogenation rate for the production of ethanol from ethyl acetate

reduction. The authors concluded that the promotor effect was most likely due to increased hydrogen surface coverage.²²¹

In this explorative study, three different additives, namely Zn, Fe and Mn oxides, were tested in the Cu-catalyzed hydrogenation of 1,3-butadiene. Focus of this study was to explore whether promotion via metal/metal oxides could boost the Cu activity in diene hydrogenation, without compromising its selectivity.

4.2 - Experimental section

Details on the chemicals used for the synthesis of the catalysts and details on the gaseous feeds can be found in **Chapter 2**.

Metal oxides promoted Cu-based catalysts were synthesized via co-impregnation of two different supports, namely SiO₂ (Davisil Grade 645, 285 m² g⁻¹, pore size of 15 nm) and carbon (graphitic nanoplatelets, GNP500, 500 m² g⁻¹). Preparation was based on incipient wetness impregnation (IWI) described in **Chapter 2** and **3** of this thesis.^{26,105,106} For all samples, the surface density of Cu atoms was 2 Cu/nm². The precursor solution was an aqueous solution of Cu(NO₃)₃ · 3H₂O acidified to pH ~ 1 by addition of HNO₃ (in order to ensure protonation of silanol groups as well as preventing early precipitation of metal salts). Promoted catalysts were prepared by introducing Fe, Mn, or Zn nitrate to the impregnation solution. An overview of the different promoter precursors, catalyst names and metal-to-Cu atomic ratio is given in Table 4.1.

Table 4.1 Catalysts prepared and investigated in this study.

Catalyst name	Promoter	Promoter precursor	M:Cu atomic ratio	HNO ₃ added [ml per 5 ml sol.]
Cu/SiO ₂	-	-	0:100	1.0
1%Fe99%Cu/SiO ₂	Fe	Fe(NO ₃) ₃ · 9H ₂ O	1:99	0.8
5%Fe95%Cu/SiO ₂	Fe	Fe(NO ₃) ₃ · 9H ₂ O	5:95	0.5
10%Fe90%Cu/SiO ₂	Fe	Fe(NO ₃) ₃ · 9H ₂ O	10:90	0
1%Mn99%Cu/SiO ₂	Mn	Mn(NO ₃) ₂ · 9H ₂ O	1:99	1.0
5%Mn95%Cu/SiO ₂	Mn	Mn(NO ₃) ₂ · 9H ₂ O	5:95	1.0
1%Zn99%Cu/SiO ₂	Zn	Zn(NO ₃) ₂ · 6H ₂ O	1:99	1.0
5%Zn95%Cu/SiO ₂	Zn	Zn(NO ₃) ₂ · 6H ₂ O	5:95	1.0

Heat treatment. Decomposition of the supported metal nitrates was carried out in tubular oven under gas flow, similarly to what is described in **Chapter 2** and **3** of this thesis.^{90,222} For each preparation, the material was placed in a 24 mm inner diameter quartz reactor tube, with a catalyst bed height of 3 mm. The catalysts prepared on silica-based supports were treated under N₂ flow to avoid formation of large crystallites and hence lower the particle size and maximize the Cu-M_xO_y contact.^{90,223} Full decomposition of the nitrates species was carried out at 450 °C for 1 h (Table 4.2). Lastly, the samples were left to cool down to room temperature, purged with 20 vol% O₂/N₂ flow (100 mL min⁻¹ g⁻¹) and heated up to 250 °C in the same gas mixture (heating ramp of 2 °C min⁻¹, isothermal hold of 2 h, 100 mL min⁻¹ gas flow for each gram of dry material). This step was performed to oxidize the sample and stabilize them for long term storage in air.

Table 4.2 Thermal treatment and gas flows used for the preparation of M_xO_y-promoted Cu catalysts supported onto silica-based support(s).

Step	Time [min]	Temperature [°C]	Heating rate [°C min ⁻¹]	N ₂ flow [cm ³ min ⁻¹]
1	5	20	0 (isothermal)	350
2	215	450	2.0	350
3	60	450	0 (isothermal)	350
4	115	20	-5.0	350
5	stop	20	0 (isothermal)	350

Characterization. Average crystallite size of copper and promoter species crystallites (as well as phase) were investigated via powder X-ray diffraction (XRD). The material was loaded in open XRD powdered-sample holder. As for these measurements, a Bruker D2 Phaser has been used, with a fixed slit of 1.0 mm and a Co K α _{1,2} X-ray source ($\lambda = 1.79026$ Å). The 2θ range investigated was 10°-80°. The average crystallite size and phase were determined by using Bruker DIFFRACT.EVA software.

Temperature programmed reduction was carried out on a Micromeritics AutoChem II 2920 Chemisorption Analyzer with H₂. Around 50 mg of fresh catalyst (pre-oxidized) was loaded in a quartz reactor. The samples were pretreated at 120 °C (10 °C/min) under an Ar flow rate of 20 cm³ (drying step). After a 15 min hold at 120 °C, the catalyst was left to cool down to room temperature under the same argon flow. Subsequently, the gas flow was switched to 5 vol% H₂/Ar and the sample was heated to 500 °C with a rate of 2.0 °C min⁻¹. The material was held at the final temperature for 10 minutes and lastly cooled down to room temperature. TPR profiles were also used to calculate the weight loading of Cu, according to this simplified reaction scheme: CuO + H₂ → Cu + H₂O.

The average weight loading of Cu was hence estimated with the following equation:

$$wt_{Cu} \% = \frac{V_{H_2} \rho_{H_2,STP} M_{Cu}}{M_{H_2} m_{sample}} * 100\%$$

where V_{H_2} represents the volume of hydrogen consumed as calculated via integration of background corrected Cu TPR area (100-280 °C), $\rho_{H_2,STP}$ the density of H₂ at standard temperature and pressure (0.08988 g NL⁻¹), M_{Cu} the atomic mass of Cu (63.55 g mol⁻¹), M_{H_2} the molar mass of H₂ (2.01 g mol⁻¹), and m_{sample} the mass of dried sample in grams. Particle sizes and particle size distributions were investigated with transmission electron microscopy (TEM). TEM samples were prepared via finely pulverizing the catalyst with mortar and pestle, followed by dry deposition on TEM grid (holey carbon Au grid, 300 mesh, Agar Scientific) and dry sonication. Samples were imaged on FEI Tecnai 20F (FEG, X-TWIN objective lens, operated at 200 kV, bright field mode. Particle size distributions were analyzed via ImageJ software.

The elemental distribution of Cu and promoter were investigated using a FEI Talos F200X (200 kV, STEM mode). Elemental maps were obtained in HAADF-STEM-EDX mode. Average particle sizes were estimated under the assumption of spherical nanoparticles. Surface (d_s) and volume (d_v) averaged particle sizes were calculated as follows:

$$d_s = \left(\frac{1}{N} \sum_{i=1}^N d_i^2 \right)^{0.5} \quad d_v = \left(\frac{1}{N} \sum_{i=1}^N d_i^3 \right)^{1/3}$$

The width of the particle distribution was calculated as the standard deviation of the particle size diameters, as below (d_i are the diameters of the single particles counted.):

$$\sigma_d = \left(\frac{\sum_i (d_i - d_s)^2}{N - 1} \right)^{0.5}$$

Full details regarding the setup employed for hydrogenation test can be found in **Chapter 2** of this thesis. Catalytic tests were carried out in a glass plug-flow reactor of 4mm ID. The reactor was loaded with 23 mg of SiO₂ supported catalyst. The catalysts were all pelletized and sieved in the range 75-150 μm and mixed with 150 mg of SiC granules (212-425 μm) to guarantee thermal uniformity of the catalyst bed. Due to the exothermic nature of the hydrogenation reaction, the controlling thermocouple was connected externally to the reactor, right next to the catalyst bed.

For the hydrogenation tests, pre-conditioning and catalytic runs were carried out as follows. Prior to the measurement, samples were reduced *in situ* at 300 °C under 40 cm³ min⁻¹ of H₂, for 1 h. The catalyst was thus cooled to 50 °C and the reaction mixture was then introduced into the reactor with a constant flow rate of 50 cm³ min⁻¹. The reaction mixture consisted of 0.3 vol% of 1,3-butadiene, 30 vol% of propene, 20 vol% of H₂ and helium as balance. Concentration of products and unconverted reactants was monitored via in line gas chromatography equipped with a flame ionization detector (GC-FID).

4.3 – Influence of additives on the structure of the fresh catalysts

The diffractograms of supported Cu nanoparticle catalysts, either pristine or additivated with Fe, Mn, or Zn on SiO₂ support are shown in Figure 4.1. Diffractograms were recorded after the final oxidation step (see [section 4.2](#)).

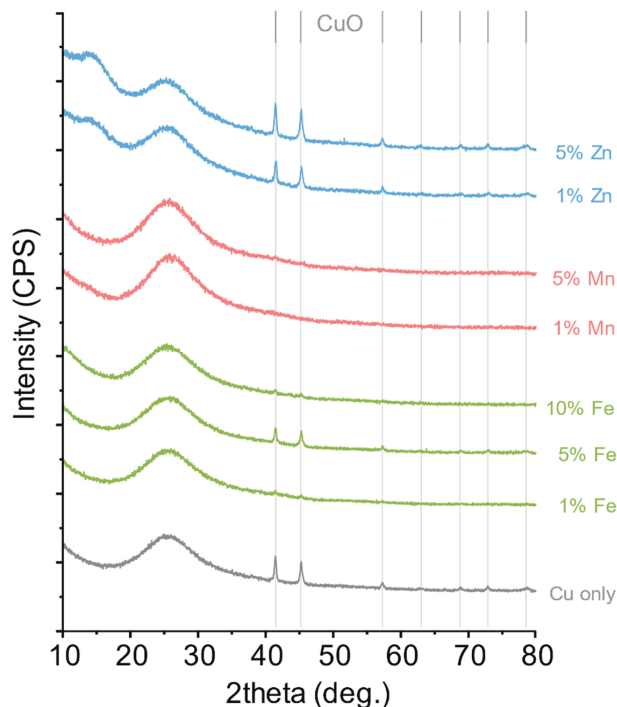


Figure 4.1 X-ray diffractograms for Cu-M_xO_y nanoparticles supported on SiO₂. Catalysts additivated with A) 1 and 5% Mn, B) 1, 5 and 10% Fe and C) 1 and 5% Zn and. The dashed lines refer to CuO crystalline phase. All figures have the Cu/SiO₂ diffractogram at the bottom as reference. Broad peak at around 25° is ascribed to amorphous SiO₂.

Regarding pure Cu on SiO₂, the as-prepared catalyst displayed sharp peaks at around 41° and 46° 2θ, that can be assigned to bulk CuO (all samples were treated in simulated air at 250 °C to guarantee stable phase for sample handling, see [section 4.2](#)). As discussed in [Chapter 2](#), these are due to the presence of few larger crystallites (>25 nm) which can be a by-product of the IWI synthesis, and are not representative of the population of crystallites present on the surface of the silica (see [Chapter 2](#), as well as [Figure 4.2](#)). Upon addition of the additives, no increase in crystallite size was observed. In particular, the CuO diffraction peaks disappeared for the Mn-promoted samples, as well as 1% and 10% Fe, indicating the presence of only small particles (<3 nm). For 5% Fe additivated samples, no substantial change was observed, while for Zn additivated samples, the CuO peaks appeared sharper and higher in intensity than for pristine Cu nanoparticles.

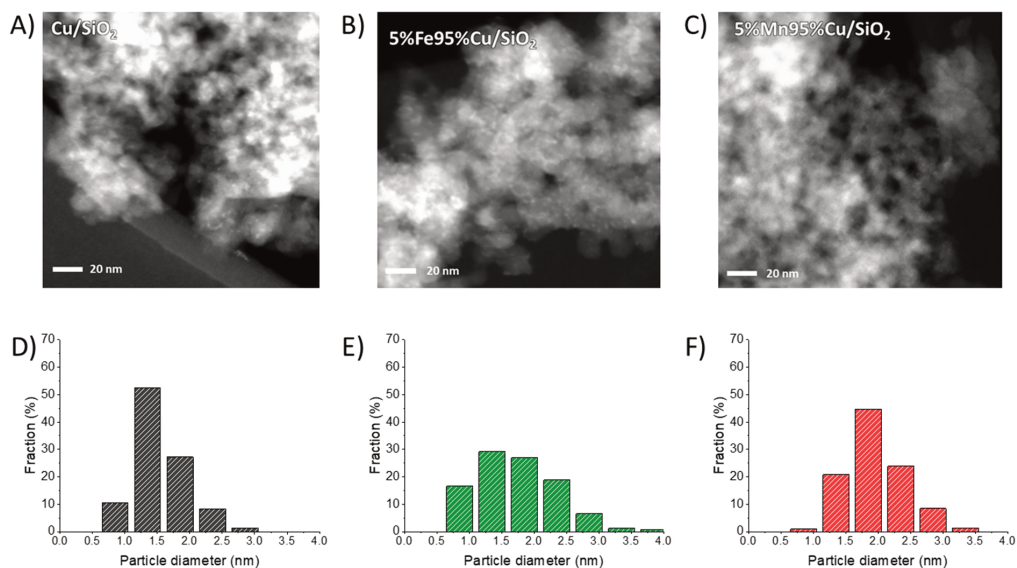


Figure 4.2 Transmission electron micrographs (dark fields) for A) Cu/SiO₂, B) 5%Fe95%Cu/SiO₂ and C) 5%Mn95%Cu/SiO₂. Particle size distributions, average particle size and particle size standard deviation for D) Cu/SiO₂, E) 5%Fe95%Cu/SiO₂ and F) 5%Mn95%Cu/SiO₂.

TEM analysis and particle size distribution for Cu/SiO₂, 5%Mn95%Cu/SiO₂ and 5%Fe95%Cu/SiO₂ is shown in Figure 4.2. The SiO₂-supported catalysts yielded small nanoparticles, around 2 nm, regardless of the modifier added (see also Figure 4.2D, E and F for particle size histograms). In the cases here investigated, the width of the distribution was less than 1 nm. The method was well established only for pure Cu supported on SiO₂, but these results shows that the presence of the metal oxide additives, at the concentrations hereby investigated, does not alter the particle size distribution of Cu (additionally, presence of Mn or Fe seems to hinder formation of larger crystallites, see also Figure 4.2 and **Chapter 2** for comparison with unpromoted Cu).

4.4 - Influence of additives on Cu reducibility

Temperature programmed reduction experiments were carried out on samples supported on SiO₂, to investigate the influence of additives on the reduction behavior of copper oxide. Before the experiment, the samples were oxidized to CuO by treating them in 20 vol% O₂/N₂ flow (100 mL min⁻¹ g⁻¹) at 250 °C (heating ramp of 2 °C min⁻¹, isothermal hold of 2 h). The TPR results are reported in Figure 4.3.

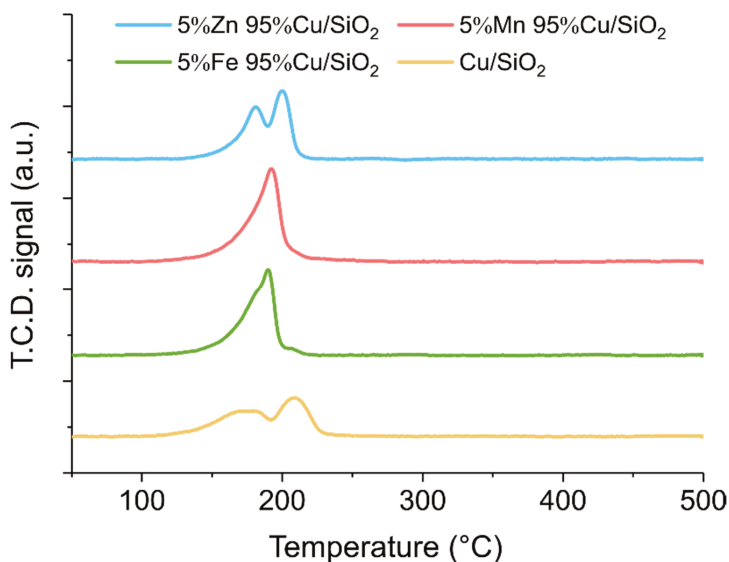


Figure 4.3 H₂-TPR profiles obtained for modified (5%-M_xO_y, 95%Cu) and pristine CuNPs on SiO₂. Samples: 5%Zn 95%Cu/SiO₂, 5%Mn 95%Cu/SiO₂, 5%Fe 95%Cu/SiO₂ and Cu/SiO₂. Reduction profiles recorded on pre-oxidized samples by heating them to 500 °C with a heating rate of 2.0 °C min⁻¹ under flow of 5 vol% H₂/Ar (20 cm³ min⁻¹, 100 mg of sample loaded).

For the pristine Cu/SiO₂ sample, two reduction peaks are observed. With a heating rate of 2 °C min⁻¹, copper undergoes a first reduction from Cu²⁺ to Cu⁺, with an onset of around 125 °C and a peak at 180 °C, and a second reduction from Cu⁺ to Cu⁰ with an onset of roughly 190 °C and peak at 210 °C. On SiO₂, our Cu NPs are hence fully reduced at 250 °C.

Regarding the 5% additivated samples, Cu was also fully reduced to metallic phase at 250 °C. Specifically, Zn additivated Cu particles show a similar 2 steps reduction of copper, with the Cu²⁺ → Cu⁺ reduction starting at around 150 °C and Cu⁺ → Cu⁰ at 200 °C. Regarding Fe and Mn promoted Cu, both samples show almost the same reduction profile, with one single reduction peak (Cu²⁺ → Cu⁰) centered at around 190 °C and with an onset temperature of 150 °C. For the sake of completeness, it is worth pointing out that the reduction might have

happened in two steps, but temperature resolution might have been too low to observe two peaks.

The addition of Mn and Fe slightly lowered the reduction temperature suggesting mild interaction between the Cu and the promoter even at low (5%) modifier concentrations, or an influence of the slightly smaller particle size. More interestingly, the addition of the two additives led to the disappearance of the bimodal reduction profile found for by pure Cu (at the conditions investigated in Figure 4.3). This suggests a possible destabilization of the transient Cu^+ and indicates close intimacy between metal oxide and Cu-based nanoparticles. This effect was not observed for the Zn-additivated Cu.

4.5 - Influence of additives on the activity of 2 nm Cu/SiO₂ catalysts

The activity of Fe, Zn- and Mn- additivated 2 nm CuNPs supported on SiO₂ is shown in Figure 4.4 in terms of 1,3-butadiene conversion as function of the reaction temperature, while Table 4.3 reports the surface-specific activities. For the sake of simplicity, only 5% M_xO_y additivated samples are discussed in this first section. Datapoints were collected during cooling down from 200 °C to 50 °C in order to keep the Cu in a reduced state (zero-valent) during the whole test (see also considerations in **Chapter 2, section 2.4** and **2.5**)

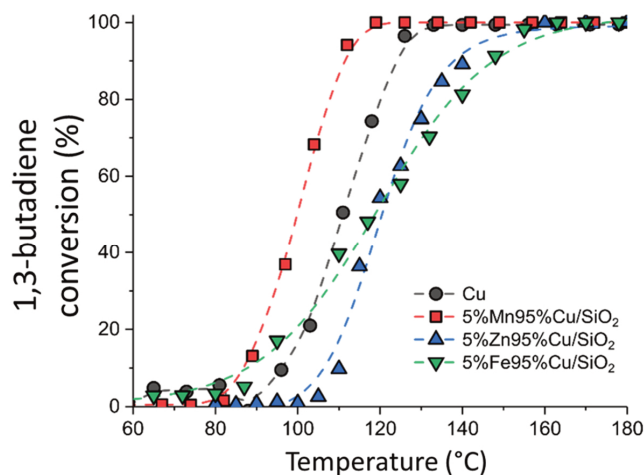


Figure 4.4 1,3-butadiene conversion as function of temperature during cooling (temperature ramp details: 0.5 °C min⁻¹, T = 200 °C → 50 °C). Dashed lines: guide for the eye. Flow rate: 50 cm³ min⁻¹. Concentration: 0.3 vol% of 1,3-butadiene, 30 vol% of propene, 20 vol% of H₂ and He as balance. Sample loading: 23 mg reduced in situ at 300 °C.

Table 4.3 Cu/SiO₂ and 5% (Mn/Fe/Zn) Cu/SiO₂ surface-averaged particle size (\pm width of the particle size distribution), catalyst activity per gram of Cu and Turnover Frequency (TOF, surface-normalized) calculated at 105 °C from the data in Figure 4.4.

Sample	ds [nm]	activity [$\mu\text{mol}_{1,3\text{-bd}} \text{gCu}^{-1} \text{s}^{-1}$]	TOF _{105 °C} [$\text{s}^{-1} 10^{-3}$]
Cu/SiO ₂	1.6 \pm 0.4	35	2.2
5%Fe95%Cu/SiO ₂	1.8 \pm 0.6	39	2.5
5%Mn95%Cu/SiO ₂	2.0 \pm 0.6	122	7.8
5%Zn95%Cu/SiO ₂	2.0 \pm 0.6	9	0.55

Before testing, it was verified that the pure metal oxide additives (100%Fe/SiO₂, 100%Mn/SiO₂, 100%Zn/SiO₂, 2 metal atoms per nm² of SiO₂, same impregnation method and pre-reduction method as used for M_xO_y-Cu samples) showed only negligible activity (in all cases less than 5% conversion up to 200 °C). The activity of the additivated catalyst displayed in Figure 4.4 is mainly due to Cu (promoted) activity.

The pure Cu NPs of 2 nm supported on SiO₂ (Cu/SiO₂) displayed a sigmoid-shaped conversion profile, with an onset temperature of around 90 °C and full 1,3-butadiene conversion reached at a temperature of 130 °C. Addition of Mn led to a higher activity (onset temperature 80 °C vs. 90 °C, full conversion at 115-120 °C). In terms of TOFs (see **Chapter 2** for TOF calculation), the 5%Mn promoted sample was around 3 times more active than Cu/SiO₂ (7.8 10⁻³ s⁻¹ vs. 2.2 10⁻³ s⁻¹). In terms of hydrogenation energy barrier, one can expect that both samples have a very similar activation energy due to the very similar slopes of the conversion plots (Figure 4.4, see also **Chapter 3**: pure Cu/SiO₂ exhibited an activation energy of ~62 kJ mol⁻¹).

Addition of Zn on the other hand decreased the activity with respect to pure Cu (onset 105 °C and full conversion at 150-160 °C, TOF at 105 °C equal to 0.55 10⁻³ s⁻¹ vs. 2.2 10⁻³ s⁻¹, respectively). The activation energy did not change significantly. So, like for Mn, Zn oxide(s) seem not to chemically affect the activity of Cu, i.e., via the different bonding energies of key reaction intermediates (see also **Chapter 3**). Their effect can hence be due to other factors such as an effect on the number of available active Cu atoms on the Cu surface and/or a decrease in available activated hydrogen.^{199,221} Possible formation of a partial alloy might be responsible of such decrease. Presence of a surface alloy, however, cannot be confirmed (or excluded) with the observations hereby reported. Lastly, it is also worth indicating that the samples additivated with Zn showed, after synthesis, a limited but not negligible presence of larger CuO crystallites (> 25 nm, see Figure 4.1), as CuO diffraction peaks were more intense than for pristine Cu. Their presence might also have played a role in reducing the observed Cu activity.

ZnO_x has been extensively studied in recent literature as Cu promotor, in particular for the hydrogenation of CO/CO₂. ZnO_x can increase the activity of Cu by an order of magnitude in case of CO/CO₂ conversion to methanol.^{7,207,219} Although its role is not fully understood, it is

clear that under methanol synthesis conditions the ZnO_x is reduced, and at least partially alloys with the Cu. As the reaction conditions for 1,3-butadiene hydrogenation are much milder and less reducing, this effect is less likely. The observed decrease in activity of 2 nm Cu particles following the addition of 5% Zn via co-impregnation might be explained by the ZnO_x covering active sites.

Lastly, the Fe-additivated sample presented a drastically different behavior, with a less steep conversion curve and an onset temperature of around 85 °C, and finally full conversion of 1,3-butadiene at around 160 °C. This suggests a lower activation energy and hence direct influence on the bonding strength of key intermediates. Overall, even though a direct comparison cannot be made (due to drastically different activation energy), the 5%Fe95%Cu/SiO₂ is less active than the other catalysts, as lower conversions were reached especially above 120 °C. To recap, for samples containing 5% M_xO_y , the activity of the catalysts followed the trend Mn>unpromoted>Zn>Fe.

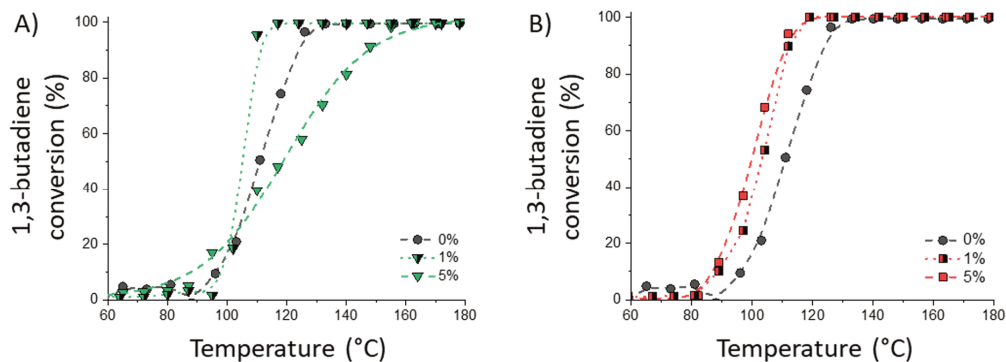


Figure 4.5 1,3-butadiene conversion profiles measured as function of the temperature during temperature programmed runs (0.5 °C min^{-1} , $T = 200\text{--}50\text{ °C}$) for A) Fe-additivated samples (green curves) and B) Mn-additivated samples (red curves). In both cases, 0% (Cu), is displayed for comparison. Dashed lines: guide for the eye. Flow rate: $50\text{ cm}^3\text{ min}^{-1}$. Concentration: 0.3 vol% of 1,3-butadiene, 30 vol% of propene, 20 vol% of H_2 and Helium as balance.

To investigate the effect of promoter loading, additional samples were prepared on silica: 1%Fe99%Cu/SiO₂ and 1%Mn/99%Cu/SiO₂. Resulting 1,3-butadiene conversion plots are shown in Figure 4.5A (Fe) and Figure 4.5B (Mn). For the Mn-promoted samples, 1% Mn gives an improved activity, while adding 5 times more (5%) only slightly further increases the activity.

Regarding iron oxide, 1% Fe addition does seem to alter 1,3-butadiene hydrogenation activity of Cu, with a somewhat steeper hydrogenation curve, while a larger amount (5%) slightly increases the activity at the lowest temperatures but decreases Cu activity at higher temperatures ($>110\text{--}120\text{ °C}$, Figure 4.4). The conversion profile suggests a lower activation energy for the 5% Fe sample 1,3-butadiene conversion (less steep profile). The lower activity, hence, must come from a simultaneous decrease in pre-exponential factor (**Chapter 3**) or, in

other words, a decrease in the number of active sites for butadiene conversion. However, the Fe-additivated catalyst also displayed a very poor selectivity (see next **section 4.6**). To better assess the overall activity of the catalysts, the total hydrogen consumption (selective + unselective conversions) must be taken into account. Figure 4.6 shows that the Fe-additivated catalyst had the lowest hydrogen consumption of all catalysts, confirming indeed that 5% Fe is detrimental for the availability/concentration of activated hydrogen on the surface of Cu particles. Mn addition led to the highest total hydrogen consumption compared to pure Cu as well as Zn and Fe-additivated Cu nanoparticles (Figure 4.6).

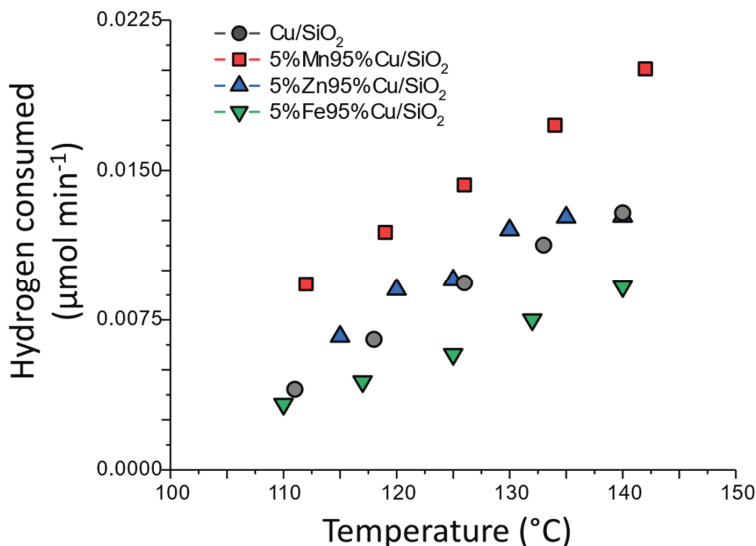


Figure 4.6 Total hydrogen consumed (obtained from hydrogen balance calculated from the concentration of all the products detected) measured during the experiments depicted in Figure 4.4. Temperature range: 110 – 140 °C.

The increase in activity post Mn addition can be explained in terms of increased surface hydrogen concentration (**Chapter 3**). There is little literature regarding the use of Mn as promoter for Cu in hydrogenation reaction. However, its possible beneficial effect on catalyst activity has already been observed. For instance, Mn can be used to improve catalyst activity in case of synthesis of methanol via direct CO₂ hydrogenation.²²⁴ The authors in this case tested 5 different transition metals (Cr, Mn, Fe, Co, Ni) and prepared promoted 7-12 nm Cu particles on SBA-15 support. Interestingly, Fe reduced the activity of Cu of about 30%, while the sample with the highest activity was the Mn-additivated one. In the work presented in this Chapter, we also observed a decrease in activity upon addition of Fe and increase in activity in case of Mn.

A more systematic study was carried on the hydrogenation of another organic compound, namely ethyl acetate. The authors, in this case, studied the activity of 5 nm Cu particles supported on carbon at different MnO_x concentrations. Although the different substrate and reaction conditions (ethyl acetate, T = 180-210 °C, 30 bar), the authors observed up to a 7-fold increase in hydrogenation activity for the 10%Mn 90%Cu sample, and around 3-fold increase for the 5%Mn 95%Cu sample, when compared to pure Cu. X-ray absorption spectra carried on these samples revealed that the oxidation state of Cu is not affected by the presence of Mn oxides (Cu remained zero-valent, and there was no strong indication of extended formation of surface alloys). At low weight loading (<10%) Mn was partially reduced, having overall oxidation state between +2 and +3. In terms of reaction kinetic, reaction rate analysis indicated that the dissociative adsorption of hydrogen was the limiting factor for this reaction. The authors concluded that the promotor effect was mostly due to increased hydrogen surface coverage,²²¹ which would be in line to what was also observed in the framework of this thesis for Cu-based catalysts (**Chapter 3**).

4.6 - Influence of additives on the selectivity of 2 nm Cu/SiO₂ catalysts

Concentration profiles for the products of the 1,3-butadiene hydrogenation (and propene hydrogenation, if any) were collected to estimate the selectivity of the catalysts. Briefly, the production of butenes (trans-2-butene, cis-2-butene, 1-butene) was considered as desired, while conversion of propene and/or butenes into propane and n-butane, respectively, was considered as unwanted. The total selectivity to butenes is hence here reported as the molar ratio between desired products and total moles of products generated by the catalyst (calculations are reported in **Chapter 3**). Results in terms of selectivity to butenes as function of 1,3-butadiene conversion are reported in Figure 4.7 (frames A-C), for the pristine and modified 2 nm Cu/SiO₂. Selectivities at 50 and 98% 1,3-butadiene conversion for the same catalysts are reported in Figure 4.7D. An explanation of the reaction mechanism and selectivity can be found in **Chapter 3**.

All samples investigated showed a very similar selectivity trends vs. 1,3-butadiene conversion except the Zn-additivated sample. In general, at low conversion values (less than 20% 1,3-butadiene conversion), the selectivity to butenes is above 90% . For both Mn and Fe-additivated samples, as well as the unpromoted catalyst, the selectivity drops significantly at higher diene conversions. For the Fe-additivated sample, the selectivity was generally lower than the one observed for pure Cu/SiO₂ (Figure 4.7C and D). Addition of Zn, resulted in very low selectivities, with a decrease in selectivity from around 98% (pure Cu) to 38% (5%Zn) already at around 10% 1,3-butadiene conversion. The Mn additivated samples, on the contrary, displayed both a very similar selectivity profile, as it can be observed by the almost full overlap of the two curves, as well as selectivity in line with the one observed for pristine Cu.

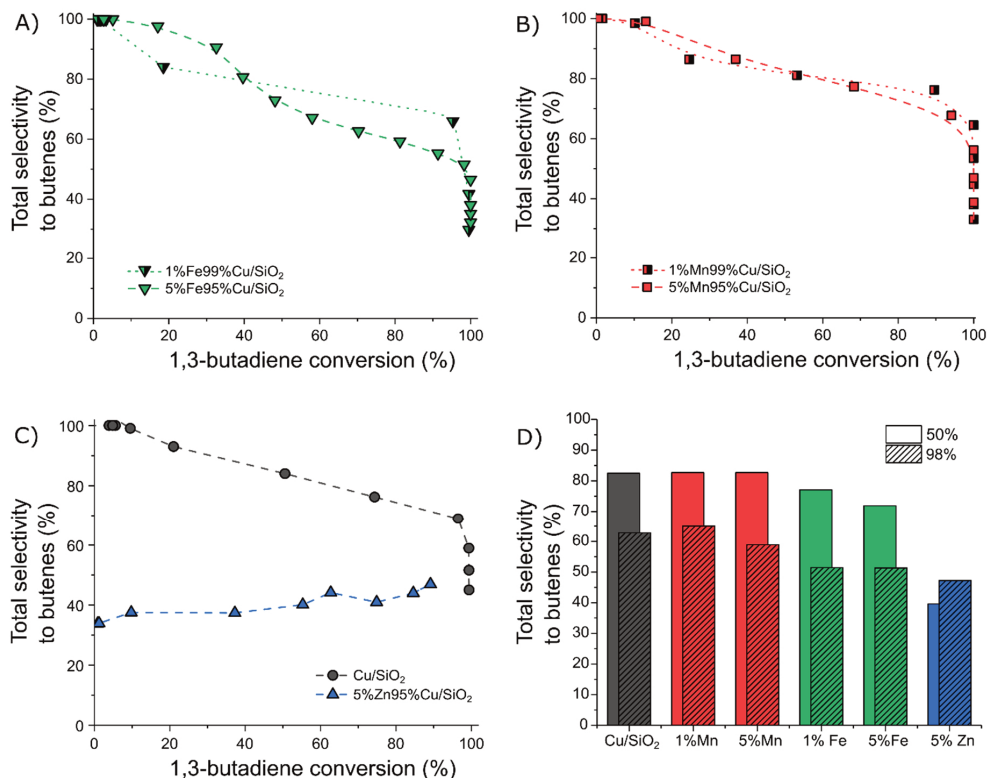


Figure 4.7 Selectivity to butenes as function of 1,3-butadiene conversion for A) 1 and 5% Fe-additivated 2 nm Cu on SiO₂, B) 1 and 5% Mn-promoted 2 nm Cu on SiO₂ and C) 5% Zn-additivated 2 nm Cu on SiO₂, as well as unpromoted 2 nm Cu/SiO₂. The data were collected during the experiments discussed and depicted in Figure 4.4 and 4.5. Frame D) reports the selectivity to butenes as measured at 50% and 98% 1,3-butadiene conversion. Data were interpolated (linearly) between two neighboring datapoints whenever there were no exact data at exactly 50 and 98% conversion (except for 5% Zn, for which the data reported in the bar plot were measured at 91% 1,3-butadiene conversion).

The primary unwanted reaction, lowering the catalysts selectivity, was the conversion of propene to propane for all the catalysts. Regarding the over hydrogenation of 1,3-butadiene and butenes to butane, the reaction was particularly limited. In all cases, less than 1% butane at around 90% conversion of butadiene was observed.

To summarize, promotion with 1 and 5% Mn preserves the original catalyst selectivity (2 nm Cu on silica), despite of the 3-fold increase in catalyst activity/TOF (Figure 4.5 and Table 4.3). There was only a slight difference between the two different concentrations of Mn.

4.7 – Conclusion

Cu nanoparticles (2 nm) supported on SiO₂ were additivated with different amounts (1-5% atomic ratio) of Mn, Fe or Zn oxide. These additives had a considerable influence on their catalytic performance for the hydrogenation of 1,3-butadiene in presence of a 100-fold excess of propene. The addition of 5% Fe oxide (5% Fe/(Cu+Fe) metal atomic percent) led to both a decrease in activity and selectivity to butenes of the catalyst. Addition of Zn did not alter the Cu activity but led to a large decrease in selectivity, which was below 45% in the whole 1,3-butadiene conversion range investigated. Addition of 1% or 5% MnOx improved the catalyst activity around 3-4-fold, while preserving the high alkenes selectivity. The result might be explained by the ability of MnOx to increase the hydrogen availability at the Cu surface, without altering the Cu oxidation state or intermediates (partially hydrogenated hydrocarbons) adsorption strength. Hence Mn oxides are proposed as promising promoter for Cu-based catalysts used in hydrogenation of polyunsaturated hydrocarbons.

4.8 – Acknowledgements

The experimental work described in this chapter was performed at the Materials Chemistry and Catalysis (MCC) group, which is part of the Debye Institute for Nanomaterials Science at Utrecht University.

This chapter is based on the data and findings from the MSc research project of Matthijs Alting (M.A.) (supervisors prof. dr. Petra E. de Jongh (P.E.d.J), Giorgio Totarella (G.T.), title: Supported Cu-based Catalysts for the Selective Hydrogenation of 1,3-Butadiene in Presence of an Excess of Propene: the Role of Promoters on the Catalytic Performance, Utrecht University, 2020). Experiments were designed by the author of this thesis (G.T), together with M.A. and the supervisors. Catalytic experiments were executed by M.A. and G.T., while M.A. and supervisors took responsibility for the final analysis and reporting of the data. G.T. prepared the first draft of the text of this chapter, which then received input from P.E.d.J. and dr. Laurent Delannoy (L.D.). The author of this thesis also gratefully acknowledges Dr. Petra Keijzer, Dr. Nynke Krans and Savannah Turner for performing TEM measurements, Dennie Wezendonk for XRD measurements, Laura Barberis for TPR measurements, and finally Jan Willem de Rijk for the technical assistance on the catalytic set-up.

5 Selective hydrogenation of 2-methyl-3-butyn-2-ol over supported Cu nanocatalysts

Abstract

Nanosized copper is an excellent alternative to noble metal-based catalysts in gas phase selective hydrogenation, but little is known about its performance in liquid phase catalysis. We investigated the activity and selectivity of 2 and 7 nm Cu on SiO₂ catalysts for the three-phase partial hydrogenation of 2-methyl-3-butyn-2-ol, a highly relevant reaction for fine chemical synthesis. Next to the desired 2-methyl-3-buten-2-ol, also 2-methyl-2-butanol was formed as a result of over-hydrogenation. The 7 nm Cu nanoparticles were intrinsically 2.5 times more active than 2 nm Cu (in terms of turnover frequency), and they were also more selective. At 180 °C the selectivity was only 15% at 50% conversion, but lowering the reaction temperature to 160 and 140°C led to 80% and even ~100% selectivity (at 50% conversion). The unselective step was around two times faster than the selective one, hence the high selectivity is due the stronger adsorption of the reactant than of the desired product, which limits over-hydrogenation.

This chapter is based on: Totarella, G., de Jongh, P. E. (2024). Selective hydrogenation of 2-methyl-3-butyn-2-ol over supported Cu nanocatalysts. Submitted.

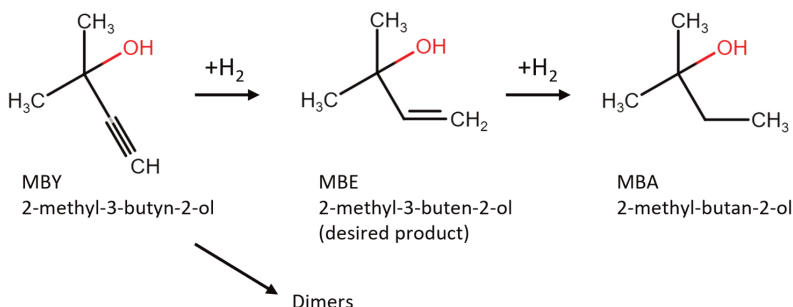
5.1 – Introduction

As already mentioned in **Chapter 1** of this thesis, another interesting and relevant application of selective hydrogenation catalysts based on Cu nanoparticles is the conversion of alkynols to alkenols.^{110,159–161,225,226} Alkenols are extensively used in fine chemistry as nucleophiles in coupling reactions e.g., with carbonyl electrophiles,^{227,228} to form C–C bonds and thus larger and more complex molecules, such as vitamins, pharmaceutical compounds and polymers.^{110,162–165} The reaction itself is often carried out in liquid phase (e.g., slurry type reactor) and shares with gas-phase hydrogenations an important challenge: the full hydrogenation of the C≡C is kinetically favoured as the second hydrogenation (C=C to C-C) is faster than the partial hydrogenation (C≡C to C=C).¹¹⁰ The use of very selective catalysts is hence essential.

Commercially, the catalyst of choice is the so called “Lindlar catalyst”,^{162–164,166} which consists of Pd nanoparticles (5% wt., typically 2-10 nm in size) supported on CaCO₃, with the addition of 2-5% Pb and organic selectivity promoters.^{99,110,167,168} The additives/promoters, however, are undesirable (especially in the final product) as they are toxic and environmentally hazardous. Copper, as it has been proven very selective for gas phase hydrogenations (see ref.^{26,153,157,158,229}, as well as results on 1,3-butadiene hydrogenation presented in this thesis) might be a valuable alternative to modified Pd-based catalysts.

Very few studies have been dedicated to the investigation of supported Cu nanoparticles for liquid phase hydrogenations.^{47,174,230,231} Most studies on Cu-based catalysts focus on Cu chromite (Cu₂Cr₂O₅).^{169–173} However, its use nowadays is restricted due to the potential presence (or later formation) of very toxic Cr⁶⁺ species.^{174,175} Regarding pure Cu, SiO₂-supported⁴⁸ and C-supported²³¹ nanoparticles showed a good selectivity in the hydrogenation of cinnamaldehyde to cinnamyl alcohol, although the preparation strategy and support choice were crucial to achieve the desired catalyst performance.^{48,231} Other examples of Cu catalyzed liquid phase hydrogenations are the conversion of acetophenone to 1-phenylethanol²³⁰ and furfural to furfuryl alcohol.¹⁷⁴

An important reaction used in particular in vitamin and fragrance synthesis is the conversion of 2-methyl-3-butyn-2-ol (MBY) to 2-methyl-3-buten-2-ol (MBE),¹⁵⁹ which will be the focus of this chapter. The only products reported in literature for the MBY hydrogenation are 2-methyl-3-buten-2-ol (desired product), 2-methyl-2-butanol (MBA, over-hydrogenation product) and oligomers (Scheme 5.1):^{232,233}



Scheme 5.1: Proposed reaction mechanism for the hydrogenation of MBY.^{232,233}

Most of the existing literature on 2-methyl-3-butyn-2-ol hydrogenation focuses on Pd-based catalysts, both in gas and liquid phase.^{110,232–235} González-Fernández *et al.*²³⁴ studied the gas phase hydrogenation of MBY at 130 °C and 1 atm total pressure (<1% MBY, balance H₂) for 1% Pd/ZnO, 1% Pd/Al₂O₃ and 5% Pd Lindlar catalyst (particle sizes between 5 and 10 nm). Relatively high selectivities (around 95 %) were achieved for Pd/ZnO but at only 10 % MBY conversion. At 60% conversion, the Lindlar-type catalyst yielded around 60% selectivity to MBE, while Pd/Al₂O₃ and Pd/ZnO displayed selectivities of around 30 % and 75 %. The authors reported MBA as main byproduct of the reaction.

Liquid phase tests for Pd-based catalysts were carried out by Shen *et al.*²³⁵, which tested pure Pd particles supported on nitrogen doped carbon(CN), as well as Zn/ZnO promoted Pd (reaction conditions: 0.245 M MBY in water, 5 bar H₂, stirring rate 1000 rpm, 35 °C). A maximum selectivity of ~85% was at around 25% conversion in case of pure Pd supported on CN (70% selectivity at 80% MBY conversion). The highest reported selectivity was measured for PdZn/ZnO: around 95% but only at low conversions (between 10 and 50% 2-methyl-3-butyn-2-ol conversion). Much better selectivities (96% at 90%) were obtained on non-supported 6-13 nm Pd for the solvent-free reaction (pure MBY) and in presence of stabilizers.²³⁶ However, it is difficult to judge the intrinsic selectivity of the metal nanoparticles in presence of stabilizers, as they potentially poison unselective centers, while separation of a colloidal or homogeneous Pd based catalyst from the reaction mixture is cumbersome.

Regarding pure Cu nanoparticles, to the best of our knowledge only one publication exists.²³⁷ Recently, Shesterkina *et al.* prepared and tested Cu-Fe nanoparticles supported on SiO₂ and Al₂O₃ and tested them in the liquid phase selective hydrogenation of 2-methyl-3-butyn-2-ol. The conditions were 0.2 M MBY solution in ethanol (15 mL), 150 °C, H₂ pressure 1.3 MPa (MBY to H₂ molar ratio equal to 1:10). It was reported that the 5%wt. Cu/SiO₂ sample tested as reference showed ~90% selectivity at 90% conversion. Unfortunately, neither particle size nor amount of catalyst loaded in the reactor were reported.

This study represents an exploration of the properties of Cu/SiO₂ catalysts in the liquid phase selective hydrogenation of 2-methyl-3-butyn-2-ol, an important intermediate in the

production of fat-soluble vitamins and fragrances. We compare catalysts with different particle size, report intrinsic (surface-based) activities and selectivities at different conversions and temperatures. The single metal Cu catalysts here reported potentially surpass unmodified Pd catalysts in terms of selectivity.

5.2 – Experimental section

The catalysts preparation methodology, as well as characterization methods, were already fully described in **section 2.2** of this thesis (samples 2nm_Cu/SiO₂ and 7nm_Cu/SiO₂).

Catalytic testing. The catalytic properties of SiO₂-supported Cu nanoparticles were investigated in the liquid-phase hydrogenation of 2-methyl-3-butyn-2-ol (MBY) to 2-methyl-3-buten-2-ol (MBE) in batch-type reactor. Prior to each experiment, the Cu catalysts were reduced under pure hydrogen at 300 °C for 2 h. The material was then transferred in an Ar glovebox in order to avoid any possible oxidation of the metallic Cu during the reactor loading procedure. The reaction media consisted of a 2% by volume solution of MBY in toluene (concentration: 0.2 mol L⁻¹; the solution was prepared and stored under N₂, with both reactant and solvent dried overnight with molecular sieves 4A).

Reaction conditions were 100 ml of solution, 200 ml head space, 14 mg total Cu loaded and 20 bar H₂, unless otherwise specified. The reactor used was a 300 mL Parr Autoclave equipped with a glass liner, gas-injection port, liquid-only sampling line and 4-blades turbine-type impeller mixer for homogeneous mixing of the reaction slurry. Once the reactor was loaded and sealed, the head space of the reactor was flushed 3 times with Argon, 3 times with H₂, and finally pressurized with H₂ to 20 bar after which the reactor was brought to the desired reaction temperature. MBE hydrogenation tests were also carried out by using the same method described for MBY. The product of the reaction was stored in a fridge (4 °C) in hermetically closed vials, for a maximum of 1 month.

Product analysis (reaction media sampled through liquid-only sampling line) to analyze the time dependence of the MBY conversion and selectivity to MBE was performed using GC-FID (Varian 430-GC, with VF-5ms column, 30 m x 0.25 mm x 0.25 μm, fused silica; integrated 5 m guard section to capture high boiling points substances that might damage the column). Quantification limits (lowest detectible concentration) for MBY, MBE and MBA were 0.005 mol L⁻¹, while 0.10 μmol L⁻¹ was the detection limit. For the byproducts acetone and methylbutene, the quantification limits was ~0.02 mol L⁻¹ and detection limit ~0.5 μmol L⁻¹) The total runtime of the GC was 7.5 minutes, with a carrier (He) flow of 3.0 mL min⁻¹. The oven temperature program consisted of a first step of 2.2 minutes at 60°C and then a fast ramp (70 °C min⁻¹) to 290 °C and an isothermal hold at the same temperature. The FID detector log frequency was 20 Hz.

Identification of byproducts was carried out by means of GC-MS (Shimadzu GCMS model QP2010, detector: single quadrupole). The column used for GC-MS analysis was equivalent to the one used for the GC-FID. The gas-chromatography step was performed between 60 and 265°C, with a heating ramp of 70 °C min⁻¹. Masses scanned/detected between 45 and 500 m/z. Lastly, the observed turnover frequency (TOF) was estimated with the following formula:

$$TOF = \frac{V * C_{MBY} * X_{MBY}}{S_{Cu} w_{Cu} 1.46 \cdot 10^{19} / N_{AV}}$$

Where V is the volume of the liquid phase (assumed constant), C_{MBY} the initial concentration of the 2-methyl-3-butyn-2-ol (MBY), X_{MBY} the measured conversion (as calculated via GC-FID data), w_{Cu} the amount of Cu in the reactor, $1.46 \cdot 10^{19}$ the number of Cu atoms per $m_{Cu}^{2,106}$ and N_{AV} the Avogadro Number.

5.3 – Conversion of MBY over Cu/SiO₂ catalysts

Prior to catalyst testing, tests without active metal phase were performed on the hydrogenation of 2-methyl-3-butyn-2-ol (MBY) using the reactor (glass liner + stirring rod and sampling line fully submerged in the reaction mixture) and the bare SiO₂ support. Data are reported in Figure 5.1. The concentration of MBY was stable during the whole duration of the test, highlighting that the conversion was negligible (<2% after 30 min 130 °C, 30 min 180 °C, 120 min 210 °C). No other compound apart from MBY was detected.

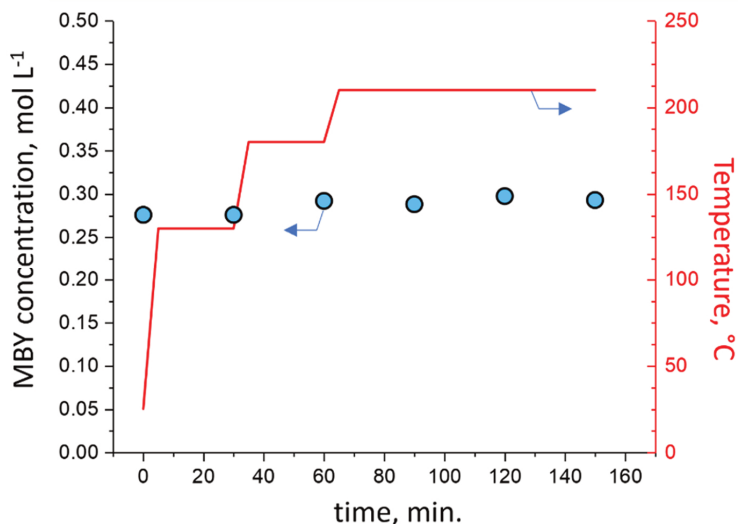


Figure 5.1 Blank test performed on the hydrogenation of 2-methyl-3-butyn-2-ol (MBY) for the empty reactor (glass liner + stirring rod and sampling line, full immersed in reaction mixture + 250 mg SiO₂ support). Reaction temperature reported in red.

In contrast, in presence of silica-supported Cu nanoparticles a significant conversion was observed. The concentrations of the components of the reaction mixture, including products formed, were determined via GC-FID. All oxidizable carbon-based products with a boiling point below 290 °C were detected (assuming that they do not thermally degrade within the 7.5 min runtime, see **section 5.2**). In this section, we will focus exclusively on the main hydrogenation reaction, which consists in the conversion of MBY (2-methyl-3-butyn-2-ol) into either MBE (2-methyl-3-buten-2-ol, the desired product of the partial hydrogenation step) and MBA (2-methyl-butan-2-ol, unwanted and formed by subsequent hydrogenation of MBE, see Scheme 5.1). Two by-products were also detected, most likely acetone and methylbutene(s). Details regarding additional by-products are reported later in the text, **section 5.4**.

Figure 5.2 shows the concentration of MBY, MBE and MBA as a function of the reaction time for tests carried out at 160 °C and 20 bar H₂. Both catalysts displayed MBY hydrogenation within 10-20 min of testing. The 2 nm Cu catalyst reached 50 % MBY conversion in 20 minutes, while for the 7 nm catalyst similar conversion was reached after around 60 min testing (mind the different time scales on the x-axes in Figure 5.2). The first product of the reaction was the desired product MBE. However, the MBE was further converted at longer reaction times, as facilitated by the excess of H₂ (H₂ to MBY ratio of 8). For 2 nm Cu nanoparticles, MBA started to be formed after 10 minutes, and at 20 minutes, a maximum in the MBE concentration was observed (0.03 mol L⁻¹). Longer reaction times resulted in full consumption of MBE and formation of MBA (max concentration reached equal to 0.10 mol L⁻¹). For 7 nm Cu nanoparticles, the formation of MBA started later (between 60 and 80 minutes). A much higher maximum MBE concentration, 0.075 mol L⁻¹, was reached. For the 2 nm catalyst, the entirety of the intermediate (and desired) MBE was further consumed in 60 min, versus 160 min for 7 nm Cu.

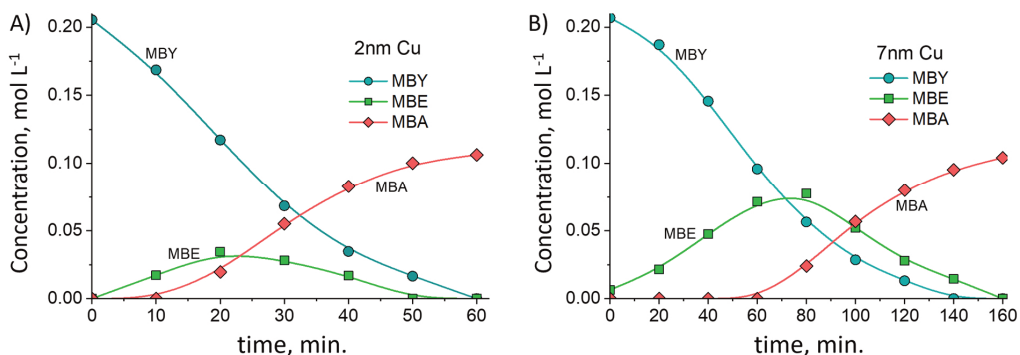


Figure 5.2. A) Concentrations of 2-methyl-3-butyn-2-ol, 2-methyl-3-buten-2-ol, 2-methylbutan-2-ol as function of reaction time for the samples 2nm_Cu/SiO₂ and B) 7nm_Cu/SiO₂ each for 14 mg Cu (right). Reaction temperature: 160 °C (details can be found in the **section 5.2**). The lines in the figure are drawn to guide the eye. Note the different x-axis (time axis) scales.

From Figure 5.2, it is clear that the 2 nm Cu catalyst displays a higher weight-based activity than 7 nm Cu. Also, the 2 nm Cu/SiO₂ catalyst displayed a stronger tendency to hydrogenate MBE to MBA, hence potentially possess a lower selectivity than the 7 nm Cu. A preliminary kinetic analysis was run on the tests reported in Figure 5.2 in order to extract reaction orders. The data are reported in Figure 5.3 in terms of natural logarithm of the consumption rate of MBY (calculated via finite difference) vs. natural logarithm of the MBY concentration. Regarding the test carried out at 160 °C, a reaction order of 0.55 (±0.08) and 0.59 (±0.07) were found respectively for 2 and 7 nm Cu on SiO₂. The intercepts estimated from this analysis are proportional to ln(*k*). Hence, the ratio between kinetic constants *k* for 7 and 2 nm samples is equal to $e^{-4.24}/e^{-4.84} = \sim 2$. This indicates that the 2nm Cu catalyst is around twice as active (per unit weight of loaded catalyst) as the 7nm Cu catalyst. It should be pointed out, however, that while reaction orders from this analysis are relevant, the difference in activity hereby discussed are based on catalyst weight (or equivalently Cu weight, since the Cu loading in the reactor was the same).

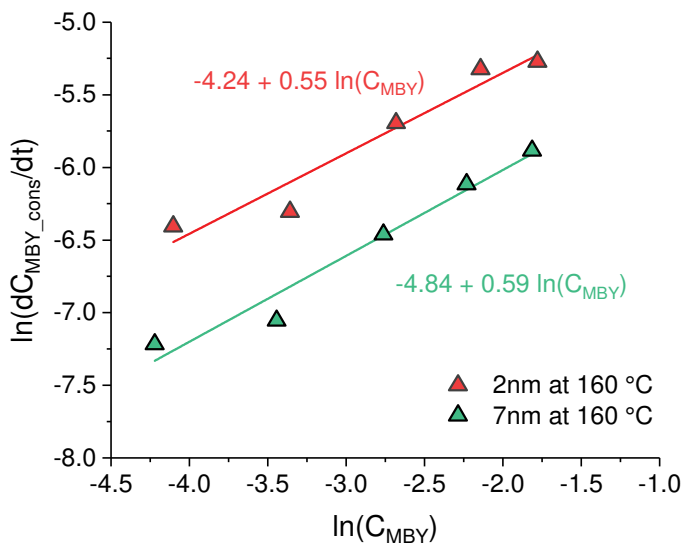


Figure 5.3 Kinetic fit of natural logarithm of the empirical reaction rate (dC_{MBY}/dt) vs. natural logarithm of the concentration of MBY. The fitted equation is equal to $\ln(dC_{\text{MBY_cons}}/dt) = \ln(k) + n \cdot \ln(C_{\text{MBY}})$. The slope of the plot corresponds to the reaction order “*n*”.

As highlighted in the Chapter 3 of this thesis, a better way to assess potential particle size effect, or better the intrinsic activity of the Cu nanoparticles, is to estimate their surface-normalized activity, as for instance in terms of TOF. In this case, the Cu surface area-based activities (turnover frequencies) for the MBY consumption were equal to 0.031 s⁻¹ for 2 nm Cu and 0.078 s⁻¹ for 7 nm. The larger particles were hence roughly 2.5 times intrinsically more active than 2 nm.

This clear particle size effect resembles that for gas phase hydrogenation reactions over Cu (e.g., methanol synthesis,⁷ 1,3-butadiene hydrogenation,^{26,199} and ethyl acetate hydrogenation²⁷), for which generally a 3-4 fold increase in intrinsic activity is observed going from ~2 nm Cu to 7-8 nm, above which the activity is size-independent. This similarity suggests that, like in these gas-phase hydrogenation reactions, the reaction rate for this liquid phase hydrogenation is probably limited by H surface availability.

A comparison with results from literature cannot easily be made. For liquid-phase hydrogenations, Cu catalysts are seldom investigated. Almost uniquely reported are Pd catalysts, which are typically very active, but show low selectivity if not modified/poisoned. Additionally, to the best of our knowledge, there is no reporting for Ni-based catalysts, which is a very common hydrogenation metal. Regarding Pd-based catalysts, Zn-promoted Pd displays TOFs between 0.02 and 0.13 s⁻¹ at 35 °C and 5 bar H₂ (0.05 mol L⁻¹ MBY in water),²³⁵ while commercial-type Lindlar catalysts (PdPb/CaCO₃) display TOF of around 2 s⁻¹ at 80 °C and 1 bar H₂ (0.25 mol L⁻¹ MBY in ethanol).²³⁸ If we would extrapolate this to 160 °C (considering an Arrhenius-type dependency of the TOF as function of the temperature, and an activation energy of 30 kJ mol⁻¹) this would correspond to a TOF of ~15 s⁻¹ (2-to-5*10³ higher activity than Cu). Also for selective hydrogenations carried out in gas phase,²⁶ Pd catalysts have typically a 3 to 6 orders of magnitude higher activity. However, given the scarcity of Pd, and the fact that selectivity is a much more crucial factor for this type of reaction, lower cost, and lower activity but high selectivity catalysts might be viable alternatives to Pd.

The shape of the concentration profiles in Figure 5.2 suggests that MBE is an intermediate in the formation of MBA. The two catalysts clearly display different selectivities. The final concentration of MBE+MBA+MBY is 0.11 mol L⁻¹, while the starting concentration of MBY was 0.2 mol L⁻¹, which indicates the formation of side products at high MBY conversions. Catalyst selectivity is discussed in more detail in the next sections.

5.4 – Side products

During the tests depicted in Figure 5.2, particularly at high MBY conversions other compounds were detected in the reaction mixture apart from MBE and MBA. The two additional side products identified (via GC-MS) were acetone and methylbutene(s). Figure 5.4 displays the concentration profile of MBY, together with the concentration of the two side-products, measured during the experiment depicted in Figure 5.2 (frame A and B) as well as the mass spectra for the two side products (frame C and D). The two products were identified by matching using the NIST mass spectral library (similarity index >95%). The concentration of methylbutene was too low to distinguish which of its 3 isomers (2-methyl-1-butene, 2-methyl-2-butene, 3-methyl-1-butene) was formed. The complete reaction scheme relevant for the experiments reported in this study is displayed in Scheme 5.2.

Although the different MBY consumption rates (see time scale in Figure 5.4A and 5.4B), the amount of methylbutene(s) formed for both the catalysts was roughly equal. For both, the concentration of methylbutene(s) was 0.04 mol L^{-1} at 100% MBY conversion (after 60 minutes for 2 nm Cu, 140 minutes for 7 nm Cu). Strikingly, for the 7 nm Cu also acetone is present. Acetone production started after 60 minutes of reaction (roughly at the same time MBA appeared, see Figure 2B). The final concentration was 0.06 mol L^{-1} (at 100% MBY conversion).

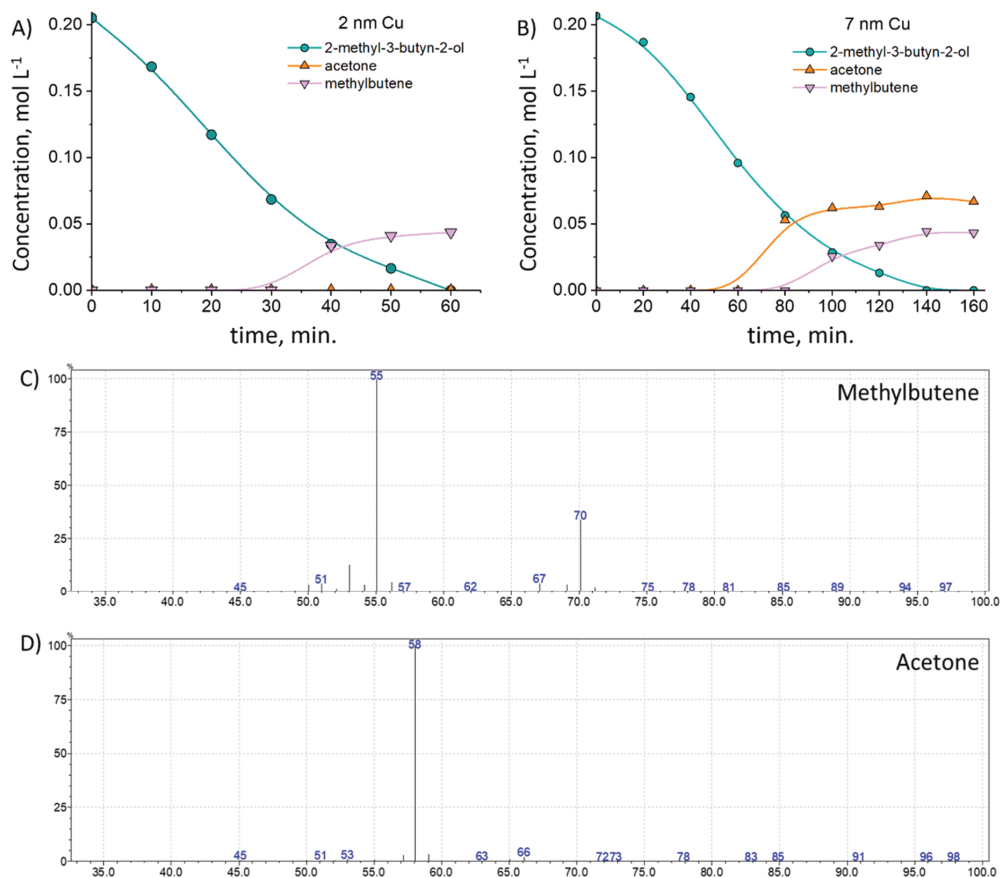
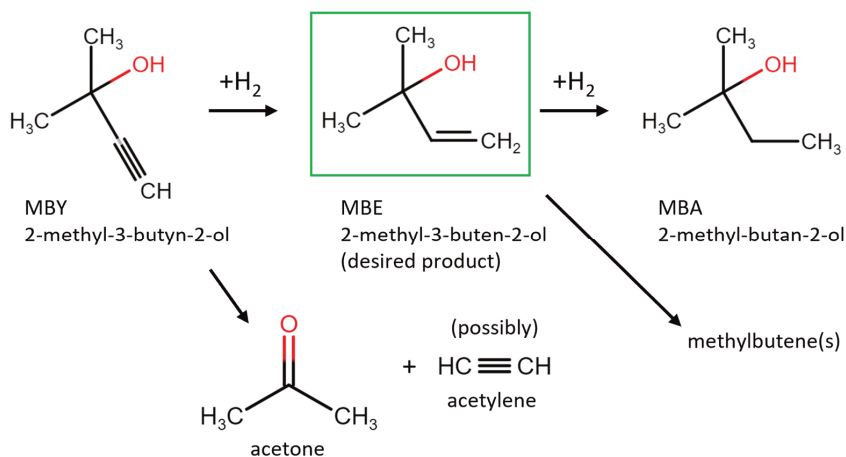


Figure 5.4 Concentrations of 2-methyl-3-butyn-2-ol and the two by-products acetone and methylbutene for A) 2 nm and B) 7 nm Cu. Reaction temperature: 160 °C (same experiment reported in Figure 5.2; details on conditions can be found in **section 5.2**). The lines in the figure are drawn to guide the eye. C) and D) are reporting the mass spectra for the two byproducts identified via GCMS as methylbutene and acetone (the acetone base peak, at $m/z=43$, is missing as MS scan was done for $m/z >45$).



Scheme 5.2. Proposed reaction scheme for the reaction investigated in this work. The only desired product of the hydrogenation of MBY (2-methyl-3-butyn-2-ol) is MBE (2-methyl-3-buten-2-ol).

Concerning the origin of the additional by-products, acetone must be formed by C-C bond cleavage, most likely cleavage of the C2-C3 bond in the MBY molecule. Concomitant formation of acetylene is expected.^{239,240} Acetylene however cannot be detected (if formed) due to its low concentration and high volatility (and/or ready hydrogenation to ethane, which is also highly volatile hence would equilibrate in the reactor head space, which during these tests was not possible to be sampled). The cleavage reaction described above is known to occur over solid catalysts having basic functionalities/sites.^{239,240} However, neither the empty reactor nor, more importantly, the support itself displayed formation of acetone from MBY when tested at similar conditions (see Figure 5.1). The formation of methylbutene(s) has not been reported before for Lindlar-type catalysts, although it is worth pointing out that byproducts of the selective hydrogenation of MBY are rarely fully characterized.

The two catalysts presented different product distributions, with the 7 nm catalyst showing a much higher yield to the desired product MBE at all MBY conversion levels. It is worth noting that the carbon balance for 7 nm Cu tested at 160 °C was around 98 % at 100% MBY conversion, while only 70 % of the carbon-containing products molar balance was detected for the less selective 2 nm Cu/SiO₂. These small particles expose a high fraction of highly undercoordinated edge and corner sides, which hence are likely to promote the formation of undesired byproducts. For this reason, we focused further investigations regarding the effect of process conditions on selectivity on the 7nm_Cu/SiO₂ catalyst.

5.5 – Effect of the temperature on activity and selectivity

Figure 5.5 displays the MBY conversion vs time (frame A) and selectivity to MBE (defined as molar ratio between MBE produced and total MBY consumed) vs MBY conversion (frame B) for different temperatures. After 20 minutes of reaction, conversions of 3, 9 and 25 % were observed at 140, 160 and 180 °C respectively. Focusing on conversion, 30% MBY consumption was obtained after 70, 40 and 20 minutes at 140, 160 and 180 °C respectively (data linearly interpolated). This roughly 2/3-fold increase in reaction rate for every 20 °C translates to an activation energy of 50-80 kJ mol⁻¹. This is well in line with activation energies generally expected for the hydrogenation of (poly)unsaturated C-C bonds (30–90 kJ mol⁻¹),^{46,47} and as expected somewhat higher than estimated for Pd-based catalysts (30 kJ mol⁻¹).¹⁵¹

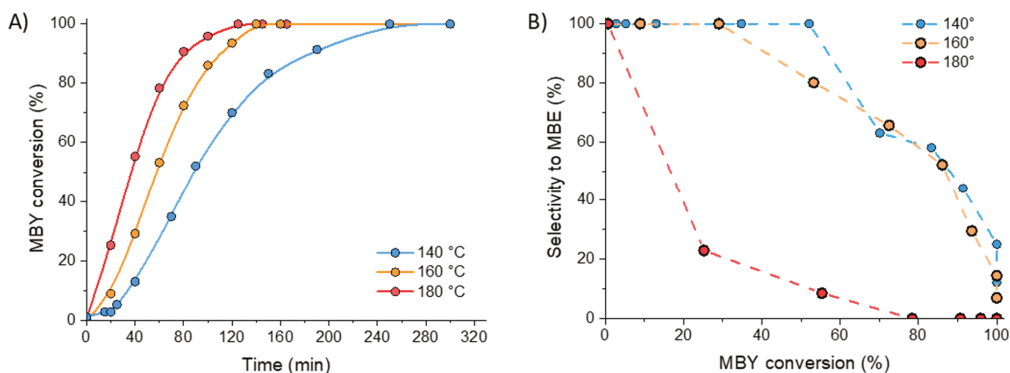


Figure 5.5 MBY conversion vs time (frame A) and selectivity of MBE vs MBY conversion (frame B) for 7nm_Cu/SiO₂ at T= 140 °C, 160 °C and 180 °C. Reaction conditions: see **section 5.2**. The lines are guides to the eye.

The selectivity (Figure 5.5B) is clearly higher to the desired 2-methyl-3-buten-2-ol at lower temperatures for a given conversion. For instance, at 25 % MBY conversion, a selectivity of 100% was achieved at 140 and 160 °C, while at 180 °C the selectivity was only 25%. At 50 % conversion, the catalyst retains 100% selectivity at 140°C, while at 160 and 180°C the selectivities were 80% and 9%, respectively. For the test carried at 180 °C, the reaction media at the end of the test appeared yellow/orange, suggesting possible formation of other compounds (possibly oligomers), however in such low concentrations that it was not possible to recover enough material for analysis.

The higher selectivity at lower temperatures is explained by a higher activation energy for the hydrogenation of MBE to MBA (unselective reaction) than for the desired MBY to MBE conversion.²³³ Regarding formation of other side products (see **section 5.4**), hydrogenolysis reactions are typically favored at higher temperatures, with activation energies of the order of 50–250 kJ mol⁻¹; much higher than the value found for the desired hydrogenation reaction

for 7nm_Cu/SiO₂. Hence it is clear that relatively low reaction temperatures should be chosen to avoid such byproducts, in which case the selectivity to the desired MBE product is mostly determined by competition with the fully hydrogenated MBA. Hence the competition between these two products is discussed in more detail in the next section.

5.6 – Catalyst selectivity

To better understand the selectivity to the desired MBE intermediate product, Figure 5.6A directly compares for the 7 nm Cu catalyst the conversion vs. reaction time for the hydrogenation of MBE alone at 160 °C (tested in a separate experiment) and that of MBY. Frame B of Figure 5.6 reports the concentration of reactant and products during the MBE hydrogenation test depicted in frame A.

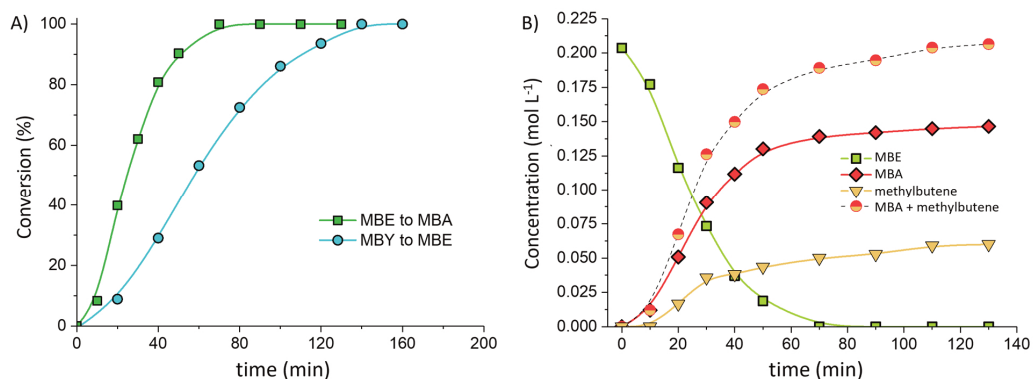


Figure 5.6 A) Conversion of MBE (2-methyl-3-buten-2-ol) to MBA (2-methylbutanol) and conversion of MBY (2-methyl-3-butyn-ol) to MBE as function of the reaction time. Reaction conditions: 0.2 mol L⁻¹ MBY (or MBE) in toluene, 14 mg Cu in the 7nm_Cu/SiO₂ catalyst), 20 bar H₂, 160 °C. The lines are drawn to guide the eye. B) Product distributions for the conversion of MBE (2-methyl-3-buten-2-ol) to MBA (2-methylbutanol). C-balance after 130 min of reaction test equal to 100%.

The hydrogenation of MBE is much faster than that of MBY. For instance, a moderate conversion of 40% is reached within 20 minutes for MBE to MBA, while for MBY to MBE conversion the same level was reached in 50 minutes. MBE hydrogenation only led to around 80 % selectivity to MBA (Figure 5.6B), with only methylbutene(s) detected as secondary product (notice that no acetone was detected, as expected from **scheme 5.2**). The hydrogenation rate of MBE is hence almost 2.5 times that of MBY under these reaction conditions. The faster hydrogenation of the alkenol due to respect to alkyne conversion was also observed in literature for Pd. For instance, commercial Pd-based catalyst (Lindlar catalyst, 5 wt % Pd/CaCO₃ modified with Pb) tested at temperatures between 40 and 80°C, also showed

apparent kinetic constant of MBE hydrogenation higher than the one for MBY hydrogenation of a factor 1.2-2.²³³

The fact that nevertheless high selectivities to MBE can be achieved means that the selectivity is probably explained by differences in adsorption strength of the compounds involved, i.e., stronger adsorption of the triple bond in the alkynol than for the double bond in the alkenol, facilitating the selectively hydrogenated product to leave the metal surface and having a small chance of being re-adsorbed and further hydrogenated. The high catalyst selectivity observed for 7nm_Cu/SiO₂, e.g., 100 % MBE selectivity at 50 % MBY conversion (140 °C, Figure 5.5) is hence explained by a much stronger adsorption and hence surface coverage of the Cu active sites with MBY rather than with MBE.

A comparison can be made with Pd and modified Pd-based catalysts. Alberto González-Fernández et. al. investigated the dependency of the MBE selectivity on the MBY conversion for 1% Pd/ZnO, 1% Pd/Al₂O₃ and 5% Pd Lindlar catalyst. The materials were tested in gas phase hydrogenation of MBY at 130 °C and 1 atm total pressure (<1% MBY, balance H₂). High selectivities (95 %) were achieved for Pd supported on ZnO at 10 % MBY conversion. The main byproduct of the reaction was MBA. At 60% conversion, Pd/Al₂O₃ and Pd/ZnO displayed selectivities of around 30 % and 75 %, while the Lindlar-type catalyst yielded around 60% selectivity to MBE. Liquid phase tests for Pd-based catalysts were carried out by Shen *et al.*²³⁵, which synthesized and tested pure Pd nanoparticles supported on nitrogen doped carbon(CN), with and without Zn/ZnO as promoter. The reaction conditions were: 0.245 M MBY in water, 5 bar H₂, stirring rate 1000 rpm, 35 °C. The authors observed a selectivity of ~75% at around 70 % conversion in case of pure Pd supported on CN (max selectivity observed: 85% at 25% MBY conversion). The highest reported selectivity was measured for PdZn/ZnO, around 95% between 10 and 50% 2-methyl-3-butyn-2-ol conversion.

This means that the MBE selectivity of close to 100% at 50% conversion for the Cu catalysts reported in this work is clearly superior to what is generally reported for unpromoted Pd-based hydrogenation catalysts. We also showed that reaction temperature is an important parameter to achieve high selectivities by avoiding formation of byproducts. Even higher selectivities might be achieved by optimizing the reaction conditions (e.g. using a lower H₂ pressure, or different solvent) or via the use of promoters.²⁴¹

5.7 – Conclusion

The activity and selectivity of supported Cu nanoparticles were assessed for the liquid phase selective hydrogenation of 2-methyl-3-butyn-2-ol to 2-methyl-3-buten-2-ol, a crucial reaction for the production of vitamins and fragrances. Our 5.7 wt% Cu/SiO₂ catalysts are rather active, with full conversion of MBY within 3 h at 160 °C (2% MBY in toluene, 250 mg of catalyst). Regarding surface-normalized activity, the 7 nm particles were twice as active as 2 nm Cu (TOF ~ 0.1 s⁻¹ @ 160 °C). In addition, the 7 nm Cu was much more selective displaying full selectivity to MBE up to 50% MBY conversion at 140 °C. This high selectivity is due to

preferential adsorption of MBY over MBE on the Cu surface, as full selectivity was obtained even though the conversion of MBE is 2.5 times faster. Lower temperatures limited both overhydrogenation to MBA as well as formation of other byproducts. Hence, Cu represents a good candidate for the selective hydrogenation of alkynol to alkenol; although higher reaction temperatures are needed, its selectivity rivals that of unpromoted Pd catalysts at similar conversions.

5.8 – Acknowledgements

The experimental work described in this chapter was performed at the Materials Chemistry and Catalysis (MCC) group, which is part of the Debye Institute for Nanomaterials Science at Utrecht University.

The author of this thesis designed and performing the catalytic experiments hereby reported, analysed the data, prepared the first draft of the text of the chapter, and carried out samples' characterization and testing. The author gratefully acknowledges Prof. dr. Petra E. de Jongh and dr. Laurent Delannoy for the supervision, for contributing to the discussion of the results of the experiment, and for contributing to the finalization of the text of this chapter. The author also gratefully acknowledges Jan Willem de Rijk for the technical assistance on the catalytic set-ups as well as in aiding the design of the experiments, Ad van der Eerden for everything concerning the safety of the high-pressure experimental setup, Ing. Pascal Wijten for his help on setting up and rationalizing GC-FID and GCMS measurements, and Dr. Remco Dalebout for his help on GC-FID.

Summary and Outlook

Catalysts enable the production of numerous compounds, such as specialty materials, bioactive compounds, fuels and indirectly even food. They do not only have an important economic and societal impact, but are also particularly important for the environment. Modern catalyst design contributes to a more sustainable human activity and healthier environment by lowering the impact of chemical processes, achieving carbon circularity, producing renewable fuels, and minimizing the negative impact of transportation. Studies on catalysts performance and their dependence on reaction conditions and catalyst structure and composition are hence crucial, both from a fundamental point of view and in the context of their deployment in relevant applications.

This thesis covers the activity, stability, and selectivity of supported Cu catalysts for relevant gas- and liquid-phase selective hydrogenation reactions. The main aim was to gain insight into the reaction mechanisms and kinetics, develop a reliable testing methodology, and to understand the mechanism governing catalyst selectivity. To this end, we synthesized and tested Cu-nanoparticles supported on either on C or SiO₂. Additionally, we adapted the catalyst synthesis procedure to obtain different nanoparticle sizes, in the range of 2 to 10 nm. The catalysts were assessed for the selective hydrogenation of trace amounts of 1,3-butadiene in large excess of propene, as well as for the hydrogenation of 2-methyl-3-butyn-2-ol, a reaction for which Cu catalysts had not been studied yet. We focused on fundamental understanding of these catalytic processes, while at the same time adopting testing conditions to mimic as closely as possible typical industrial working conditions.

Chapter 1 provides a general overview on Cu nanoparticles and on the basics of nanoparticle catalysis and synthesis methodologies. The uniqueness of Cu is explained, both in terms of d-band theory as well as based on established literature concerning its use in relevant processes, such as methanol synthesis and selective hydrogenation of unsaturated organic moieties. A brief review on particle size effects is provided, with specific focus on Cu. Lastly, a detailed introduction to the selective hydrogenation of 1,3-butadiene, from a molecular point of view to practical applications, is given.

Chapter 2 focuses on the use of nanoparticulate Cu in the selective hydrogenation of 1,3-butadiene in the presence of a 100-fold excess of propene. The reaction is particularly relevant for the production of high-quality olefins and subsequent more complex products. From a fundamental viewpoint, it presents an important challenge as virtually full selectivity to alkenes is required for the catalyst, i.e. exclusive hydrogenation of the trace amount of 1,3-butadiene while leaving the olefins untouched. Cu-based catalysts had been reported as active for the selective hydrogenation of different unsaturated hydrocarbons, however, their poor stability limited further investigation. A crucial point is the testing methodology, which is critical for catalysts prone to oxidation. We demonstrate that the use of inert supports and accurate particle size control via incipient wetness impregnation, are valuable strategies to

produce highly selective to butenes (~99%) and stable Cu nanoparticulate catalysts. An explanation for the high catalyst selectivity is provided, as well as reflections on the hydrogenation kinetics, which are more widely of relevance for other Cu-catalyzed selective hydrogenations.

Chapter 3 discussed in more detail the particle size effect on activity and selectivity of Cu nanoparticles in the selective hydrogenation of 1,3-butadiene. All nanoparticle-based catalysts are expected to show size-dependent activities. However, the specific trends depend on both the reaction and the active metal itself. The particle size effect can lead to interesting behavior in terms of activity and selectivity of the catalyst, deviating from just scaling with the exposed metal surface area. The activities and selectivities of 2, 3, 4, 7 and 10 nm Cu nanoparticles supported on SiO₂ are reported. Maximum activity (normalized to the Cu surface area) was observed for particles of 4 to 7 nm, which were 3 to 4 times more active than 2 nm particles. This higher activity was explained by the fraction of kinks and steps sites, which are essential to activate hydrogen, which was observed being the rate limiting step for the selective conversion of 1,3-butadiene. In terms of preferential hydrogenation of 1,3-butadiene to butenes, the nanoparticles of 4 and 7 nm were also the ones with the highest selectivity in the investigated series.

Kinetic analysis of propene hydrogenation, the unwanted reaction, as well as adsorption and calorimetric experiments, established that the selectivity is due to the preferred adsorption of 1,3-butadiene with respect to propene and butenes on the Cu surface. The findings of this chapter may guide both testing and catalyst design for reactions where hydrogen surface availability and specific moiety selectivity play a key role.

Chapter 4 presents a preliminary investigation of the effect of common metal/metal oxide additives for Cu-based hydrogenation catalysts. Cu nanoparticles were synthesized via incipient wetness co-impregnation in the presence of Mn, Fe or Zn oxide precursors, and tested for the reaction that was also reported in Chapter 2 and 3. The experiments showed that Fe oxides mildly suppressed Cu hydrogenation activity and decreased Cu selectivity already at very low concentration of modifier, i.e., 1:99 Fe:Cu atomic ratio. The addition of Zn oxides did not have a significant effect on total hydrogenation activity, but altered the rate with which 1,3-butadiene and propene were hydrogenated, leading to a strong decrease in catalyst selectivity (<50%, even at low 1,3-butadiene conversion). Mn oxides, on the other hand, improved the catalyst activity 2 to 3-fold, while completely retaining the high selectivity to butenes of the unmodified sample.

Chapter 5 moves from selective hydrogenation in gas phase, to the same type of reaction in liquid phase. Cu/SiO₂ was tested for the selective (partial) hydrogenation of alkynols to alkenols, a highly relevant conversion step widely employed in the synthesis of fat-soluble vitamins, pharmaceuticals, and fragrances. This conversion presents an interesting challenge, as the unwanted conversion of the alkenols is faster (around twice as fast) than the hydrogenation of the alkynol, hence a very high selectivity of the catalyst is required. We show that 7 nm Cu nanoparticles are 2.5 times more active (surface normalized) than 2 nm

ones. At the same time, the larger particles showed much higher selectivities, around ~100% at 50% conversion ($T_{\text{reaction}}=140\text{ }^{\circ}\text{C}$). Cu nanoparticles showed selectivities that rivals the one of Pd (unpromoted), a commonly used active metal for hydrogenation processes.

To summarize, supported Cu nanoparticles are very promising for the selective (partial) hydrogenation of polyunsaturated (or highly unsaturated) compounds. Monometallic Cu-based catalysts, which are known in literature to be prone to deactivation during hydrogenation of polyunsaturated molecules (i.e., due to formation of long-chain oligomers), can be made more stable by suppressing unwanted side reactions. This can be obtained by careful control of Cu nanoparticle size, reaction conditions, and by adopting inert supports such as C and SiO_2 .

Catalyst design allows to tune catalyst activity and selectivity, which are maximum at a particle size of 4 to 7 nm. Hydrogenation of polyunsaturated compounds is rate limited by hydrogen surface availability. This governs the catalyst activity (such as its dependency on particle size) and, together with preferential adsorption of polyunsaturated vs. monounsaturated moieties, also the catalyst selectivity. Other examples of nanoparticulate Cu catalyzed reactions for which activity and selectivity depend on the concentration of hydrogen at the catalyst surface, such as methanol synthesis and the hydrogenation of ethyl acetate, were recently reported in the scientific literature. This indicates that the knowledge gathered in this thesis is relevant also for other Cu-catalyzed (or base metal-catalyzed) hydrogenation processes. The advanced understanding of the behavior of this base active metal, and its catalytic properties, may assist in developing very selective and stable hydrogenation catalysts. Cu is a promising alternative to noble-metal based hydrogenation catalysts, which regularly require the use of potentially hazardous stabilizers and selectivity additives. Its use hence may assist in developing a more efficient use of energy, material and resources in applied hydrogenation catalysis.

Nederlandse samenvatting

Katalysatoren zijn essentieel voor het maken van dagelijkse producten zoals plastic, medicijnen, brandstoffen en voedingsstoffen. Ze zijn niet alleen van groot economisch belang, maar ook relevant voor het milieu en de energietransitie. Moderne katalysatoren kunnen bijdragen aan het verlagen van het energie-, materialen- en grondstoffengebruik; ze dragen bij aan circulariteit en verminderen van de CO₂ uitstoot en andere negatieve emissies in de transportsector. Het begrijpen van de eigenschappen en hoe hun effectiviteit afhangt van procescondities, katalysatorstructuur en -samenstelling is erg belangrijk, zowel vanuit wetenschappelijk oogpunt als voor praktisch gebruik.

Het onderzoek beschreven in dit **proefschrift** gaat over de activiteit, selectiviteit en stabiliteit van gedragen koperkatalysatoren voor relevante gas- en vloeistoffase selectieve hydrogeneringsreacties. Het voornaamste doel was om inzicht te verkrijgen in reactiemechanismen en kinetiek, om een betrouwbare testmethodologie te ontwikkelen, en om te begrijpen welke factoren bepalend zijn voor de selectiviteit van katalysatoren. Om dit doel te bereiken, onderzochten we kopernanodeeltjes aangebracht op poreus koolstof of silica. Een bereidingsmethode werd ontwikkeld om verschillende grootten kopernanodeeltjes te verkrijgen, tussen de 2 en 10 nm in diameter. Deze katalysatoren werden getest in een reactie waarbij sporen 1,3-butadien in een grote overmaat aan propaan gehydrogeneerd werden. Ook werden voor de eerste keer koperkatalysatoren getest om 2-methyl-3-butyn-2-ol te hydrogeneren. Hoewel begrip het hoofddoel was, werden de reactiecondities zodanig gekozen dat ze de industriële procescondities zo goed mogelijk benaderden.

Hoofdstuk 1 geeft achtergrond met betrekking tot kopernanodeeltjes en de katalytische eigenschappen en synthesemethoden voor nanodeeltjes. Koper is uniek, zowel in zijn elektronische (d-band) structuur als ook als unieke katalysator voor bepaalde chemische reacties zoals de synthese van methanol en de selectieve hydrogenering van onverzadigde koolstof-koolstof-bindingen. Na een korte uitleg over deeltjesgrootte-effecten, bevat dit hoofdstuk als laatste zowel moleculaire and toepassingsrelevante informatie over de selectieve hydrogenering van 1,3-butadien.

Hoofdstuk 2 richt zich specifiek op kopernanodeeltjes voor 1,3-butadien hydrogenering in een honderdvoudige overmaat van propaan. Deze reactie is erg relevant om alkenen en daaruit weer nog complexere producten zoals polymeren te maken. Wetenschappelijk is dit uitdagend omdat de *selectiviteit* kritisch is: sporen van 1,3-butadien moeten volledig omgezet worden, terwijl de grote overmaat aan alkenen onaangeroerd moet blijven. Tot nu toe beschouwden weinigen koperkatalysatoren als relevant voor selectieve hydrogeneringsreacties, waarschijnlijk vanwege de geringe stabiliteit. De juiste testprocedure is essentieel voor dit type katalysatoren dat erg gevoelig is voor oxidatie. Wij laten zien dat ons gebruik van inerte dragermaterialen en goede controle over de deeltjesgrootte door impregnatie (juist voldoende metaalzoutoplossing toe dienen om de poriën van de drager te

vullen en dan door verhitting dit om te zetten in metaal nanodeeltjes op de drager), een succesvolle aanpak is om katalysatoren te maken die zeer selectief buteen maken (~99%) en bovendien erg stabiel zijn. Deze grote selectiviteit wordt onderbouwd, en inzicht wordt gegeven in de kinetiek van de hydrogenatie, wat ook relevant is voor koper-gekatalyseerde selectieve hydrogenering van andere moleculen.

Hoofdstuk 3 gaat in detail in op de invloed van deeltjesgrootte op de activiteit en selectiviteit van kopernanodeeltjeskatalysatoren. Voor alle gedragen metaalkatalysatoren is de deeltjesgrootte belangrijk voor hoe actief ze zijn, maar hoe die afhankelijkheid precies is hangt af van het type metaal en reactie. Hoewel je zou verwachten dat de activiteit schaaft met het specifieke metaaloppervlak (m^2/g) is dat vaak niet het geval. Katalysatoren met 2, 3, 4, 7 en 10 nm koperdeeltjes gedragen op silica werden bestudeerd. Genormaliseerd naar het koperoppervlak waren de 4 tot 7 nm koperdeeltjes het meest selectief en het meest actief, zo'n 3 tot 4 keer actiever dan de 2 nm deeltjes. Dit komt omdat bij deze 4 tot 7 nm deeltje een groot deel van het metaaloppervlak kristalvlakken betreft met veel monoatomaire treden (een hoge Miller index), en/of vlakken waarvoor alle drie de Miller indices verschillend zijn, en deze treden ook nog regelmatig verspringen. De snelheidsbepalende stap in de hydrogenering van butadien is namelijk de adsorptie en splitsing van diatomaire waterstofmoleculen, en dit proces verloopt bijzonder snel op bovengenoemde plekken op het metaaloppervlak. Analyse van de snelheid waarmee propen wordt gehydrogeneerd (de ongewenste reactie), gecombineerd met adsorptie- en warmteopnamemetingen, toonde aan dat de hoge selectiviteit te wijten was aan het feit dat 1,3-butadien heel veel sterker adsorbeert op het kopermetaaloppervlak. Op het metaaloppervlak aanwezig waterstofatomen binden dus bij voorkeur aan dit molecuul simpelweg omdat het metaaloppervlak hiermee bedekt is, en niet met andere moleculen die eventueel gehydrogeneerd zouden kunnen worden. Dit is een belangrijk inzicht voor het op de juiste wijze testen en ontwerpen van katalysatoren waarbij de beschikbaarheid van waterstof op het metaaloppervlak om bepaalde groepen te hydrogeneren de limiterende factor is.

Hoofdstuk 4 is een eerste verkenning van het toevoegen van metaaloxide, die vaak worden gebruikt als additieven, maar niet voor de door ons bestudeerde koper-gebaseerde hydrogeneringskatalysatoren. De kopernanodeeltjes werden afgezet in aanwezigheid van Mn, Fe of Zn zouten, en getest als katalysatoren voor dezelfde reactie die ook in hoofdstuk 2 en 3 beschreven staat. Ijzeroxiden maakten de koperkatalysator minder actief en ook met slechts 1% ijzeroxide nam de selectiviteit al af. Zinkoxiden hadden weinig effect op de activiteit van de koperkatalysator, maar veranderden de snelheid waarmee 1,3-butadien en propen werden omgezet, waardoor de selectiviteit bijzonder laag werd (<50% zelfs wanneer nauwelijks butadien werd omgezet). Daarentegen verbeterde het toevoegen van mangaanoxiden de activiteit van de katalysator met een factor twee tot drie, terwijl de zeer hoge selectiviteit naar buteen behouden bleef.

Hoofdstuk 5 behandelt ook hydrogenering, maar niet zoals in de andere hoofdstukken van gassen, maar met een vloeibaar reactiemedium. Cu/SiO_2 werd gebruikt om alkynolen te hydrogeneren naar een alkenolen. Dit is een belangrijke reactiestap om vet-oplosbare

vitaminen te maken, maar ook medicijnen en geurstoffen. De omzetting is een interessante uitdaging omdat de volgende reactie stap waarin C-C binding volledig verzadigd wordt, normaal gesproken twee keer zo snel verloopt als de eerste stap naar het gewenste product. Een selectieve katalysator is dus essentieel. Oppervlakte-genormaliseerd waren 7 nm kopernanodeeltjes 2.5 keer zo actief als 2 nm deeltjes. Belangrijk was dat de grotere deeltjes ook veel selectiever waren, met vrijwel volledige selectiviteit bij 50% omzetting ($T_{\text{reactie}}=140\text{ }^{\circ}\text{C}$). Kopernanodeeltjes zijn hiermee net zo selectief als palladium (zonder additieven), het algemeen gebruikte metaal om deze reactie te katalyseren.

Samenvattend kunnen we stellen dat kopernanodeeltjes zeer veelbelovend zijn voor de hydrogenering van meervoudig onverzadigde moleculen. Tot nu toe werd koper als een weinig stabiele katalysator beschouwd, waarbij het activiteitsverlies waarschijnlijk te wijten was aan geleidelijke bedekking van het metaaloppervlak met polymeren, die gevormd werden door nevenreacties. Wij laten echter zien dat dit voorkomen kan worden door zorgvuldig de kopernanodeeltjesgrootte en reactiecondities te kiezen, en gebruik te maken van weinig reactieve dragermaterialen zoals koolstof en silica. Zowel activiteit als selectiviteit zijn maximaal bij een koperdeeltjesgrootte van 4 tot 7 nm. De snelheidsbepalende stap bij de hydrogenering is de beschikbaarheid van waterstof op het metaaloppervlak waar de reactie plaats vindt. De beschikbaarheid van waterstof verklaart zowel waarom deze deeltjesgrootte optimaal is voor de activiteit als de selectiviteit, wanneer ook in aanmerking wordt genomen dat meervoudig onverzadigde moleculen sterker geadsorbeerd worden dan moleculen met eenvoudig onverzadigde bindingen (en dus een veel hogere oppervlakte-bedekkingsgraad hebben).

De nieuwe kennis in dit onderzoek verkregen en in dit proefschrift beschreven is ook relevant voor andere hydrogeneringsreacties die door koper gekatalyseerd kunnen worden, zoals methanol synthese en ester hydrogenering. Het kan leiden tot het ontwikkelen van relatief goedkope en zeer selectieve en stabiele katalysatoren. Koper is daarmee een veelbelovend alternatief voor edelmetalen, die vaak ook potentieel gevaarlijke of milieuonvriendelijke additieven nodig hebben, en kan leiden tot efficiënter gebruik van energie, metalen en andere grondstoffen in grootschalige hydrogeneringsprocessen.

Riepilogo in italiano

Cenni di catalisi eterogenea

Con il termine *catalisi* ci si riferisce al fenomeno per cui la velocità di una reazione chimica è modificata (accelerata) dall'azione di una sostanza o materiale detto *catalizzatore*. Quest'ultimo è generalmente presente in piccole quantità - se comparato alla concentrazione dei reagenti - e non partecipa direttamente alla reazione, restando dunque inalterato nel tempo. Grazie all'azione di un catalizzatore, ad esempio, reazioni che potrebbero portarsi a compimento in tempi nell'ordine di anni o più, sono in grado di verificarsi nel giro di ore, minuti o anche tempi inferiori al secondo. In altre parole, la catalisi rende accessibile la produzione di determinate sostanze in tempi compatibili con la vita stessa.

Non sorprende, dunque, che i sistemi biologici come il corpo umano posseggano numerosissimi catalizzatori, detti *enzimi* (chimicamente, proteine). Alcuni esempi: gli enzimi *proteolitici* scindono i legami peptidici, consentendo la digestione di proteine, il ricambio cellulare e la coagulazione del sangue. Le *amilasi* agiscono sull'amido rendendolo digeribile. La *catalasi* modula la concentrazione di specie reattive dell'ossigeno, ed è lo stesso enzima responsabile per la formazione di schiuma quando si utilizza dell'acqua ossigenata nella disinfezione di una ferita (le bollicine non sono nient'altro che ossigeno prodotto dalla scissione dell'acqua ossigenata in ossigeno e comune acqua). Questa lista è ben lontana dall'essere esaustiva. È importante però aggiungere che tutti questi enzimi non sono solo in grado di accelerare reazioni chimiche, ma sono anche specifici. Ovvero accelerano solo specifiche reazioni chimiche, legandosi a specifiche sostanze/reagenti (un po' come ad una serratura corrisponde un'unica chiave) e producendo determinati prodotti.

I catalizzatori non sono presenti esclusivamente nei sistemi biologici; oltre agli enzimi, esistono altre tipologie di catalizzatori, sia presenti in natura o sintetizzabili in laboratorio. Tutti hanno sentito parlare della cosiddetta marmitta catalitica (o convertitore catalitico), un dispositivo che, ad esempio, accelera l'ossidazione di vapori di idrocarburi incombusti ed il tossico monossido di carbonio - questo nel caso dei catalizzatori ossidanti - riducendo l'impatto delle automobili su ambiente e salute umana. Nell'industria chimica sono numerosissimi gli esempi di catalizzatori utilizzati per la produzione di sostanze e materiali. Basti pensare che la catalisi è indirettamente responsabile per circa il 35% del Prodotto Interno Lordo mondiale e di circa il 90% (in volume) della produzione di sostanze chimiche (**Capitolo 1**). Senza la catalisi industriale non sarebbe possibile produrre fertilizzanti, carburanti e biocarburanti, idrogeno (mediante processi elettro- o fotoelettro- catalitici), fibre sintetiche, plastiche, vernici e farmaci. In aggiunta, oggi la catalisi gioca un ruolo fondamentale nel ridurre l'impatto ambientale di mezzi di trasporto, processi chimici e produzione industriale.

Ma come funzionano i catalizzatori? Le reazioni chimiche, al fine di verificarsi, richiedono il superamento di una barriera energetica, detta *energia di attivazione*; questa barriera energetica può essere “superata” ad esempio incrementando la temperatura dei reagenti fino ad “innescare” la reazione. Il ruolo del catalizzatore è quello di abbassare l’energia di attivazione senza perturbare energia di prodotti e reagenti. Esemplicando, il lettore può immaginare questa barriera energetica come una montagna nel mezzo del percorso che collega due città distanti. Una opzione - *non catalizzata* - potrebbe essere quella di muoversi da una città all’altra scalando la montagna, il che richiederebbe una grande quantità di energia. La seconda opzione - *catalizzata* - consisterebbe invece nell’attraversare la montagna tramite un tunnel. Nell’ultimo caso, il risultato sarebbe lo stesso, ma lo sforzo necessario sarebbe di gran lunga inferiore ed il percorso più rapido. In questo caso la compagnia di costruzione del tunnel farebbe le veci di *catalizzatore*. L’uso di un catalizzatore, in pratica, può comportare una riduzione dell’energia necessaria al sostentamento di una reazione (o processo) chimico, portando alla formazione più rapida ed efficiente di prodotti chimici e parallelamente una minore produzione di scarti.

Questo lavoro di **tesi** si sofferma principalmente su catalizzatori a base di rame (simbolo chimico *Cu*). Il rame è un metallo presente in natura in grandi quantità, facilmente estraibile, che gode di importanti proprietà chimico-fisiche, come ad esempio elevata conducibilità termica ed elettrica. Cu è anche già largamente utilizzato in importanti processi chimici, come la sintesi di metanolo, molecola fondamentale per la produzione di una grande quantità di sostanze chimiche di interesse industriale.

Tuttavia, il rame, così come tanti altri metalli, non può essere utilizzato direttamente come catalizzatore nella sua forma originale e macroscopica. Infatti, le reazioni catalitiche (eterogenee) sono processi che avvengono in corrispondenza della superficie di contatto tra catalizzatore e reagenti. Dunque, una valida strategia per aumentare l’efficienza di utilizzo di un catalizzatore solido è quello di produrlo sottoforma di particelle fini, incrementandone esponenzialmente la superficie esposta. Nell’industria chimica, così come nell’ambito della ricerca chimica, è di ampio interesse la sintesi e l’utilizzo di particelle di diametri estremamente ridotti, dell’ordine di 1-100 nanometri (cosiddette *nanoparticelle*). Si tenga conto che 1 nanometro corrisponde 1 miliardesimo di metro (0.000000001 metri, o 10^{-9} metri). Per dare un’idea al lettore delle dimensioni in gioco, si immagini una collana di perle, ogni perla delle dimensioni di un nanometro. La collana dovrebbe essere formata da un quarto di milione di perle (250’000) affinché abbia la stessa circonferenza di un capello umano. Equivalentemente, si immagini che il rapporto di dimensione che esiste fra una grande arancia e l’intero pianeta Terra è lo stesso presente fra un’arancia ed una nanoparticella di 1 nanometro.

La strategia di preparazione di catalizzatori a base di nanoparticelle non è semplicemente guidata dall’obiettivo di massimizzare la superficie di contatto tra metallo e reagenti. Le nanoparticelle hanno, difatti, proprietà chimico-fisiche differenti dal materiale di dimensioni macroscopiche. È necessario, dunque, controllare la loro struttura e morfologia superficiale in fase di sintesi. Difatti, nonostante le nanoparticelle metalliche possano possedere struttura

cristallina, gruppi di atomi che ne ricoprono la superficie possono essere organizzati in diverse geometrie. Ognuna delle suddette geometrie può rendere il catalizzatore più o meno attivo e selettivo, e talune possono favorire la produzione di certi prodotti anziché altri.

Una volta preparate, le nanoparticelle raramente vengono utilizzate tal quali. Nel caso di catalizzatori solidi, queste vengono depositate su supporti porosi, come ad esempio carboni attivi, gel di silice, allumina o materiali ceramici ed ossidi metallici. Ciò al fine di evitare la loro coagulazione, migliorarne l'usabilità e per garantire facile separazione dai prodotti finiti. Il supporto stesso può essere inerte nei confronti della reazione, parteciparvi come co-catalizzatore, o cambiare le proprietà delle nanoparticelle. Inoltre, è possibile l'aggiunta di sostanze additive al fine di migliorarne le prestazioni catalitiche. Ciò, insieme alla loro ridotta dimensione, rende sintesi ed il loro studio complesso. Basti pensare che al fine di "fotografarle" (per misurarne il diametro e forma) si adoperano microscopi elettronici con un costo che può superare le centinaia di migliaia di euro e che richiedono edifici appositamente costruiti ed isolati da ogni vibrazione. Il loro studio, sia dal punto di vista teorico e pratico, è però fondamentale e può avere risvolti importanti sulla società.

Contenuto della tesi

Questa **tesi** riguarda lo studio dell'attività, la stabilità e la selettività di catalizzatori a base di nanoparticelle di rame supportate su materiali porosi, per rilevanti reazioni di idrogenazione selettiva in fase gassosa e liquida. L'obiettivo dello studio alla base di questa tesi era quello di ottenere informazioni sui meccanismi e sulla cinetica di reazione, sviluppare una metodologia di test affidabile, verificare la dipendenza delle prestazioni catalitiche sulla base del diametro particellare, e comprendere il meccanismo che governa la selettività del catalizzatore. A tal fine, sono stati sintetizzate e testate nanoparticelle di Cu supportate su C o SiO₂. La procedura di sintesi del catalizzatore è stata adattata al fine di ottenere diverse dimensioni delle nanoparticelle, specificatamente nell'intervallo da 2 a 10 nm. I catalizzatori sono stati testati nella reazione di idrogenazione selettiva di tracce di 1,3-butadiene presenti in largo eccesso di propene, nonché per l'idrogenazione di 2-metil-3-butin-2-olo (quest'ultima una reazione per la quale i catalizzatori di Cu non erano ancora stati studiati). Lo studio si è soffermato sulla comprensione fondamentale di questi processi catalitici, allo stesso tempo adottando condizioni di prova quanto più fedeli possibili alle tipiche condizioni di lavoro industriali.

Il **Capitolo 1** fornisce una panoramica generale sulle nanoparticelle di Cu, su concetti basilari di catalisi e sulle metodologie per la sintesi di catalizzatori metallici a base di nanoparticelle. Le peculiarità delle nanoparticelle di Cu è spiegata sia in termini di "teoria della banda *d*", sia sulla base della letteratura riguardante il loro utilizzo in processi di rilevanza industriale, come la sintesi di metanolo e l'idrogenazione selettiva di composti organici insaturi. Viene fornito, inoltre, un breve resoconto sulla dipendenza delle proprietà catalitiche in funzione della dimensione delle nanoparticelle (*particle size effect*), con

particolare attenzione al Cu. Infine, nel capitolo viene riportata un'introduzione dettagliata all'idrogenazione selettiva dell'1,3-butadiene, da un punto di vista sia molecolare che riguardante gli aspetti pratici ed industriali.

Il **Capitolo 2** si concentra sull'uso di nanoparticelle di Cu nell'idrogenazione selettiva dell'1,3-butadiene in presenza di un largo eccesso (100x) di propene. La reazione è particolarmente rilevante per la produzione di olefine di alta qualità e per la produzione, mediante suddette olefine, di successivi prodotti a più alto peso molecolare. Da un punto di vista fondamentale, la reazione qui descritta richiede elevatissime selettività (verso la produzione di alcheni), in quanto la reazione desiderata è l'idrogenazione esclusiva di 1,3-butadiene (presente in concentrazione pari a migliaia di ppm) lasciando intatte le olefine (come ad esempio il propene). La letteratura corrente descrive i catalizzatori a base di rame come attivi per l'idrogenazione selettiva di diversi idrocarburi (poli)insaturi. Tuttavia, la scarsa stabilità di catalizzatori a base di Cu ha limitato ulteriori indagini. Un punto importante è la metodologia utilizzata per testare le proprietà di questi catalizzatori, che si è rivelata di sostanziale importanza per catalizzatori soggetti a rapida ossidazione. In questa tesi viene dimostrato che l'uso di supporti inerti ed un accurato controllo del diametro delle particelle tramite impregnazione incipiente, sono valide strategie per la produzione di catalizzatori nanoparticellari di Cu altamente selettivi (~99%) e stabili. Viene infine fornita una spiegazione sui meccanismi alla base della loro elevata selettività, così come valutazioni sulla cinetica di idrogenazione, che sono più ampiamente rilevanti per altre idrogenazioni selettive catalizzate da Cu.

Il **Capitolo 3** espone l'effetto del diametro delle particelle sulle proprietà catalitiche di Cu nanoparticellare, nel contesto dell'idrogenazione selettiva di 1,3-butadiene. In linea di principio, tutti i catalizzatori basati su nanoparticelle dovrebbero mostrare attività dipendenti dalle dimensioni delle stesse. Tuttavia, gli intervalli di diametri alla quale questo effetto è visibile dipendono sia dalla reazione che dal metallo attivo. La modulazione dei diametri particellari può portare all'ottimizzazione dell'attività catalitica e a maggiori selettività del catalizzatore, mostrando un comportamento che non è banalmente funzione lineare della superficie specifica esposta.

Questo capitolo si concentra specificatamente su attività e selettività delle nanoparticelle di Cu con diametri di 2, 3, 4, 7 e 10 nm supportate su SiO₂. La massima attività (normalizzata alla superficie di Cu) è stata osservata per particelle da 4 a 7 nm, che erano da 3 a 4 volte più attive delle particelle da 2 nm. Questa maggiore attività può essere ascritta alla maggiore densità di siti attivi di quali *kinks* e *steps*, siti che risultano essenziali per attivazione dell'idrogeno. Questa reazione, difatti, è il passaggio cineticamente limitante per la conversione selettiva dell'1,3-butadiene. Per nanoparticelle di 4 e 7 nm, è stato osservato anche la più alta selettività nell'intera serie. L'analisi cinetica dell'idrogenazione del propene (si noti, reazione indesiderata), nonché esperimenti di adsorbimento e misure calorimetriche, hanno stabilito che la più alta selettività delle particelle di 4 e 7 nm è dovuta al più forte adsorbimento, sulla superficie di Cu, di 1,3-butadiene contro l'adsorbimento propene e buteni. Le osservazioni riportate in questo capitolo possono essere potenzialmente estese alla

preparazione (ed analisi) di catalizzatori per idrogenazioni selettive, laddove la concentrazione superficiale di idrogeno (attivato) e selettività a specifici gruppi funzionali altamente insaturi giocano un ruolo fondamentale sulle performance catalitiche.

Il **Capitolo 4** presenta un'indagine preliminare sull'effetto dei comuni additivi metallici (o ossidi metallici) per catalizzatori di idrogenazione a base di rame. In questo caso, le nanoparticelle di Cu sono state sintetizzate tramite co-impregnazione incipiente ed in presenza di precursori di ossidi di Mn, Fe o Zn. I catalizzatori così sintetizzati sono stati testati nella reazione descritta nei Capitoli 2 e 3. Gli esperimenti hanno dimostrato che gli ossidi di Fe hanno un effetto deleterio sia per quanto riguarda l'attività di idrogenazione delle nanoparticelle di Cu, sia riguardo la loro selettività. Peggiori prestazioni catalitiche si sono osservate a una concentrazione molto bassa di additivo, specificatamente 1:99 di rapporto atomico Fe:Cu. L'aggiunta di ossidi di Zn non ha avuto effetti significativi sull'attività di idrogenazione totale (consumo totale di idrogeno), ma ha alterato il rapporto tra velocità di idrogenazione di 1,3-butadiene e propene. Ciò ha comportato una forte diminuzione della selettività del catalizzatore (<50%, anche a bassa conversione di 1,3-butadiene). Gli ossidi di Mn, d'altra parte, hanno migliorato l'attività del catalizzatore di un fattore 2-3, pur mantenendo sorprendentemente l'elevata selettività delle nanoparticelle.

Il **Capitolo 5** si sofferma sull'idrogenazione selettiva in fase liquida di 2-metil-3-butin-2-olo a 2-metil-3-buten-2-olo. La reazione fa parte del gruppo delle idrogenazioni selettive (parziale) di alcoli polinsaturi in alcoli monoinsaturi, un processo di conversione di estrema rilevanza nella sintesi di vitamine, prodotti farmaceutici e fragranze liposolubili. Questa conversione richiede catalizzatori altamente selettivi, in quanto la conversione indesiderata degli alcoli monoinsaturi è più veloce dell'idrogenazione degli alcoli polinsaturi (circa due volte più veloce, reazione indesiderata). Mostriamo che le nanoparticelle di Cu dal diametro di 7 nm sono 2,5 volte più attive (attività normalizzata alla superficie esposta di Cu) rispetto a quelle da 2 nm. Allo stesso tempo, le particelle più grandi hanno mostrato selettività molto più elevate (verso la specie monoinsaturata) di circa ~100% al 50% di conversione (reazione T = 140 °C). Le nanoparticelle di Cu hanno mostrato una selettività che compete, se non superiore, a quella del Pd (non promosso), un metallo attivo comunemente usato per i processi di idrogenazione.

In conclusione, le nanoparticelle di Cu sono molto promettenti nelle reazioni di idrogenazione parziale di composti polinsaturi, in particolar modo quando alte selettività sono necessarie. Il metallo attivo, che è tipicamente considerato instabile per questa classe di processi, può essere reso stabile da un attento controllo della dimensione delle particelle, delle condizioni di reazione e dall'adozione di supporti inerti come C e SiO₂. Il design del catalizzatore consente di regolare l'attività e la selettività del catalizzatore, che sono massime a una dimensione delle particelle compresa tra 4 e 7 nm. L'idrogenazione dei composti polinsaturi è limitata dalla disponibilità superficiale dell'idrogeno, che riteniamo essere alla base di molte altre idrogenazioni mediate da Cu. Le conoscenze qui raccolte sono rilevanti per altri processi di idrogenazione catalizzati da Cu (o catalizzati da metalli di base). Per quanto riguarda il Cu, la comprensione del comportamento di questo metallo attivo di base e delle sue proprietà

catalitiche può aiutare a sviluppare catalizzatori di idrogenazione largamente selettivi e stabili. Il Cu è un'alternativa promettente ai catalizzatori di idrogenazione a base di metalli nobili, che normalmente richiedono l'uso di stabilizzanti e additivi (per migliorarne la selettività) potenzialmente tossici e nocivi. Il suo utilizzo può quindi portare ad un uso più efficiente di energia, materiali e risorse nei processi di idrogenazione catalitica.

References

- (1) Greene, J. E. Tracing the 5000-Year Recorded History of Inorganic Thin Films from ~3000 BC to the Early 1900s AD. *Appl. Phys. Rev.* **2014**, *1*, 041302-1 – 041302-36.
- (2) Stanczak, M. A brief history of copper. <https://web.archive.org/web/20150203154021/http://www.csa.com/discoveryguides/copper/overview.php> (accessed Jan 22, 2022).
- (3) Matthews, R.; Fazeli, H. Copper and Complexity: Iran and Mesopotamia in the Fourth Millennium B.C. *Iran* **2004**, *42*, 61–75.
- (4) Harishchandra, B. D.; Pappuswamy, M.; PU, A.; Shama, G.; A, P.; Arumugam, V. A.; Periyaswamy, T.; Sundaram, R. Copper Nanoparticles: A Review on Synthesis, Characterization and Applications. *Asian Pac. J. Cancer Biol.* **2020**, *5*, 201–210.
- (5) Ma, Z.; Zaera, F. Heterogeneous Catalysis by Metals. In *Encyclopedia of Inorganic Chemistry*; Wiley, **2006**.
- (6) Rothenberg, G. *Catalysis: Concepts and Green Applications*; Wiley, **2008**.
- (7) Van Den Berg, R.; Prieto, G.; Korpershoek, G.; van der Wal, L. I.; van Bunningen, A. J.; Lægsgaard-Jørgensen, S.; de Jongh, P. E.; de Jong, K. P. Structure Sensitivity of Cu and CuZn Catalysts Relevant to Industrial Methanol Synthesis. *Nat. Commun.* **2016**, *7*, 13057.
- (8) Prieto, G.; Zečević, J.; Friedrich, H.; de Jong, K. P.; de Jongh, P. E. Towards Stable Catalysts by Controlling Collective Properties of Supported Metal Nanoparticles. *Nat. Mater.* **2013**, *12*, 34–39.
- (9) Prieto, G.; Shakeri, M.; de Jong, K. P.; de Jongh, P. E. Quantitative Relationship between Support Porosity and the Stability of Pore-Confined Metal Nanoparticles Studied on CuZnO/SiO₂ Methanol Synthesis Catalysts. *ACS Nano* **2014**, *8*, 2522–2531.
- (10) Gokhale, A. A.; Dumesic, J. A.; Mavrikakis, M. On the Mechanism of Low-Temperature Water Gas Shift Reaction on Copper. *J. Am. Chem. Soc.* **2008**, *130*, 1402–1414.
- (11) Zhang, Z.; Wang, S.-S.; Song, R.; Cao, T.; Luo, L.; Chen, X.; Gao, Y.; Lu, J.; Li, W.-X.; Huang, W. The Most Active Cu Facet for Low-Temperature Water Gas Shift Reaction. *Nat. Commun.* **2017**, *8*, 488.
- (12) Gargiulo, N.; Caputo, D.; Totarella, G.; Lisi, L.; Cimino, S. Me-ZSM-5 Monolith Foams for the NH₃-SCR of NO. *Catal. Today* **2018**, *304*, 112–118.
- (13) Pereda-Ayo, B.; De La Torre, U.; Illán-Gómez, M. J.; Bueno-López, A.; González-Velasco, J. R. Role of the Different Copper Species on the Activity of Cu/Zeolite Catalysts for SCR of NO_x with NH₃. *Appl. Catal. B Environ.* **2014**, *147*, 420–428.
- (14) Kim, D.; Kley, C. S.; Li, Y.; Yang, P. Copper Nanoparticle Ensembles for Selective Electroreduction of CO₂ to C₂–C₃ Products. *PNAS* **2017**, *114*, 10560–10565.

- (15) Dongare, S.; Singh, N.; Bhunia, H. Electrocatalytic Reduction of CO₂ to Useful Chemicals on Copper Nanoparticles. *Appl. Surf. Sci.* **2021**, *537*, 148020.
- (16) Tian, H.; Zhang, X. L.; Scott, J.; Ng, C.; Amal, R. TiO₂-Supported Copper Nanoparticles Prepared via Ion Exchange for Photocatalytic Hydrogen Production. *J. Mater. Chem. A* **2014**, *2*, 6432–6438.
- (17) Hosseini, S. R.; Ghasemi, S.; Ghasemi, S. A. Effect of Surfactants on Electrocatalytic Performance of Copper Nanoparticles for Hydrogen Evolution Reaction. *J. Mol. Liq.* **2016**, *222*, 1068–1075.
- (18) Shi, Z. Z.; Wang, X.; Kang, W. J.; Bai, Y. M.; Yang, J.; Liu, H.; Dong, C. K.; Yin, P. F.; Du, X. W. Copper Nanoparticles with Abundant Defects as a pH-Universal Catalyst for Hydrogen Evolution Reaction. *ACS Appl. Energy Mater.* **2023**, *6*, 10012–10019.
- (19) Hasan, M. M.; Tolba, S. A.; Allam, N. K. In Situ Formation of Graphene Stabilizes Zero-Valent Copper Nanoparticles and Significantly Enhances the Efficiency of Photocatalytic Water Splitting. *ACS Sustain. Chem. Eng.* **2018**, *6*, 16876–16885.
- (20) de Brito, J. F.; Tavella, F.; Genovese, C.; Ampelli, C.; Zanoni, M. V. B.; Centi, G.; Perathoner, S. Role of CuO in the Modification of the Photocatalytic Water Splitting Behavior of TiO₂ Nanotube Thin Films. *Appl. Catal. B Environ.* **2018**, *224*, 136–145.
- (21) Camats, M.; Pla, D.; Gómez, M. Copper Nanocatalysts Applied in Coupling Reactions: A Mechanistic Insight. *Nanoscale* **2021**, *13*, 18817–18838.
- (22) Goswami, M.; Das, A. M. Synthesis of Cellulose Impregnated Copper Nanoparticles as an Efficient Heterogeneous Catalyst for C–N Coupling Reactions under Mild Conditions. *Carbohydr. Polym.* **2018**, *195*, 189–198.
- (23) Guo, X.; Hao, C.; Jin, G.; Zhu, H.-Y.; Guo, X.-Y. Copper Nanoparticles on Graphene Support: An Efficient Photocatalyst for Coupling of Nitroaromatics in Visible Light. *Angew. Chemie - Int. Ed.* **2014**, *53*, 1973–1977.
- (24) Yoshida, K.; Gonzalez-Arellano, C.; Luque, R.; Gai, P. L. Efficient Hydrogenation of Carbonyl Compounds Using Low-Loaded Supported Copper Nanoparticles under Microwave Irradiation. *Appl. Catal. A Gen.* **2010**, *379*, 38–44.
- (25) Wang, D.; Yang, G.; Ma, Q.; Wu, M.; Tan, Y.; Yoneyama, Y.; Tsubaki, N. Confinement Effect of Carbon Nanotubes: Copper Nanoparticles Filled Carbon Nanotubes for Hydrogenation of Methyl Acetate. *ACS Catal.* **2012**, *2*, 1958–1966.
- (26) Totarella, G.; Beerthuis, R.; Masoud, N.; Louis, C.; Delannoy, L.; de Jongh, P. E. Supported Cu Nanoparticles as Selective and Stable Catalysts for the Gas Phase Hydrogenation of 1,3-Butadiene in Alkene-Rich Feeds. *J. Phys. Chem. C* **2021**, *125*, 366–375.
- (27) Beerthuis, R.; de Rijk, J. W.; Deeley, J. M. S.; Sunley, G. J.; de Jong, K. P.; de Jongh, P. E. Particle Size Effects in Copper-Catalyzed Hydrogenation of Ethyl Acetate. *J. Catal.* **2020**, *388*, 30–37.

- (28) Bond, G. C. *Metal-Catalysed Reactions of Hydrocarbons*, Springer US, **2005**.
- (29) Pande, S.; Saha, A.; Jana, S.; Sarkar, S.; Basu, M.; Pradhan, M.; Sinha, A. K.; Saha, S.; Pal, A.; Pal, T. Resin-Immobilized CuO and Cu Nanocomposites for Alcohol Oxidation. *Org. Lett.* **2008**, *10*, 5179–5181.
- (30) Han, C.; Yu, M.; Sun, W.; Yao, X. Ligand-Promoted, Copper Nanoparticles Catalyzed Oxidation of Propargylic Alcohols with TBHP or Air as Oxidant. *Synlett* **2011**, *16*, 2363–2368.
- (31) Gawande, M. B.; Goswami, A.; Felpin, F.-X.; Asefa, T.; Huang, X.; Silva, R.; Zou, X.; Zboril, R.; Varma, R. S. Cu and Cu-Based Nanoparticles: Synthesis and Applications in Catalysis. *Chem. Rev.* **2016**, *116*, 3722–3811.
- (32) Ertl, G.; Knözinger, H.; Weitkamp, J. *Handbook of Heterogeneous Catalysis*, 2nd ed.; Wiley, **2008**; Vol. 1–5.
- (33) Schlögl, R. Heterogeneous Catalysis. *Angew. Chemie - Int. Ed.* **2015**, *54*, 3465–3520.
- (34) Rase, H. F. *Handbook of Commercial Catalysts*, CRC Press, **2016**.
- (35) Anastas, P. T.; Kirchhoff, M. M.; Williamson, T. C. Catalysis as a Foundational Pillar of Green Chemistry. *Appl. Catal. A Gen.* **2001**, *221*, 3–13.
- (36) Barberis, L.; Hakimioun, A. H.; Plessow, P. N.; Visser, N. L.; Stewart, J. A.; Vandegehuchte, B. D.; Studt, F.; de Jongh, P. E. Competition between Reverse Water Gas Shift Reaction and Methanol Synthesis from CO₂: Influence of Copper Particle Size. *Nanoscale* **2022**, *14*, 13551–13560.
- (37) Gandeepan, P.; Müller, T.; Zell, D.; Cera, G.; Warratz, S.; Ackermann, L. 3d Transition Metals for C-H Activation. *Chem. Rev.* **2019**, *119*, 2192–2452.
- (38) Ojha, N. K.; Zyryanov, G. V.; Majee, A.; Charushin, V. N.; Chupakhin, O. N.; Santra, S. Copper Nanoparticles as Inexpensive and Efficient Catalyst: A Valuable Contribution in Organic Synthesis. *Coord. Chem. Rev.* **2017**, *353*, 1–57.
- (39) Anilkumar, G.; Saranya, S. *Copper Catalyst in Organic Synthesis*; Wiley, **2020**.
- (40) McCann, S. D.; Stahl, S. S. Copper-Catalyzed Aerobic Oxidations of Organic Molecules: Pathways for Two-Electron Oxidation with a Four-Electron Oxidant and a One-Electron Redox-Active Catalyst. *Acc. Chem. Res.* **2015**, *48*, 1756–1766.
- (41) Sambiagio, C.; Marsden, S. P.; Blacker, A. J.; McGowan, P. C. Copper Catalysed Ullmann Type Chemistry: From Mechanistic Aspects to Modern Development. *Chem. Soc. Rev.* **2014**, *43*, 3525–3550.
- (42) Yoshikai, N.; Nakamura, E. Mechanisms of Nucleophilic Organocopper(I) Reactions. *Chem. Rev.* **2012**, *112*, 2339–2372.
- (43) Reymond, S.; Cossy, J. Copper-Catalyzed Diels - Alder Reactions. *Chem. Rev.* **2008**, *108*, 5359–5406.
- (44) Kattel, S.; Ramírez, P. J.; Chen, J. G.; Rodriguez, J. A.; Liu, P. Active Sites for CO₂

- Hydrogenation to Methanol on Cu/ZnO Catalysts. *Science* **2017**, *355*, 1296–1299.
- (45) Beerthuis, R. PhD thesis: Carbon-Supported Copper for Gas-Phase Hydrogenation Catalysis, Utrecht University, **2020**.
- (46) Phillipson, J. J.; Wells, P. B.; Wilson, G. R. The Hydrogenation of Alkadienes. Part III. The Hydrogenation of Buta-1,3-Diene Catalysed by Iron, Cobalt, Nickel, and Copper. *J. Chem. Soc. A* **1969**, 1351–1363.
- (47) Marchi, A. J.; Gordo, D. A.; Trasarti, A. F.; Apesteguía, C. R. Liquid Phase Hydrogenation of Cinnamaldehyde on Cu-Based Catalysts. *Appl. Catal. A Gen.* **2003**, *249*, 53–67.
- (48) Gutierrez, V.; Alvarez, M.; Volpe, M. A. Liquid Phase Selective Hydrogenation of Cinnamaldehyde over Copper Supported Catalysts. *Appl. Catal. A Gen.* **2012**, *413–414*, 358–365.
- (49) Tisseraud, C.; Comminges, C.; Belin, T.; Ahouari, H.; Soualah, A.; Pouilloux, Y.; Le Valant, A. The Cu-ZnO Synergy in Methanol Synthesis from CO₂, Part 2: Origin of the Methanol and CO Selectivities Explained by Experimental Studies and a Sphere Contact Quantification Model in Randomly Packed Binary Mixtures on Cu-ZnO Coprecipitate Catalysts. *J. Catal.* **2015**, *330*, 533–544.
- (50) Pan, W. X.; Cao, R.; Roberts, D. L.; Griffin, G. L. Methanol Synthesis Activity of Cu ZnO Catalysts. *J. Catal.* **1988**, *114*, 440–446.
- (51) Furlong, B. K.; Hightower, J. W.; Chan, T. Y.-L.; Sarkany, A.; Gucci, L. 1,3-Butadiene Selective Hydrogenation Over Pd/Alumina and CuPd/Alumina Catalysts. *Appl. Catal. A, Gen.* **1994**, *117*, 41–51.
- (52) Delannoy, L.; Thrimurthulu, G.; Reddy, P. S.; Méthivier, C.; Nelayah, J.; Reddy, B. M.; Ricolleau, C.; Louis, C. Selective Hydrogenation of Butadiene over TiO₂ Supported Copper, Gold and Gold-Copper Catalysts Prepared by Deposition-Precipitation. *Phys. Chem. Chem. Phys.* **2014**, *16*, 26514–26527.
- (53) Hammer, B.; Nørskov, J. K. Theoretical Surface Science and Catalysis—Calculations and Concepts. *Adv. Catal.* **2000**, *45*, 71–129.
- (54) Hammer, B.; Nørskov, J. K. Why Gold Is the Noblest of All the Metals. *Nature* **1995**, *376*, 238–240.
- (55) Calle-Vallejo, F.; Koper, M. T. M.; Bandarenka, A. S. Tailoring the Catalytic Activity of Electrodes with Monolayer Amounts of Foreign Metals. *Chem. Soc. Rev.* **2013**, *42*, 5210–5230.
- (56) Ruban, A.; Hammer, B.; Stoltze, P.; Skriver, H. L.; Nørskov, J. K. Surface Electronic Structure and Reactivity of Transition and Noble Metals. *J. Mol. Catal. A Chem.* **1997**, *115*, 421–429.
- (57) Hammer, B.; Nørskov, J. K. Electronic Factors Determining the Reactivity of Metal Surfaces. *Surf. Sci.* **1995**, *343*, 211–220.

- (58) Hanefeld, U.; Lefferts, L. *Catalysis: An Integrated Textbook for Students*, Wiley, **2017**.
- (59) Scholten, J. J. F.; Pijpers, A. P.; Hustings, A. M. L. Surface Characterization of Supported and Unsupported Hydrogenation Catalysts. *Catal. Rev.* **1985**, *27*, 151–206.
- (60) Li, J. J.; Liu, Z.; Guan, Z. J.; Han, X. S.; Shi, W. Q.; Wang, Q. M. A 59-Electron Non-Magic-Number Gold Nanocluster Au₉₉(C≡CR)₄₀ Showing Unexpectedly High Stability. *J. Am. Chem. Soc.* **2022**, *144*, 690–694.
- (61) Tsunoyama, H.; Tsukuda, T. Magic Numbers of Gold Clusters Stabilized by PVP. *J. Am. Chem. Soc.* **2009**, *131*, 18216–18217.
- (62) Mori, T.; Hegmann, T. Determining the Composition of Gold Nanoparticles: A Compilation of Shapes, Sizes, and Calculations Using Geometric Considerations. *J. Nanoparticle Res.* **2016**, *18*, 295.
- (63) Somorjai, G. A. The Structure Sensitivity and Insensitivity of Catalytic Reactions in Light of the Adsorbate Induced Dynamic Restructuring of Surfaces. *Catal. Letters* **1990**, *7*, 169–182.
- (64) Boudart, M. Catalysis by Supported Metals. *Adv. Catal.* **1969**, *20*, 153–166.
- (65) Van Santen, R. A. Complementary Structure Sensitive and Insensitive Catalytic Relationships. *Acc. Chem. Res.* **2009**, *42*, 57–66.
- (66) Zambelli, T.; Wintterlin, J.; Trost, J.; Ertl, G. Identification of the “Active Sites” of a Surface-Catalyzed Reaction. *Science* **1996**, *273*, 1688–1690.
- (67) van Hardeveld, R.; van Montfoort, A. The Influence of Crystallite Size on the Adsorption of Molecular Nitrogen on Nickel, Palladium and Platinum. An Infrared and Electron-Microscopic Study. *Surf. Sci.* **1966**, *4*, 396–430.
- (68) Somorjai, G. A.; *Introduction to Surface Chemistry and Catalysis*, Wiley, **1995**.
- (69) den Breejen, J. P.; Radstake, P. B.; Bezemer, G. L.; Bitter, J. H.; Frøseth, V.; Holmen, A.; de Jong, K. P. On the Origin of the Cobalt Particle Size Effects in Fischer-Tropsch Catalysis. *J. Am. Chem. Soc.* **2009**, *131*, 7197–7203.
- (70) Torres Galvis, H. M.; Bitter, J. H.; Davidian, T.; Ruitenbeek, M.; Dugulan, A. I.; de Jong, K. P. Iron Particle Size Effects for Direct Production of Lower Olefins from Synthesis Gas. *J. Am. Chem. Soc.* **2012**, *134*, 16207–16215.
- (71) Bezemer, G. L.; Bitter, J. H.; Kuipers, H. P. C. E.; Oosterbeek, H.; Holewijn, J. E.; Xu, X.; Kapteijn, F.; Van Diilen, A. J.; de Jong, K. P. Cobalt Particle Size Effects in the Fischer-Tropsch Reaction Studied with Carbon Nanofiber Supported Catalysts. *J. Am. Chem. Soc.* **2006**, *128*, 3956–3964.
- (72) Gigola, C. E.; Aduriz, H. R.; Bodnariuk, P. Particle Size Effect in the Hydrogenation of Acetylene under Industrial Conditions. *Appl. Catal.* **1986**, *27*, 133–144.
- (73) Neri, G.; Musolino, M. G.; Milone, C.; Pietropaolo, D.; Galvagno, S. Particle Size Effect in the Catalytic Hydrogenation of 2,4-dinitrotoluene over Pd/C Catalysts. *Appl. Catal. A Gen.* **2001**, *208*, 307–316.

- (74) Coq, B.; Tijani, A.; Figuéras, F. Particle Size Effect on the Kinetics of *p*-chloronitrobenzene Hydrogenation over Platinum/Alumina Catalysts. *J. Mol. Catal.* **1991**, *68*, 331–345.
- (75) Hub, S.; Hilaire, L.; Touroude, R. Hydrogenation of But-1-yne and But-1-ene on Palladium Catalysts. Particle Size Effect. *Appl. Catal.* **1988**, *36*, 307–322.
- (76) Plomp, A. J.; Vuori, H.; Krause, A. O. I.; de Jong, K. P.; Bitter, J. H. Particle Size Effects for Carbon Nanofiber Supported Platinum and Ruthenium Catalysts for the Selective Hydrogenation of Cinnamaldehyde. *Appl. Catal. A Gen.* **2008**, *351*, 9–15.
- (77) Stakheev, A. Y.; Batkin, A. M.; Teleguina, N. S.; Bragina, G. O.; Zaikovskiy, V. I.; Prosvirin, I. P.; Khudorozhkov, A. K.; Bukhtiyarov, V. I. Particle Size Effect on CH₄ Oxidation over Noble Metals: Comparison of Pt and Pd Catalysts. *Top. Catal.* **2013**, *56*, 306–310.
- (78) Isaifan, R. J.; Ntais, S.; Baranova, E. A. Particle Size Effect on Catalytic Activity of Carbon-Supported Pt Nanoparticles for Complete Ethylene Oxidation. *Appl. Catal. A Gen.* **2013**, *464–465*, 87–94.
- (79) Eckle, S.; Augustin, M.; Anfang, H.-G.; Behm, R. J. Influence of the Catalyst Loading on the Activity and the CO Selectivity of Supported Ru Catalysts in the Selective Methanation of CO in CO₂ Containing Feed Gases. *Catal. Today* **2012**, *181*, 40–51.
- (80) Sakpal, T.; Lefferts, L. Structure-Dependent Activity of CeO₂ Supported Ru Catalysts for CO₂ Methanation. *J. Catal.* **2018**, *367*, 171–180.
- (81) Kesavan, J. K.; Luisetto, I.; Tuti, S.; Meneghini, C.; Iucci, G.; Battocchio, C.; Mobilio, S.; Casciardi, S.; Sisto, R. Nickel Supported on YSZ: The Effect of Ni Particle Size on the Catalytic Activity for CO₂ Methanation. *J. CO₂ Util.* **2018**, *23*, 200–211.
- (82) Hayden, B. E. Particle Size and Support Effects in Electrocatalysis. *Acc. Chem. Res.* **2013**, *46*, 1858–1866.
- (83) Mayrhofer, K. J. J.; Blizanac, B. B.; Arenz, M.; Stamenkovic, V. R.; Ross, P. N.; Markovic, N. M. The Impact of Geometric and Surface Electronic Properties of Pt-Catalysts on the Particle Size Effect in Electrocatalysis. *J. Phys. Chem. B* **2005**, *109*, 14433–14440.
- (84) Shao, M.; Peles, A.; Shoemaker, K. Electrocatalysis on Platinum Nanoparticles: Particle Size Effect on Oxygen Reduction Reaction Activity. *Nano Lett.* **2011**, *11*, 3714–3719.
- (85) Mukerjee, S. Particle Size and Structural Effects in Platinum Electrocatalysis. *J. Appl. Electrochem.* **1990**, *20*, 537–548.
- (86) Reske, R.; Mistry, H.; Behafarid, F.; Roldan Cuenya, B.; Strasser, P. Particle Size Effects in the Catalytic Electroreduction of CO₂ on Cu Nanoparticles. *J. Am. Chem. Soc.* **2014**, *136*, 6978–6986.
- (87) Crampton, A. S.; Rötzer, M. D.; Ridge, C. J.; Schweinberger, F. F.; Heiz, U.; Yoon, B.; Landman, U. Structure Sensitivity in the Non-scalable Regime Explored via Catalysed Ethylene Hydrogenation on Supported Platinum Nanoclusters. *Nat. Commun.* **2016**, *7*,

- 10389.
- (88) de Jong, K. P. *Synthesis of Solid Catalysts*, Wiley-VCH, 2009.
- (89) Liu, L.; Corma, A. Metal Catalysts for Heterogeneous Catalysis: From Single Atoms to Nanoclusters and Nanoparticles. *Chem. Rev.* **2018**, *118*, 4981–5079.
- (90) Munnik, P.; de Jongh, P. E.; de Jong, K. P. Recent Developments in the Synthesis of Supported Catalysts. *Chem. Rev.* **2015**, *115*, 6687–6718.
- (91) Wang, Z.; Brouri, D.; Casale, S.; Delannoy, L.; Louis, C. Exploration of the Preparation of Cu/TiO₂ Catalysts by Deposition-Precipitation with Urea for Selective Hydrogenation of Unsaturated Hydrocarbons. *J. Catal.* **2016**, *340*, 95–106.
- (92) Pompe, C. E. PhD thesis: Stability of Copper Catalysts for Methanol Synthesis, Utrecht University, **2019**.
- (93) van Den Berg, R.; Elkjaer, C. F.; Gommès, C. J.; Chorkendorff, I.; Sehested, J.; de Jongh, P. E.; de Jong, K. P.; Helveg, S. Revealing the Formation of Copper Nanoparticles from a Homogeneous Solid Precursor by Electron Microscopy. *J. Am. Chem. Soc.* **2016**, *138*, 3433–3442.
- (94) van den Berg, R.; Zečević, J.; Sehested, J.; Helveg, S.; de Jongh, P. E.; de Jong, K. P. Impact of the Synthesis Route of Supported Copper Catalysts on the Performance in the Methanol Synthesis Reaction. *Catal. Today* **2016**, *272*, 87–93.
- (95) Van Der Grift, C. J. G.; Elberse, P. A.; Mulder, A.; Geus, J. W. Preparation of Silica-Supported Copper Catalysts by Means of Deposition-Precipitation. *Appl. Catal.* **1990**, *59*, 275–289.
- (96) Lee, B. H.; Park, S.; Kim, M.; Sinha, A. K.; Lee, S. C.; Jung, E.; Chang, W. J.; Lee, K.-S.; Kim, J. H.; Cho, S. P.; Kim, H.; Nam, K. T.; Hyeon, T. Reversible and Cooperative Photoactivation of Single-Atom Cu/TiO₂ Photocatalysts. *Nat. Mater.* **2019**, *18*, 620–626.
- (97) Yahiro, H.; Iwamoto, M. Copper Ion-Exchanged Zeolite Catalysts in deNO_x Reaction. *Appl. Catal. A Gen.* **2001**, *222*, 163–181.
- (98) Cepollaro, E. M.; Botti, R.; Franchin, G.; Lisi, L.; Colombo, P.; Cimino, S. Cu/ZSM5-Geopolymer 3D-Printed Monoliths for the NH₃-SCR of NO_x. *Catalysts* **2021**, *11*, 1212.
- (99) Witte, P. T.; Berben, P. H.; Boland, S.; Boymans, E. H.; Vogt, D.; Geus, J. W.; Donkervoort, J. G. BASF NanoSelect™ Technology: Innovative Supported Pd- and Pt-Based Catalysts for Selective Hydrogenation Reactions. *Top. Catal.* **2012**, *55*, 505–511.
- (100) Manthiram, K.; Beberwyck, B. J.; Alivisatos, A. P. Enhanced Electrochemical Methanation of Carbon Dioxide with a Dispersible Nanoscale Copper Catalyst. *J. Am. Chem. Soc.* **2014**, *136*, 13319–13325.
- (101) Lomelí-Rosales, D. A.; Delgado, J. A.; Díaz de los Bernardos, M.; Pérez-Rodríguez, S.; Gual, A.; Claver, C.; Godard, C. A General One-Pot Methodology for the Preparation of Mono- and Bimetallic Nanoparticles Supported on Carbon Nanotubes: Application in the Semi-Hydrogenation of Alkynes and Acetylene. *Chem. Eur. J.* **2019**, *25*, 8321–

- 8331.
- (102) Ren, X.; Chen, D.; Tang, F. Shape-Controlled Synthesis of Copper Colloids with a Simple Chemical Route. *J. Phys. Chem. B* **2005**, *109*, 15803–15807.
- (103) Isomura, Y.; Narushima, T.; Kawasaki, H.; Yonezawa, T.; Obora, Y. Surfactant-Free Single-Nano-Sized Colloidal Cu Nanoparticles for Use as an Active Catalyst in Ullmann-Coupling Reaction. *Chem. Commun.* **2012**, *48*, 3784–3786.
- (104) Ben Aissa, M. A.; Tremblay, B.; Andrieux-Ledier, A.; Maisonhaute, E.; Raouafi, N.; Courty, A. Copper Nanoparticles of Well-Controlled Size and Shape: a New Advance in Synthesis and Self-Organization. *Nanoscale* **2015**, *7*, 3189–3195.
- (105) Wang, G.; van den Berg, R.; de Mello Donega, C.; de Jong, K. P.; de Jongh, P. E. Silica-Supported Cu₂O Nanoparticles with Tunable Size for Sustainable Hydrogen Generation. *Appl. Catal. B Environ.* **2016**, *192*, 199–207.
- (106) Munnik, P.; Wolters, M.; Gabrielsson, A.; Pollington, S. D.; Headdock, G.; Bitter, J. H.; de Jongh, P. E.; de Jong, K. P. Copper Nitrate Redispersion to Arrive at Highly Active Silica-Supported Copper Catalysts. *J. Phys. Chem. C* **2011**, *115*, 14698–14706.
- (107) Toupance, T.; Kermarec, M.; Louis, C. Metal Particle Size in Silica-Supported Copper Catalysts. Influence of the Conditions of Preparation and of Thermal Pretreatments. *J. Phys. Chem. B* **2000**, *104*, 965–972.
- (108) Veldsink, J. W.; Bouma, M. J.; Schönö, N. H.; Beenackers, A. A. C. M. Heterogeneous Hydrogenation of Vegetable Oils: A Literature Review. *Catal. Rev. Sci. Eng.* **1997**, *39*, 253–318.
- (109) Chen, B.; Dingerdissen, U.; Krauter, J. G. E.; Lansink Rotgerink, H. G. J.; Möbus, K.; Ostgard, D. J.; Panster, P.; Riermeier, T. H.; Seebald, S.; Tacke, T.; Trauthwein, H. New Developments in Hydrogenation Catalysis Particularly in Synthesis of Fine and Intermediate Chemicals. *Appl. Catal. A Gen.* **2005**, *280*, 17–46.
- (110) Bonrath, W.; Medlock, J.; Schutz, J.; Wustenberg, B.; Netscher, T. Hydrogenation in the Vitamins and Fine Chemicals Industry – An Overview. In *Hydrogenation*; IntechOpen, 2012.
- (111) Blaser, H.-U.; Malan, C.; Pugin, B.; Spindler, F.; Steiner, H.; Studer, M. Selective Hydrogenation for Fine Chemicals: Recent Trends and New Developments. *Adv. Synth. Catal.* **2003**, *345*, 103–151.
- (112) Koga, N.; Morokuma, K. Potential Energy Surface of Olefin Hydrogenation by Wilkinson Catalyst. In *The Challenge of d and f Electrons*. **1989**, 77–91.
- (113) Daniel, C.; Koga, N.; Han, J.; Fu, X. Y.; Morokuma, K. Ab Initio MO Study of the Full Catalytic Cycle of Olefin Hydrogenation by the Wilkinson Catalyst RhCl(PR₃)₃. *J. Am. Chem. Soc.* **1988**, *110*, 3773–3787.
- (114) Pogorelić, I.; Filipan-Litvić, M.; Merkaš, S.; Ljubić, G.; Capanec, I.; Litvić, M. Rapid, Efficient and Selective Reduction of Aromatic Nitro Compounds with Sodium

- Borohydride and Raney Nickel. *J. Mol. Catal. A Chem.* **2007**, *274*, 202–207.
- (115) Dörfelt, C.; Kolvenbach, R.; Wirth, A. S.; Albert, M.; Köhler, K. Catalytic Properties of a Novel Raney-Nickel Foam in the Hydrogenation of Benzene. *Catal. Letters* **2016**, *146*, 2425–2429.
- (116) Monguchi, Y.; Fujita, Y.; Hashimoto, S.; Ina, M.; Takahashi, T.; Ito, R.; Nozaki, K.; Maegawa, T.; Sajiki, H. Palladium on Carbon-Catalyzed Solvent-Free and Solid-Phase Hydrogenation and Suzuki-Miyaura Reaction. *Tetrahedron* **2011**, *67*, 8628–8634.
- (117) Pérez-Cadenas, A. F.; Kapteijn, F.; Zieverink, M. M. P.; Moulijn, J. A. Selective Hydrogenation of Fatty Acid Methyl Esters over Palladium on Carbon-Based Monoliths. Structural Control of Activity and Selectivity. *Catal. Today* **2007**, *128*, 13–17.
- (118) Díaz, E.; Mohedano, A. F.; Calvo, L.; Gilarranz, M. A.; Casas, J. A.; Rodríguez, J. J. Hydrogenation of Phenol in Aqueous Phase with Palladium on Activated Carbon Catalysts. *Chem. Eng. J.* **2007**, *131*, 65–71.
- (119) Lévy, K.; Tóth, K. D.; Kárpáti, T.; Hegedüs, L. Heterogeneous Catalytic Hydrogenation of 3-Phenylpropionitrile over Palladium on Carbon. *ACS Omega* **2020**, *5*, 5487–5497.
- (120) Hill, T.; Haake, M.; Schwab, E.; Frenzel, A.; Worz, H. Selective Catalytic Gas-Phase Hydrogenation of Alkynes, Dienes, Alkenynes and/or Polyenes. US 2003/0069458 A1, **2003**.
- (121) Arganbright, R. P. Selective Hydrogenation of Dienes and Acetylenes in C₃ Streams. WO 94/04477, **1994**.
- (122) Putman, H. M.; Adams, J. R. Process and Catalyst for Selective Hydrogenation of Dienes and Acetylenes. US 8,227,650 B2, **2012**.
- (123) Sugeta, M.; Fukada, H. Catalyst for Selective Hydrogenation of Acetylene Compounds in 1,3-Butadiene, Method for Producing the Same and Method of Using the Same. EP 2 329 879 A1, **2011**.
- (124) Ryu, Y. J. Selective Hydrogenation Process and Catalyst. WO 2006/044005 A2, **2006**.
- (125) Beerthuis, R.; Sunley, John, G.; de Jong, K.; de Jongh, P. E. Selective Hydrogenation of Polyunsaturates. WO2019/233961 A1, **2019**.
- (126) Ren, T.; Patel, M.; Blok, K. Olefins from Conventional and Heavy Feedstocks: Energy Use in Steam Cracking and Alternative Processes. *Energy* **2006**, *31*, 425–451.
- (127) Červený, L. *Catalytic Hydrogenation*; Elsevier, **1986**.
- (128) Nikolaev, S. A.; Zhanavskina, L. N.; Smirnov, V. V.; Averyanov, V. A.; Zhanavskina, K. L. Catalytic Hydrogenation of Alkyne and Alkadiene Impurities from Alkenes. Practical and Theoretical Aspects. *Russ. Chem. Rev.* **2009**, *78*, 231–247.
- (129) Bender, M. An Overview of Industrial Processes for the Production of Olefins – C₄ Hydrocarbons. *ChemBioEng Rev.* **2014**, *1*, 136–147.

- (130) Che, C.; Liang, Y.; Qian, Y.; Han, W.; Zhang, F.; Gou, G.; Jing, X.; Chang, X.; Gui, Q.; Gu, L.; Xie, W.; Zhang, Z.; Huang, D.; Tan, D.; Gao, Y.; Cheng, L. Palladium-Based Supported Hydrogenation Catalyst, And Preparation Method And Application Thereof. US 10,800,717 B2, 2020.
- (131) Borodziński, A.; Bond, G. C. Selective Hydrogenation of Ethyne in Ethene-Rich Streams on Palladium Catalysts, Part 2: Steady-State Kinetics and Effects of Palladium Particle Size, Carbon Monoxide, and Promoters. *Catal. Rev. Sci. Eng.* **2008**, *50*, 379–469.
- (132) Chinayon, S.; Mekasuwandumrong, O.; Praserttham, P.; Panpranot, J. Selective Hydrogenation of Acetylene over Pd Catalysts Supported on Nanocrystalline α -Al₂O₃ and Zn-Modified α -Al₂O₃. *Catal. Commun.* **2008**, *9*, 2297–2302.
- (133) Ravanchi, M. T.; Sahebdehfar, S.; Fard, M. R.; Fadaerayeni, S.; Bigdeli, P. Pd-Ag/ α -Al₂O₃ Catalyst Deactivation in Acetylene Selective Hydrogenation Process. *Chem. Eng. Technol.* **2016**, *39*, 301–310.
- (134) Piccolo, L.; Piednoir, A.; Bertolini, J. C. Pd-Au Single-Crystal Surfaces: Segregation Properties and Catalytic Activity in the Selective Hydrogenation of 1,3-Butadiene. *Surf. Sci.* **2005**, *592*, 169–181.
- (135) Piccolo, L.; Valcarcel, A.; Bausach, M.; Thomazeau, C.; Uzio, D.; Berhault, G. Tuning the Shape of Nanoparticles to Control Their Catalytic Properties: Selective Hydrogenation of 1,3-Butadiene on Pd/Al₂O₃. *Phys. Chem. Chem. Phys.* **2008**, *10*, 5504–5506.
- (136) Vignola, E.; Steinmann, S. N.; Vandegehuchte, B. D.; Curulla, D.; Sautet, P. C₂H₂-Induced Surface Restructuring of Pd-Ag Catalysts: Insights from Theoretical Modeling. *J. Phys. Chem. C* **2016**, *120*, 26320–26327.
- (137) Jin, Y.; Datye, A. K.; Rightor, E.; Gulotty, R.; Waterman, W.; Smith, M.; Holbrook, M.; Maj, J.; Blacksony, J. The Influence of Catalyst Restructuring on the Selective Hydrogenation of Acetylene to Ethylene. *J. Catal.* **2001**, *203*, 292–306.
- (138) Nuss, P.; Eckelman, M. J. Life Cycle Assessment of Metals: A Scientific Synthesis. *PLoS One* **2014**, *9*, e101298.
- (139) Kang, M.; Song, M. W.; Kim, T. W.; Kim, K. L. γ -Alumina Supported Cu-Ni Bimetallic Catalysts: Characterization and Selective Hydrogenation of 1,3-Butadiene. *Can. J. Chem. Eng.* **2002**, *80*, 63–70.
- (140) Wang, Z.; Wang, G.; Louis, C.; Delannoy, L. Bimetallic Ni-Zn/TiO₂ Catalysts for Selective Hydrogenation of Alkyne and Alkadiene Impurities from Alkenes Stream. *Res. Chem. Intermed.* **2021**, *47*, 91–116.
- (141) Grant, J.; Moyes, R. B.; Oliver, R. G.; Wells, P. B. The Hydrogenation of Alkadienes. VII. 1,2-Butadiene Hydrogenation Catalyzed by Two Forms of Nickel. *J. Catal.* **1976**, *42*, 213–220.
- (142) Silvestre-Albero, J.; Rupprechter, G.; Freund, H. J. Atmospheric Pressure Studies of Selective 1,3-Butadiene Hydrogenation on Well-Defined Pd/Al₂O₃/NiAl(110) Model Catalysts: Effect of Pd Particle Size. *J. Catal.* **2006**, *240*, 58–65.

- (143) Ahn, I. Y.; Lee, J. H.; Kim, S. K.; Moon, S. H. Three-Stage Deactivation of Pd/SiO₂ and Pd-Ag/SiO₂ Catalysts during the Selective Hydrogenation of Acetylene. *Appl. Catal. A Gen.* **2009**, *360*, 38–42.
- (144) Cooper, A.; Bachiller-Baeza, B.; Anderson, J. A.; Rodríguez-Ramos, I.; Guerrero-Ruiz, A. Design of Surface Sites for the Selective Hydrogenation of 1,3-Butadiene on Pd Nanoparticles: Cu Bimetallic Formation and Sulfur Poisoning. *Catal. Sci. Technol.* **2014**, *4*, 1446–1455.
- (145) Seth, D.; Sarkar, A.; Ng, F. T. T.; Rempel, G. L. Selective Hydrogenation of 1,3-Butadiene in Mixture with Isobutene on a Pd/ α -Alumina Catalyst in a Semi-Batch Reactor. *Chem. Eng. Sci.* **2007**, *62*, 4544–4557.
- (146) Yan, H.; Cheng, H.; Yi, H.; Lin, Y.; Yao, T.; Wang, C.; Li, J.; Wei, S.; Lu, J. Single-Atom Pd₁/Graphene Catalyst Achieved by Atomic Layer Deposition: Remarkable Performance in Selective Hydrogenation of 1,3-Butadiene. *J. Am. Chem. Soc.* **2015**, *137*, 10484–10487.
- (147) Bates, A. J.; Leszczynski, Z. K.; Phillipson, J. J.; Wells, P. B.; Wilson, G. R. The Hydrogenation of Akladienes. Part IV. the Reaction of Buta-1,3-Diene with Deuterium Catalysed by Rhodium, Palladium, and Platinum. *J. Chem. Soc. A* **1970**, 2435–2441.
- (148) Masoud, N.; Delannoy, L.; Schaink, H.; van der Eerden, A.; de Rijk, J. W.; Silva, T. A. G.; Banerjee, D.; Meeldijk, J. D.; de Jong, K. P.; Louis, C.; de Jongh, P. E. Superior Stability of Au/SiO₂ Compared to Au/TiO₂ Catalysts for the Selective Hydrogenation of Butadiene. *ACS Catal.* **2017**, *7*, 5594–5603.
- (149) Masoud, N.; Delannoy, L.; Calers, C.; Gallet, J. J.; Bournel, F.; de Jong, K. P.; Louis, C.; de Jongh, P. E. Silica-Supported Au–Ag Catalysts for the Selective Hydrogenation of Butadiene. *ChemCatChem* **2017**, *9*, 2418–2425.
- (150) Moyes, R. B.; Wells, P. B.; Grant, J.; Salman, N. Y. Electronic Effects in Butadiene Hydrogenation Catalysed by the Transition Metals. *Appl. Catal. A Gen.* **2002**, *229*, 251–259.
- (151) Wehrli, J. T.; Thomas, D. J.; Wainwright, M. S.; Trimm, D. L.; Cant, N. W. Selective Hydrogenation of Propyne over Supported Copper Catalysts: Influence of Support. *Appl. Catal.* **1991**, *70*, 253–262.
- (152) Nishimura, E.; Inoue, Y.; Yasumori, I. The Mechanism of the Selective Hydrogenation of 1,3-Butadiene on Copper Surfaces. *Bull. Chem. Soc. Jpn.* **1975**, *48*, 803–807.
- (153) Koeppl, R. A.; Wehrli, J. T.; Wainwright, M. S.; Trimm, D. L.; Cant, N. W. Selective Hydrogenation of C₄-Alkynes over a Copper on Silica Catalyst. *Appl. Catal. A, Gen.* **1994**, *120*, 163–177.
- (154) Ossipoff, N. J.; Cant, N. W. The Hydrogenation and Oligomerization of Propyne over an Ion-Exchanged Copper on Silica Catalyst. *J. Catal.* **1994**, *148*, 125–133.
- (155) Wehrli, J. T.; Thomas, D. J.; Wainwright, M. S.; Trimm, D. L.; Cant, N. W. Selective Hydrogenation of Propyne over an Ion-Exchanged Copper on Silica Catalyst. *Appl.*

- Catal.* **1990**, *66*, 199–208.
- (156) Cervantes, G. G.; Santos, F. J. C.; Bertolini, J. C. Compared Properties of Pd on Thermo-Conductor Supports (SiC, Si₃N₄) and Pd on Oxide Supports (Al₂O₃, SiO₂) for the 1,3-Butadiene Hydrogenation Reaction. *J. Catal.* **2003**, *214*, 26–32.
- (157) Wang, Z.; Wang, G.; Louis, C.; Delannoy, L. Novel Non-Noble Bimetallic Cu-Zn/TiO₂ Catalysts for Selective Hydrogenation of Butadiene. *J. Catal.* **2017**, *347*, 185–196.
- (158) Studt, F.; Abild-Pedersen, F.; Bligaard, T.; Sørensen, R. Z.; Christensen, C. H.; Nørskov, J. K. Identification of Non-Precious Metal Alloy Catalysts for Selective Hydrogenation of Acetylene. *Science* **2008**, *320*, 1320–1322.
- (159) Bonrath, W.; Eggersdorfer, M.; Netscher, T. Catalysis in the Industrial Preparation of Vitamins and Nutraceuticals. *Catal. Today* **2007**, *121*, 45–57.
- (160) Kholkina, E. K. A.; Nikoshvili, L. Z.; Bykov, A. V.; Morozov, A. S.; Bessonov, I. V.; Kiwi-Minsker, L.; Sulman, E. Selective Hydrogenation of Alkynols in Ethanol Medium in a Batch Mode Using Polyamine-Supported Pd Catalysts. *Chem. Eng. Trans.* **2017**, *61*, 883–888.
- (161) Molnár, Á.; Sárkány, A.; Varga, M. Hydrogenation of Carbon-Carbon Multiple Bonds: Chemo-, Regio- and Stereo-Selectivity. *J. Mol. Catal. A Chem.* **2001**, *173*, 185–221.
- (162) Chen, X.; Shi, C.; Liang, C. Highly Selective Catalysts for the Hydrogenation of Alkynols: A Review. *Chinese J. Catal.* **2021**, *42*, 2105–2121.
- (163) Winterbottom, J. M.; Marwan, H.; Viladevall, J.; Sharma, S.; Raymahasay, S. Selective Catalytic Hydrogenation of 2-Butyne-1,4-Diol to Cis-2-Butene-1,4-Diol in Mass Transfer Efficient Slurry Reactors. *Stud. Surf. Sci. Catal.* **1997**, *108*, 59–66.
- (164) Natividad, R.; Kulkarni, R.; Nuithitikul, K.; Raymahasay, S.; Wood, J.; Winterbottom, J. M. Analysis of the Performance of Single Capillary and Multiple Capillary (Monolith) Reactors for the Multiphase Pd-Catalyzed Hydrogenation of 2-Butyne-1,4-Diol. *Chem. Eng. Sci.* **2004**, *59*, 5431–5438.
- (165) Vernuccio, S.; Meier, A.; von Rohr, P. R. Kinetic Investigation of the Solvent-Free Hydrogenation of Dehydroisophytol. *Ind. Eng. Chem. Res.* **2017**, *56*, 4929–4937.
- (166) Tschan, R.; Schubert, M. M.; Baiker, A.; Bonrath, W.; Lansink-Rotgerink, H. Continuous Semihydrogenation of a Propargylic Alcohol over Amorphous Pd₈₁Si₁₉ in Dense Carbon Dioxide: Effect of Modifiers. *Catal. Letters* **2001**, *75*, 31–36.
- (167) Mallát, T.; Szabó, S.; Petró, J. The Role of Lead in the Selectivity of Palladium-Lead (Lindlar Type) Catalysts. *Appl. Catal.* **1987**, *29*, 117–123.
- (168) García-Mota, M.; Gómez-Díaz, J.; Novell-Leruth, G.; Vargas-Fuentes, C.; Bellarosa, L.; Bridier, B.; Pérez-Ramírez, J.; López, N. A Density Functional Theory Study of the “Mythic” Lindlar Hydrogenation Catalyst. *Theor. Chem. Acc.* **2011**, *128*, 663–673.
- (169) Johansson, L. E.; Lundin, S. T. Copper Catalysts in the Selective Hydrogenation of Soybean and Rapeseed Oils: I. The Activity of the Copper Chromite Catalyst. *J. Am. Oil*

- Chem. Soc.* **1979**, *56*, 974–980.
- (170) Capece, F. M.; Di Castro, V.; Furlani, C.; Mattogno, G.; Fragale, C.; Gargano, M.; Rossi, M. “Copper Chromite” Catalysts: XPS Structure Elucidation and Correlation with Catalytic Activity. *J. Electron Spectros. Relat. Phenomena* **1982**, *27*, 119–128.
- (171) Fragale, C.; Gargano, M.; Ravasio, N.; Rossi, M.; Santo, I. Catalytic Hydrogenation of Vegetable Oils: III. A Comparison of Reactivity and Selectivity between Cyclic Polyenes and Polyunsaturated Fatty Acids with Copper Chromite as Catalyst. *Inorganica Chim. Acta* **1984**, *82*, 157–160.
- (172) Ilseemann, K.; Mukherjee, K. D. Continuous Hydrogenation of Fats and Fatty Acids at Short Contact Times. *J. Am. Oil Chem. Soc.* **1978**, *55*, 892–896.
- (173) Koritala, S.; Moulton, K. J.; Friedrich, J. P.; Frankel, E. N.; Kwolek, W. F. Continuous Slurry Hydrogenation of Soybean Oil with Copper-Chromite Catalyst at High Pressure. *J. Am. Oil Chem. Soc.* **1984**, *61*, 909–913.
- (174) Villaverde, M. M.; Bertero, N. M.; Garetto, T. F.; Marchi, A. J. Selective Liquid-Phase Hydrogenation of Furfural to Furfuryl Alcohol over Cu-Based Catalysts. *Catal. Today* **2013**, *213*, 87–92.
- (175) Nagaraja, B. M.; Padmasri, A. H.; David Raju, B.; Rama Rao, K. S. Vapor Phase Selective Hydrogenation of Furfural to Furfuryl Alcohol over Cu–MgO Coprecipitated Catalysts. *J. Mol. Catal. A Chem.* **2007**, *265*, 90–97.
- (176) Hou, X.; Qing, S.; Liu, Y.; Xi, H.; Wang, T.; Wang, X.; Gao, Z. Reshaping CuO on Silica to Generate a Highly Active Cu/SiO₂ Catalyst. *Catal. Sci. Technol.* **2016**, *6*, 6311–6319.
- (177) Briot, P.; Primet, M. Catalytic Oxidation of Methane over Palladium Supported on Alumina. Effect of Aging under Reactants. *Appl. Catal.* **1991**, *68*, 301–314.
- (178) Yadav, O. P.; Palmqvist, A.; Cruise, N.; Holmberg, K. Synthesis of Platinum Nanoparticles in Microemulsions and Their Catalytic Activity for the Oxidation of Carbon Monoxide. *Colloids Surfaces A Physicochem. Eng. Asp.* **2003**, *221*, 131–134.
- (179) Hugon, A.; Delannoy, L.; Louis, C. Supported Gold Catalysts for Selective Hydrogenation of 1,3-Butadiene in the Presence of an Excess of Alkenes. *Gold Bull.* **2008**, *41*, 127–138.
- (180) Sárkány, A. Formation of C₄ Oligomers in Hydrogenation of Acetylene over Pd/Al₂O₃ and Pd/TiO₂ Catalysts. *React. Kinet. Catal. Lett.* **2001**, *74*, 299–307.
- (181) Bond, G. C.; Wells, P. B. The Mechanism of the Hydrogenation of Unsaturated Hydrocarbons on Transition Metal Catalysts. *Adv. Catal.* **1965**, *15*, 91–226.
- (182) Silvestre-Albero, J.; Rupprechter, G.; Freund, H. J. From Pd Nanoparticles to Single Crystals: 1,3-Butadiene Hydrogenation on Well-Defined Model Catalysts. *Chem. Commun.* **2006**, 80–82.
- (183) Maccoll, A.; Ross, R. A. The Hydrogen Bromide Catalyzed Isomerization of n-Butenes. I. Equilibrium Values. *J. Am. Chem. Soc.* **1965**, *87*, 1169–1170.

- (184) Hugon, A.; Delannoy, L.; Louis, C. Influence of the Reactant Concentration in Selective Hydrogenation of 1,3-Butadiene over Supported Gold Catalysts under Alkene Rich Conditions: a Consideration of Reaction Mechanism. *Gold Bull.* **2009**, *42*, 310–320.
- (185) Bridier, B.; López, N.; Pérez-Ramírez, J. Partial Hydrogenation of Propyne over Copper-Based Catalysts and Comparison with Nickel-Based Analogues. *J. Catal.* **2010**, *269*, 80–92.
- (186) Bridier, B.; Karhánek, D.; Pérez-Ramírez, J.; López, N. Molecular Understanding of Enyne Hydrogenation over Palladium and Copper Catalysts. *ChemCatChem* **2012**, *4*, 1420–1427.
- (187) Kaeffler, N.; Larmier, K.; Fedorov, A.; Copéret, C. Origin of Ligand-Driven Selectivity in Alkyne Semihydrogenation over Silica-Supported Copper Nanoparticles. *J. Catal.* **2018**, *364*, 437–445.
- (188) van der Hoeven, J. E. S.; Jelic, J.; Olthof, L. A.; Totarella, G.; van Dijk-Moes, R. J. A.; Krafft, J. M.; Louis, C.; Studt, F.; van Blaaderen, A.; de Jongh, P. E. Unlocking Synergy in Bimetallic Catalysts by Core–Shell Design. *Nat. Mater.* **2021**, *20*, 1216–1220.
- (189) Lucci, F. R.; Liu, J.; Marcinkowski, M. D.; Yang, M.; Allard, L. F.; Flytzani-Stephanopoulos, M.; Sykes, E. C. H. Selective Hydrogenation of 1,3-Butadiene on Platinum-Copper Alloys at the Single-Atom Limit. *Nat. Commun.* **2015**, *6*, 8550.
- (190) Hu, N.; Li, X. Y.; Liu, S. M.; Wang, Z.; He, X. K.; Hou, Y. X.; Wang, Y. X.; Deng, Z.; Chen, L. H.; Su, B. L. Enhanced Stability of Highly-Dispersed Copper Catalyst Supported by Hierarchically Porous Carbon for Long Term Selective Hydrogenation. *Chinese J. Catal.* **2020**, *41*, 1081–1090.
- (191) Musselwhite, N.; Somorjai, G. A. Investigations of Structure Sensitivity in Heterogeneous Catalysis: From Single Crystals to Monodisperse Nanoparticles. *Top. Catal.* **2013**, *56*, 1277–1283.
- (192) Taghavi, M. B.; Pajonk, G. M.; Teichner, S. J. On the Structure-Sensitive and Structure-Insensitive Catalytic Reactions and Their New Characteristics, Demonstrated with Copper-Supported Catalysts. *J. Colloid Interface Sci.* **1979**, *71*, 451–465.
- (193) Pant, K. K.; Gupta, S. K.; Ahmad, E. *Catalysis for Clean Energy and Environmental Sustainability*. Springer International Publishing, **2021**.
- (194) Bridier, B.; López, N.; Pérez-Ramírez, J. Molecular Understanding of Alkyne Hydrogenation for the Design of Selective Catalysts. *Dalt. Trans.* **2010**, *39*, 8412–8419.
- (195) Jackson, S. D.; McLellan, G. D.; Webb, G.; Conyers, L.; Keegan, M. B. T.; Mather, S.; Simpson, S.; Wells, P. B.; Whan, D. A.; Whyman, R. Supported Metal Catalysts: Preparation, Characterization, and Function: V. Activities and Selectivities of Platinum Catalysts in the Reactions of Cyclopropane, Ethene, 1,3-Butadiene, and 2-butyne with Dihydrogen. *J. Catal.* **1996**, *162*, 10–19.
- (196) Cremer, P. S.; Somorjai, G. A. Surface Science and Catalysis of Ethylene Hydrogenation. *J. Chem. Soc. Faraday Trans.* **1995**, *91*, 3671–3677.

- (197) Boitiaux, J. P.; Cosyns, J.; Robert, E. Liquid Phase Hydrogenation of Unsaturated Hydrocarbons on Palladium, Platinum and Rhodium Catalysts. Part I: Kinetic Study of 1-Butene, 1,3-Butadiene and 1-Butyne Hydrogenation on Platinum. *Appl. Catal.* **1987**, *32*, 145–168.
- (198) Yang, J. W.; Zheng, W. T.; Hu, Z.; Zhang, M.; Xu, B.-Q. Do Olefin Hydrogenation Reactions Remain Structure Insensitive over Pt in Nanostructured Pt-on-Au Catalyst? *ACS Catal.* **2018**, *8*, 10254–10260.
- (199) Totarella, G.; de Rijk, J. W.; Delannoy, L.; de Jongh, P. E. Particle Size Effects in the Selective Hydrogenation of Alkadienes over Supported Cu Nanoparticles. *ChemCatChem* **2022**, *14*, e202200348.
- (200) Wang, H.; Lu, J. A Review on Particle Size Effect in Metal-Catalyzed Heterogeneous Reactions. *Chinese J. Chem.* **2020**, *38*, 1422–1444.
- (201) van Helden, P.; Ciobică, I. M.; Coetzer, R. L. J. The Size-Dependent Site Composition of FCC Cobalt Nanocrystals. *Catal. Today* **2016**, *261*, 48–59.
- (202) Van Hardeveld, R.; Hartog, F. The Statistics of Surface Atoms and Surface Sites on Metal Crystals. *Surf. Sci.* **1969**, *15*, 189–230.
- (203) Einstein, T. L. Equilibrium Shape of Crystals. In *Handbook of Crystal Growth: Second Edition*; Elsevier, **2015**.
- (204) Laidler, K. J.; Townshend, R. E. Kinetics of the Ethylene Hydrogenation on Evaporated Nickel and Iron Films. *Trans. Faraday Soc.* **1961**, *57*, 1590–1602.
- (205) Chorkendorff, I.; Niemantsverdriet, J. W. *Concepts of Modern Catalysis and Kinetics*; Wiley-VCH, **2003**.
- (206) Twigg, M. V.; Spencer, M. S. Deactivation of Supported Copper Metal Catalysts for Hydrogenation Reactions. *Appl. Catal. A Gen.* **2001**, *212*, 161–174.
- (207) Behrens, M.; Studt, F.; Kasatkin, I.; Kühl, S.; Hävecker, M.; Abild-Pedersen, F.; Zander, S.; Girgsdies, F.; Kurr, P.; Knief, B. L.; Tovar, M.; Fischer, R. W.; Nørskov, J. K.; Schlögl, R. The Active Site of Methanol Synthesis over Cu/ZnO/Al₂O₃ Industrial Catalysts. *Science* **2012**, *336*, 893–897.
- (208) Sharma, S. K.; Khan, T. S.; Singha, R. K.; Paul, B.; Poddar, M. K.; Sasaki, T.; Bordoloi, A.; Samanta, C.; Gupta, S.; Bal, R. Design of Highly Stable MgO Promoted Cu/ZnO Catalyst for Clean Methanol Production through Selective Hydrogenation of CO₂. *Appl. Catal. A Gen.* **2021**, *623*, 118239.
- (209) Chang, F.-W.; Kuo, W.-Y.; Yang, H.-C. Preparation of Cr₂O₃-Promoted Copper Catalysts on Rice Husk Ash by Incipient Wetness Impregnation. *Appl. Catal. A Gen.* **2005**, *288*, 53–61.
- (210) Santacesaria, E.; Carotenuto, G.; Tesser, R.; Di Serio, M. Ethanol Dehydrogenation to Ethyl Acetate by Using Copper and Copper Chromite Catalysts. *Chem. Eng. J.* **2012**, *179*, 209–220.

- (211) Edwards, M. A.; Whittle, D. M.; Rhodes, C.; Ward, A. M.; Rohan, D.; Shannon, M. D.; Hutchings, G. J.; Kiely, C. J. Microstructural Studies of the Copper Promoted Iron Oxide/Chromia Water-Gas Shift Catalyst. *Phys. Chem. Chem. Phys.* **2002**, *4*, 3902–3908.
- (212) Sourav, S.; Wachs, I. E. Cr-Free, Cu Promoted Fe Oxide-Based Catalysts for High-Temperature Water-Gas Shift (HT-WGS) Reaction. *Catalysts* **2020**, *10*, 305.
- (213) Yan, H.; Qin, X.-T.; Yin, Y.; Teng, Y.-F.; Jin, Z.; Jia, C.-J. Promoted Cu-Fe₃O₄ Catalysts for Low-Temperature Water Gas Shift Reaction: Optimization of Cu Content. *Appl. Catal. B Environ.* **2018**, *226*, 182–193.
- (214) Topsøe, N.-Y.; Topsøe, H. Characterization of the Structures and Active Sites in Sulfided CoMo Al₂O₃ and NiMo Al₂O₃ Catalysts by NO Chemisorption. *J. Catal.* **1983**, *84*, 386–401.
- (215) Manrique, R.; Rodríguez-Pereira, J.; Rincón-Ortiz, S. A.; Bravo-Suárez, J. J.; Baldovino-Medrano, V. G.; Jiménez, R.; Karelovic, A. The Nature of the Active Sites of Pd-Ga Catalysts in the Hydrogenation of CO₂ to Methanol. *Catal. Sci. Technol.* **2020**, *10*, 6644–6658.
- (216) Sankar, M.; Dimitratos, N.; Miedziak, P. J.; Wells, P. P.; Kiely, C. J.; Hutchings, G. J. Designing Bimetallic Catalysts for a Green and Sustainable Future. *Chem. Soc. Rev.* **2012**, *41*, 8099–8139.
- (217) Guzzi, L. Structure and Promotion of Bimetallic Catalysts: Activity and Selectivity. *Catal. Letters* **1990**, *7*, 205–212.
- (218) Spencer, M. S. The Role of Zinc Oxide in Cu/ZnO Catalysts for Methanol Synthesis and the Water-Gas Shift Reaction. *Top. Catal.* **1999**, *8*, 259–266.
- (219) Dalebout, R.; Barberis, L.; Totarella, G.; Turner, S. J.; La Fontaine, C.; de Groot, F. M. F.; Carrier, X.; van der Eerden, A. M. J.; Meirer, F.; de Jongh, P. E. Insight into the Nature of the ZnO_x Promoter during Methanol Synthesis. *ACS Catal.* **2022**, *12*, 6628–6639.
- (220) Brands, D. S.; Poels, E. K.; Blik, A. Ester Hydrogenolysis over Promoted Cu/SiO₂ Catalysts. *Appl. Catal. A Gen.* **1999**, *184*, 279–289.
- (221) Beerthuis, R.; Visser, N. L.; van der Hoeven, J. E. S.; Ngene, P.; Deeley, J. M. S.; Sunley, G. J.; de Jong, K. P.; de Jongh, P. E. Manganese Oxide Promoter Effects in the Copper-Catalyzed Hydrogenation of Ethyl Acetate. *J. Catal.* **2021**, *394*, 307–315.
- (222) Pompe, C. E.; Slagter, M.; de Jongh, P. E.; de Jong, K. P. Impact of Heterogeneities in Silica-Supported Copper Catalysts on their Stability for Methanol Synthesis. *J. Catal.* **2018**, *365*, 1–9.
- (223) Kikhtyanin, O.; Pospelova, V.; Aubrecht, J.; Lhotka, M.; Kubička, D. Effect of Atmosphere Calcination and Temperature on the Hydrogenolysis Activity and Selectivity of Copper-Zinc Catalysts. *Catalysts* **2018**, *8*, 446.
- (224) Yan, Y.; King, S. C.; Li, M.; Galy, T.; Marszewski, M.; Kang, J. S.; Pilon, L.; Hu, Y.; Tolbert, S. H. Exploring the Effect of Porous Structure on Thermal Conductivity in Templated

- Mesoporous Silica Films. *J. Phys. Chem. C* **2019**, *123*, 21721–21730.
- (225) Bruehwiler, A.; Semagina, N.; Grasmann, M.; Renken, A.; Kiwi-Minsker, L.; Saaler, A.; Lehmann, H.; Bonrath, W.; Roessler, F. Three-Phase Catalytic Hydrogenation of a Functionalized Alkyne: Mass Transfer and Kinetic Studies with in Situ Hydrogen Monitoring. *Ind. Eng. Chem. Res.* **2008**, *47*, 6862–6869.
- (226) Cherkasov, N.; Ibhaddon, A. O.; McCue, A. J.; Anderson, J. A.; Johnston, S. K. Palladium-Bismuth Intermetallic and Surface-Poisoned Catalysts for the Semi-Hydrogenation of 2-methyl-3-butyn-2-ol. *Appl. Catal. A Gen.* **2015**, *497*, 22–30.
- (227) Ho, C.-Y.; Schleicher, K. D.; Chan, C.-W.; Jamison, T. F. Catalytic Addition of Simple Alkenes to Carbonyl Compounds by Use of Group 10 Metals. *Synlett* **2009**, *16*, 2565–2582.
- (228) Nguyen, K. D.; Park, B. Y.; Luong, T.; Sato, H.; Garza, V. J.; Krische, M. J. Metal-Catalyzed Reductive Coupling Ofolefin-Derived nucleophiles: Reinventing Carbonyl Addition. *Science* **2016**, *354*, aah5133.
- (229) Zhao, B.; Zhang, R.; Huang, Z.; Wang, B. Effect of the Size of Cu Clusters on Selectivity and Activity of Acetylene Selective Hydrogenation. *Appl. Catal. A Gen.* **2017**, *546*, 111–121.
- (230) Bertero, N. M.; Apesteguía, C. R.; Marchi, A. J. Catalytic and Kinetic Study of the Liquid-Phase Hydrogenation of Acetophenone over Cu/SiO₂ Catalyst. *Appl. Catal. A Gen.* **2008**, *349*, 100–109.
- (231) Liu, Z.; Yang, Y.; Mi, J.; Tan, X.; Song, Y. Synthesis of Copper-Containing Ordered Mesoporous Carbons for Selective Hydrogenation of Cinnamaldehyde. *Catal. Commun.* **2012**, *21*, 58–62.
- (232) Fernández-Roperero, A. J.; Zawadzki, B.; Kowalewski, E.; Pieta, I. S.; Krawczyk, M.; Matus, K.; Lisovytskiy, D.; Śrębowata, A. Continuous 2-methyl-3-butyn-2-ol Selective Hydrogenation on Pd/γ-Al₂O₃ as a Green Pathway of Vitamin a Precursor Synthesis. *Catalysts* **2021**, *11*, 501.
- (233) Vernuccio, S.; von Rohr, P. R.; Medlock, J. General Kinetic Modeling of the Selective Hydrogenation of 2-Methyl-3-Butyn-2-Ol over a Commercial Palladium-Based Catalyst. *Ind. Eng. Chem. Res.* **2015**, *54*, 11543–11551.
- (234) González-Fernández, A.; Pischetola, C.; Kiwi-Minsker, L.; Cárdenas-Lizana, F. Partial Hydrogenation of 2-Methyl-3-butyn-2-ol over Pd/ZnO: Effect of Reduction Temperature on Alloy Formation and Catalytic Response. *J. Phys. Chem. C* **2020**, *124*, 3681–3691.
- (235) Shen, L.; Mao, S.; Li, J.; Li, M.; Chen, P.; Li, H.; Chen, Z.; Wang, Y. PdZn Intermetallic on a CN@ZnO Hybrid as an Efficient Catalyst for the Semihydrogenation of Alkynols. *J. Catal.* **2017**, *350*, 13–20.
- (236) Semagina, N.; Renken, A.; Laub, D.; Kiwi-Minsker, L. Synthesis of Monodispersed Palladium Nanoparticles to Study Structure Sensitivity of Solvent-Free Selective

REFERENCES

- Hydrogenation of 2-Methyl-3-butyn-2-ol. *J. Catal.* **2007**, *246*, 308–314.
- (237) Shesterkina, A. A.; Strekalova, A. A.; Shuvalova, E. V.; Kapustin, G. I.; Tkachenko, O. P.; Kustov, L. M. CuO-Fe₂O₃ Nanoparticles Supported on SiO₂ and Al₂O₃ for Selective Hydrogenation of 2-Methyl-3-butyn-2-ol. *Catalysts* **2021**, *11*, 625.
- (238) Mao, S.; Zhao, B.; Wang, Z.; Gong, Y.; Lü, G.; Ma, X.; Yu, L.; Wang, Y. Tuning the Catalytic Performance for the Semi-Hydrogenation of Alkynols by Selectively Poisoning the Active Sites of Pd Catalysts. *Green Chem.* **2019**, *21*, 4143–4151.
- (239) Brei, V. V. Correlation between the Strength of the Basic Sites of Catalysts and Their Activity in the Decomposition of 2-Methyl-3-butyn-2-ol as a Test Reaction. *Theor. Exp. Chem.* **2008**, *44*, 320–324.
- (240) Lauron-Pernot, H.; Luck, F.; Popa, J. M. Methylbutynol: A New and Simple Diagnostic Tool for Acidic and Basic Sites of Solids. *Appl. Catal.* **1991**, *78*, 213–225.
- (241) Sulman, E. M.; Nikoshvili, L. Z.; Matveeva, V. G.; Tyamina, I. Y.; Sidorov, A. I.; Bykov, A. V.; Demidenko, G. N.; Stein, B. D.; Bronstein, L. M. Palladium Containing Catalysts Based on Hypercrosslinked Polystyrene for Selective Hydrogenation of Acetylene Alcohols. *Top. Catal.* **2012**, *55*, 492–497.

List of publications and presentations

This thesis is amongst others based on the following publications

Totarella, G., Beerthuis, R., Masoud, N., Louis, C., Delannoy, L., & De Jongh, P. E. (2020). Supported Cu Nanoparticles as Selective and Stable Catalysts for the Gas Phase Hydrogenation of 1,3-Butadiene in Alkene-Rich Feeds. *The Journal of Physical Chemistry C*, 125(1), 366-375. First authors Giorgio Totarella and Rolf Beerthuis contributed equally.

Totarella, G., de Rijk, J. W., Delannoy, L., de Jongh, P. E. (2022). Particle Size Effects in the Selective Hydrogenation of Alkadienes over Supported Cu Nanoparticles. *ChemCatChem*, 14(19), e202200348.

Totarella, G., de Jongh, P.E., Selective Hydrogenation of 2-Methyl-3-butyn-2-ol Over Supported Cu Nanocatalysts. Submitted (2024).

Other publications from the author

Cimino, S., **Totarella, G.**, Tortorelli, M., Lisi, L. (2017). Combined Poisoning Effect of K⁺ and its Counter-Ion (Cl⁻ Or NO³⁻) On MnO_x/TiO₂ Catalyst During the Low Temperature NH₃-SCR of NO. *Chemical Engineering Journal*, 330, 92-101.

Cimino, S., Lisi, L., **Totarella, G.**, Barison, S., Musiani, M., Verlato, E. (2018). Highly Stable Core-Shell Pt-CeO₂ Nanoparticles Electrochemically Deposited onto FeCrAlloy Foam Reactors for the Catalytic Oxidation of CO. *Journal of Industrial and Engineering Chemistry*, 66, 404-410.

Gargiulo, N., Caputo, D., **Totarella, G.**, Lisi, L., Cimino, S. (2018). Me-ZSM-5 Monolith Foams for the NH₃-SCR Of NO. *Catalysis Today*, 304, 112-118.

Balsamo, M., Erto, A., Lancia, A., **Totarella, G.**, Montagnaro, F., Turco, R. (2018). Post-Combustion CO₂ Capture: on the Potentiality of Amino Acid Ionic Liquid as Modifying Agent of Mesoporous Solids. *Fuel*, 218, 155-161.

van der Hoeven, J. E., Jelic, J., Olthof, L. A., **Totarella, G.**, van Dijk-Moes, R. J., Krafft, J. M., Louis, C., Studt, F., van Blaaderen, A., de Jongh, P. E. (2021). Unlocking Synergy in Bimetallic Catalysts by Core-Shell Design. *Nature Materials*, 20(9), 1216-1220.

Dalebout, R., Barberis, L., **Totarella, G.**, Turner, S. J., La Fontaine, C., De Groot, F. M., Carrier, X., van der Eerden, A. M. J., Meirer, F., de Jongh, P. E. (2022). Insight into the Nature of the ZnO_x Promoter during Methanol Synthesis. *ACS catalysis*, 12(11), 6628-6639.

Oral presentations

Totarella, G.; Donoeva, B.; de Jongh, P.E. Selective Hydrogenation of 1,3-Butadiene over SiO₂-Supported Cu Nanoparticles, CatConf 2020- Catalysis: From Science to Industry, Tomsk (Russia, held online), 6-10 October **2020**.

Totarella, G.; Delannoy, L.; de Jongh, P.E. Selective hydrogenation of 1,3-butadiene over supported Cu nanoparticles, NWO Chemistry as Innovating Science 2020 (CHAINS2020), Netherlands (held online), 8-9 December **2020**.

Totarella, G.; Delannoy, L.; P. Ngene, de Jongh, P.E. Supported Cu Nanoparticles as Selective and Stable Catalysts for the Gas Phase Hydrogenation of 1,3-Butadiene in Alkene-Rich Feeds, XXII Netherlands' Catalysis and Chemistry Conference 2021 (NCCC2021), Netherlands (held online), 1 March **2021**.

Totarella, G.; Delannoy, L.; de Jongh, P.E. Supported Cu Nanoparticles as Selective and Stable Catalysts for the Gas Phase Hydrogenation of 1,3-Butadiene in Alkene-Rich Feeds, ACS SPRING 2021, USA (held online), 5-30 April **2021**.

Poster presentations

Totarella, G.; Donoeva, B.; de Jongh, P.E. Supported Cu-based Catalysts for Selective Hydrogenation, XX Netherlands Catalysis and Chemistry Conference (NCCC2019), Noordwijkerhout (Netherlands). 4-6 March **2019**

Totarella, G.; Donoeva, B.; de Jongh, P.E. Supported Cu-based Catalysts for Selective Hydrogenation, 3rd EFCATS-CNRS European Summer School on Catalyst Preparation (CatPrep2019), Vogüé – Ardèche (France), 16-21 June **2019**.

Totarella, G.; Donoeva, B.; de Jongh, P.E. Silica-supported Copper Nanoparticles as Selective and Stable Catalysts for the Hydrogenation of 1,3-Butadiene, XXI Netherlands Catalysis and Chemistry Conference (NCCC2019), Noordwijkerhout (Netherlands). 2-4 March **2020**

Curriculum vitae

Giorgio Totarella was born on the 30th of May 1992 in Campobasso, Italy. He completed his pre-university education at the Istituto Tecnico Industriale Statale “G. Marconi” (Campobasso, Italy) where he graduated as Food Technologist. After his graduation, he started his BSc studies in Industrial Chemistry at the University of Naples “Federico II” (Naples, Italy) in 2014, where he defended his BSc thesis and graduated 110/110 *cum laude*. At the same university, the author received his MSc (110/110), with *magna cum laude*, in Science and Technology of Industrial Chemistry in 2016. His MSc research project was focused on the synthesis, characterization and testing of novel supported ionic liquid-based materials for CO₂ capture from flue-gas. Afterwards, the author joined the Institute for Research on Combustion (National Research Council of Italy, Naples) as graduate research fellow from 2016 to 2017. Here the author worked on the set-up of three experimental projects for the investigation of activity, stability and selectivity of catalysts intended for pollution control (de-NO_x) and flameless combustion. During this time, he contributed to 4 peer-reviewed articles.



From end 2017 to 2022 Giorgio worked as a PhD candidate in the Materials Chemistry and Catalysis group at Utrecht University, under supervision of prof. dr. Petra de Jongh and dr. Laurent Delannoy. During his research project, the author contributed to improvement of catalytic set-ups and testing for hydrogenation catalysts, sharing knowledge on his practical scientific and engineering background, in particular regarding kinetics measurements on flow set-ups. The author supervised two BSc projects, one MSc project, one joined MSc project and two practical lab courses (Research Project Debye). His research was presented at several national and international conferences. Part of the work discussed in this thesis has been published in peer-reviewed journals.

At the time of publication, the author joined ASML (2022, the Netherlands) as Physics Design Engineer. In his free time, Giorgio likes travelling, coding, boxing, running, playing with his two cats and spending time with friends.